JGERI
Journal of Green Energy Research and Innovation
ISSN: 3041-9018

Journal of Green Energy Research and Innovation

Volume 2, Issue 2, Spring 2025

PUBLISHER
Arak University

Journal of Green Energy Research and Innovation (JGERI)

Publisher: **Arak University**

Director-in-Charge: **Dr. Ali Asghar Ghadimi**

Editor-in-Chief: **Prof. Gevork B. Gharehpetian**

Deputy Editor: **Dr. Abolghasem Daeichian**

Managing and Executive Editor**: Dr. Mahyar Abasi**

Coverage area: **International**

Journal Type: **Scientific and technical**

Scientific Rank (Iran MSRT): **B**

Language: **English**

Frequency: **Quarterly**

Review Time: **4-8 Weeks**

Publication Type: **Electronic**

Open Access: **Yes**

Policy: **Peer-Reviewed**

DOI**: 10.61186/jgeri**

E-mails: **jgeri@araku.ac.ir**

Website: **https://jgeri.araku.ac.ir/**

Address: **Department of Electrical Engineering, Faculty of Engineering, Arak University, Arak, Iran.**

P.O. Box: **38156-8-8349**

Tel: **086-32625099**

Editorial Board

About Journal

JGERI is an international, open-access, and free-of-charge journal in the field of green and renewable energies, published quarterly, only electronically, in cooperation with the Renewable Energy Research Institute (**RERI**) of Arak University and Iranian Association of Electrical and Electronics Engineers (**IAEEE**). Articles accepted and published by **JGERI** are in three formats: research articles, review articles, and applied articles. **JGERI** accepts manuscripts that provide results of scientific achievements in a very wide scope of fundamental, engineering, and industrial research focusing on green energy.

The following articles are acceptable:

- **Research articles** are expected to present innovative solutions, new concepts, or creative ideas that can help solve existing or emerging technical challenges in the field of green and renewable energy.
- **Review articles** are expected to provide enlightening and specialized reviews, trainings, or case studies on an important topic, timely and widely in the field of green and renewable energies.
- **Applied articles** are expected to share the results of the industry's valuable experiences in dealing with challenging technical issues, developing/adopting new standards, applying new technologies or solving complex problems in the field of green and renewable energies. These articles can have a significant impact on the strategic plans of the industry in the coming years.

Aims and Scope

JGERI is interested on the qualified international multidisciplinary research results related to all aspects of green energy. The scope of **JGERI** is very broad, and welcomes original, novel fundamental and engineering research. We also publish reviews and industrial reports of green energy and its impact on the eco-environment.

We welcome research papers that focus on, but are not limited to, the following areas:

- Policies and Strategies for Green Energy Systems
- Fundamental And Industrial Applications for Green Energy Systems
- Energy Conversion, Control Techniques, and Grid Interactive Systems for Green Energy Systems
- Environmental Impacts of Energy Technologies and Pollution Control
- Materials And Catalysis for Green Energy Systems
- Green Energy Consumption
- Artificial Intelligence, Machine Learning, and Computational Methods in Green Energy Systems
- Public Awareness and Education for Green Energy Systems
- Solar Energy and Photovoltaic
- Wind Energy
- Hydrogen Energy and Energy Storage
- Biofuel and Bioenergy
- Utilization of Green Energies in the Structure of Power Systems
- Development of Manufacturing Technology for Green Energy Production Tools
- Electricity Market in the Presence of Green Energies
- The Effects of Green Energy Production on Power Quality of the Power System
- Impact of Expansion Planning of Power Systems on the Development of Green Energy Generation
- Operation of Green Energy-Based Microgrids
- Control and Protection of Power Systems in Networks Equipped with Green and Renewable Generation
- Energy Management in Networks Consisting of Green Energies
- Studies on the Technology of Hybrid Vehicles Based on Green Energy Fuels
- The Future Perspective of the Electricity Industry in the Presence of Production-Based Technologies and Green Energy-Based Consumers
- Green Energy Storage Technologies
- Communication Infrastructures and Protocols and Internet in Green Energy-Based Power Systems
- Cyber Security and Defense Activities in the Field of Green Energy Management

Each manuscript will go through a rigors peer-review process. you can visit our Guide for Authors page for information on preparing your manuscript.

Guide for Authors

1. Important points and rules for manuscript submission and publication

-Submitting a manuscript to a journal means that the manuscript is not under review or has not been published anywhere in any other language before.
-The submission of the manuscript for publication by the author, implicitly or explicitly, implies the approval of the organization or body where the author works and has used its affiliation.
-By submitting the manuscript, all authors officially declare their agreement to grant the copyright of the manuscript in case of acceptance to Arak University and **JGERI**. However, the authors are responsible for all the contents published in the manuscript, and the journal is only a reviewer and publisher.
- All authors are required to declare any actual or potential conflicts of interest, including financial, personal, or relationships with individuals or organizations that could affect their work.
- Each of the authors must declare their contribution and role in the manuscript on the Title Page to the journal. The statement of approval of all authors and their role in the manuscript is the responsibility of the corresponding author.
- Authors should note that all manuscripts sent to **JGERI** are checked with Authenticate's CrossCheck software to analyze the authenticity of the content. In this analysis, the overlap and similar texts presented in the submitted manuscripts will be determined.
- **JGERI** makes its manuscripts open to access after publication and there is no charge (APC) for reviewing and publication of manuscripts, and readers can download and use the articles for free.
- All authors, if they had financial support in conducting research related to this manuscript, should briefly state their role. If financial source(s) have no role in the results of the research published by the article, this should also be mentioned by the authors.
- Acknowledgments to individuals and institutions can be mentioned in a separate section at the end of the manuscript before References, and they must not be included as footnotes or in any other form. In this section, it is recommended to mention the names of those who have collaborated during the research (such as those helping in the language correctness aspect of the manuscript, assisting in writing the manuscript or proofreading it, and other cases).
- Non-commercial use of the manuscript will be governed by the Creative Commons Attribution-NonCommercial 4.0 International License, which is currently available at the link (https://creativecommons.org/licenses/by-nc/4.0/). This certificate allows others to use the authors' work in a non-commercial way and utilize it in their research work, although in the new work, they need to acknowledge the authors and mention its non-commercial nature.

2. Initial submission of the manuscript

Submission to this journal is online and you will be accompanied in all the steps of creating a user account and uploading files. All correspondence, including notification of the editor's decision and request for revision, will be made via email. To submit your manuscript, just click on the **Submit Manuscript** option on the journal page. Then, click on **Register** to create an author account. A message will be sent to your email containing your username and password. Then, log in to the manuscript submission system on the Users login page, where you need to enter the username and password and submit your new manuscript. Once you are logged in, you can change your password by clicking on My Home in the top menu. For the next time, just log in to your account. Please include the names, addresses, and email addresses of at least three potential academic reviewers with the paper. Please include reviewers' names and their academic rank, affiliation, and contact information (mail address is mandatory). However, only the editor has the right to decide on the use of suggested reviewers. All the submitted manuscripts undergo the process of plagiarism check with IThenticate software and the review process begins. According to the journal policy, there is a difference between the requirements for initial and revised submission files. Required files for initial submission include three files: **JGERI_Main_Manuscript**, **JGERI_Form_for _Copyright_Transfer_Statement and Conflict_ of_ Interest_ Disclosure** and **JGERI_Cover_Letter**, all three of which must be sent to the journal in PDF format. You can use the links below to download the requirements and suggestions files of these three files.

- JGERI_Guideline_for_Main_Manuscript
- JGERI_Guideline_for_Cover_Letter
- JGERI_Form_for_Copyright_Transfer_Statement and Conflict_ of_ Interest_ Disclosure

3. Submission of the revised manuscript

If the submitted manuscript, after going through the initial review process, is evaluated by the officials and reviewers of the journal and a decision is made to make corrections and revisions in the form of minor or major, the authors are obliged to make the corrections and prepare the response letter to the reviewers within the time specified by the journal. Three files must be sent to the journal at this stage: WORD and PDF files of the revised manuscript (changes should be highlighted), PDF file of the response to the reviewers (including the comments and responses of each of the reviewers separately), Title Page and Authorship file in WORD format (containing two main forms: Title Page and Authorship). The link to download the necessary files along with their requirements and instructions is given below. Points raised in the file **JGERI_Revised_Manuscript** must be followed for compiling the revised manuscript.

The authors are obliged to submit the revised file in PDF and WORD format to the journal. Also, different parts of the file **JGERI_Form_for_Title_Page_ and_ Authorship** needs to be completed and signed by the corresponding author, but **JGERI_Response_to_the_Reviewers_Comments** is suggested by the journal and it is not necessary to follow all the points of that file. It should be noted that all the stages of page layout and editing in the form of final publication are the responsibility of the journal. In the completion stages of this process, the cooperation of the authors is needed, and we will inform you at each stage. Thus, the minimum requirements for file compilation are provided in the template file.

- JGERI_Guideline_for_Revised_Manuscript
- JGERI_Form_for_Title_Page_ and_ Authorship
- JGERI_Guideline_for_Response_to_the_Reviewers_Comments

4. After the final acceptance of the manuscript

After announcing the final acceptance of the manuscript (reviews may happen several times), the files **JGERI_Revised_Manuscript** and **JGERI_Form_for_ Title_Page_ and_ Authorship** will be sent to the paging unit for page layout and final editing. After the final acceptance announcement, the authors will be asked to send a graphic abstract included in a single file. Then, the process of compilation of the manuscript will be completed by the journal and finally, the proof version of the manuscript will be sent to the authors. The authors are obliged to check the proof file completely and report to the journal if they find any ambiguity or error in the final file. In some cases, along with the final proof file of the manuscript, there may be a series of errors and ambiguities in the manuscript, which are sent to the author in the form of comments along with the proof version of the manuscript. The corresponding author is obliged to clarify and resolve these problems and ambiguities in the specified time.

5. After publication on the journal's website

After announcing the initial acceptance, the information of the article without its content will be indexed in the Articles in the Press section of the website. After including the article in the issue selected by the journal, the desired article will be indexed in the Current Issue unit along with Vol., No., and pp. Also, the electronic file of the article can be introduced in all scientific references through the DOI link. The important point is that, after acceptance and indexing, the names of the authors cannot be changed, that is, it will not be possible to add, delete, or change the order of the names of the authors and their organizational affiliations.

Cooperative Publication Organization

Renewable Energy Research Institute of Arak University
http://araku.ac.ir/web/riren

Iranian Association of Electrical and Electronics Engineers
https://iaeee.ir/

Iranian Wind Energy Association
https://www.irwea.org/fa/

Indexing Databases and Social Networks

Iran MSRT: https://journals.msrt.ir/home/detail/21538/

Magiran: https://www.magiran.com/magazine/8484

Google Scholar: https://scholar.google.com/citations?user=47bsJFoAAAAJ&hl=en

Linkedin: https://www.linkedin.com/in/jgeri-arak-university-0818872b9

Academia:https://independent.academia.edu/JournalofGreenEnergyResearchandInnovationJGERI

MyScineceWork: https://www.mysciencework.com/profile/j.green.energy.res.innov.jgeri

Contents

Journal of Green Energy Research and Innovation

A Multi-Objective Framework for Smart Energy Hubs: Leveraging Compressed Air Storage and Demand Response

Pouria Hajiamoosha, Abdollah Rastgou, Hadi Afshar

Highlights

- **A multi-carrier energy hub generates and delivers electricity, heating, and cooling from diverse sources.**
- **The hub participates in demand response to reduce peak demand and enhance system efficiency.**
- **We use a mixed-integer linear programming approach to minimize costs and carbon emissions.**
- **Case study results demonstrate significant cost and emission reductions while improving energy hub efficiency.**

Graphical Abstract

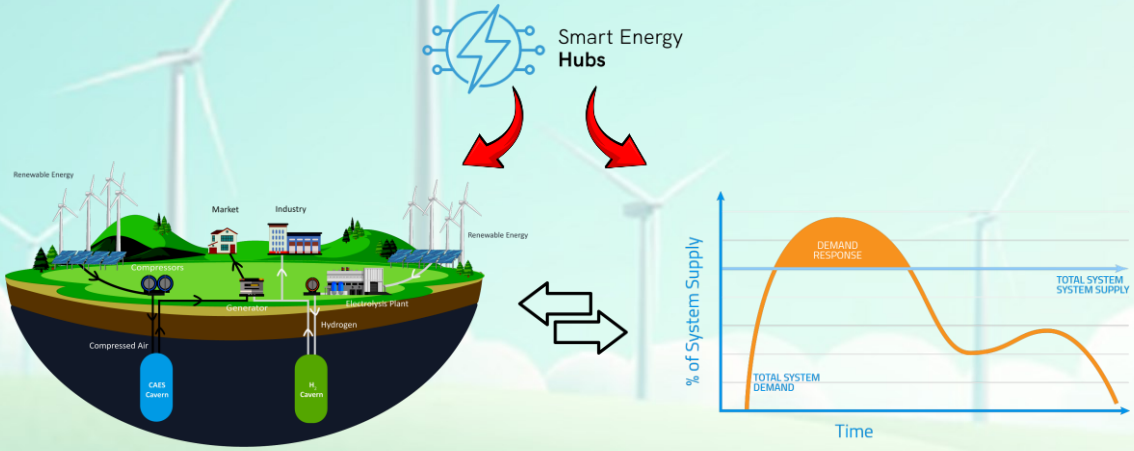

Use your device to scan and read the article online

Citation

P. Hajiamoosha, A. Rastgou, and H. Afshar," A Multi-Objective Framework for Smart Energy Hubs: Leveraging Compressed Air Storage and Demand Response," *Journal of Green Energy Research and Innovation*, vol. 2, no. 2, pp. 1-25, 2025.

https://doi.org/10.61186/jgeri.2.2.1

Journal of Green Energy Research and Innovation 2.2 (2025) 1-25

Online ISSN: 3041-9018

Journal of Green Energy Research and Innovation

Journal Homepage: www.jgeri.araku.ac.ir

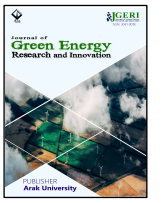

A Multi-Objective Framework for Smart Energy Hubs: Leveraging Compressed Air Storage and Demand Response

Pouria Hajiamoosha [1], Abdollah Rastgou [1,*], Hadi Afshar [2]

[1] *Department of Electrical Engineering, Kermanshah Branch, Islamic Azad University, Kermanshah, Iran.*

[2] *Electrical and Computer Engineering Faculty, Semnan University, Semnan, Iran.*

A R T I C L E I N F O

Keywords:
Energy hub,
Multi-objective programming,
Storage devices,
Optimization.

Article History:
Received: 05 March 2025;
Revised: 11 March 2025;
Accepted: 15 March 2025.

Article type:
Research Article

* ***Corresponding author***
E-mail address
abdollah.rastgou@iau.ac.ir (A. Rastgou)

A B S T R A C T

In this paper, a multi-carrier energy hub that can generate and deliver electricity, heating, and cooling energy from different sources, such as wind, solar, fuel cells, batteries, and compressed air is proposed. The intelligent energy hub can also participate in electrical and thermal demand response, which aims to reduce peak demand and enhance overall system efficiency. The scheduling problem is a mixed-integer linear programming problem that seeks to minimize the system cost and carbon dioxide emissions. To obtain optimal solutions that strike a balance between cost, emissions, and decision maker's preferences, an augmented epsilon-constraint min-max fuzzy method is employed. The proposed strategy's advantages are demonstrated through a case study, where it is compared with other methods. The results show that the proposed approach effectively reduces the cost and emissions of the smart energy hub while improving the load shape and energy hub efficiency. Moreover, the results showed that the integration of compressed air systems and demand response programs enhances the performance of the smart energy hub, making it more flexible and reliable. The GAMS software is employed for the modeling and resolution of the scheduling issue.

1. Introduction

The increasing concerns over environmental sustainability and the need for efficient utilization of energy resources have driven the development of innovative energy systems [1-3]. In recent years, numerous research studies have concentrated on the integration of various renewable energy sources, such as fuel cells, photovoltaic (PV) systems, and energy storage systems, to create hybrid energy systems [4]. These hybrid systems offer the potential for improved reliability, reduced environmental impact, and enhanced energy efficiency [5]. Nevertheless, the effective implementation and management of hybrid energy systems in practical environments present multifaceted challenges [6]. One significant challenge is the presence of demand response programs, which aim to optimize energy consumption by adjusting demand based on supply conditions. These programs introduce variability in the energy demand, thus influencing the performance and cost-effectiveness of the hybrid energy systems [7,8]. The energy hub (EH) represents a novel approach to energy systems, serving as a crucial link between diverse energy sources [9]. By enabling the smooth convergence of diverse energy systems, such as electrical grids and natural gas infrastructures, EHs foster a synchronized and effective functioning. [10]. Reference [11], proposed a microgrid that incorporates a combined heating, cooling, and power (CCHP) system, utilizing electricity and gas as energy carriers. This EH system aims to optimize the utilization of energy resources. The integration of renewable energies into the CCHP system enhances the economic and environmental aspects, which have been thoroughly investigated as delineated in [12]. In [13], the CCHP systems are studied, which employ a variety of energy suppliers, including gas turbines (GTs), gas boilers (GBs), and electric and absorption chillers, to meet the demands for heat, cooling, and power. In reference [14], a proposed EH system introduces the concept of a versatile infrastructure capable of storing and converting multiple energy carriers. In an EH framework, the requisites for cooling, power, and heating are addressed through the strategic utilization of electricity and gas, which constitute the primary energy vectors commonly in use [15]. In [16], the focus is on examining the optimization of multi-energy carriers within an EH system through the utilization of a non-linear programming model. Reference [17], presents a thorough examination of EHs in the role of decision-makers and proposes a multi-period, multi-energy operational framework designed to enhance coordination across various energy networks.

A proposed analysis of energy consumption in smart multi-energy carriers, functioning as an EH system, is presented in [18] for residential applications. In [19] Optimization of EH systems for residential loads while considering customer preferences and comfortability is solved in real time. A novel approach is presented in Reference [20] for managing the charging process of plug-in hybrid electric vehicles (PHEVs) within the structure of EHs, which utilizes a multi-objective optimization framework to determine the optimal charging patterns for PHEVs, taking into account both the perspectives of vehicle owners and system operators. Reference [10] has developed a residential EH model that demonstrates the operation of multiple energy carriers in a home. They propose an integrated infrastructure and an optimization problem to enhance the performance of a smart home.

Demand response (DR) programs are becoming increasingly prevalent in the context of microgrids. These programs allow for the efficient management and utilization of energy resources by adjusting consumer demand to match the available supply. By engaging participants to temporarily reduce or shift their energy consumption during peak periods, DR programs optimize the overall operation of the EH. Through intelligent communication and control systems, these programs enable the seamless integration of distributed energy resources, such as solar panels and battery storage, into the grid, providing a reliable and sustainable solution for the ever-increasing energy demand. Reference [21] and [22] have studied DR programs in multi-energy systems. In [23], the DR program and energy generation for various customer types in a microgrid are modeled using a two-stage stochastic function. A stochastic energy procurement model that considers the effects of DR is proposed in reference[24]. This model is designed for large electricity consumers and demonstrates operational cost reductions by shifting the load from peak to off-peak periods. Reference [25] presents a concept of electricity shifting potential to determine the maximum reduction of electricity from the grid to the distributed multi-generation system, based on a profitability map of DR incentives. The optimal solutions and scheduling in DR in multi-energy carriers have been investigated in fewer studies compared with studies that investigate the potential and modeling analysis of DR in multi-energy carriers. In [26], the economic performance of the gas-fired CCHP system is thoroughly examined, taking into account various factors that influence its overall efficiency. A sensitivity analysis is also conducted to assess the system's robustness under different scenarios.

The motivation of this paper is to develop a model of a smart grid in the EH concept in which different forms of energy such as power, heat, and cold, are integrated into it, and different energy carriers such as gas and electricity support the EH with the different multi-generation unit are in the model. This paper proposes a scheduling strategy for a smart multi-carrier EH (SMEH) that can provide electricity, heating, and cooling from various sources. The SMEH includes a wind turbine (WT), a solar panel, a micro-turbine, a fuel cell, a boiler, an absorption chiller, a battery, and a compressed air energy storage (CAES) system. The SMEH can also join electrical and thermal DR programs to lower the peak demand and improve the system's efficiency. We model the scheduling problem as a mixed-integer linear programming (MILP) problem that aims to minimize the system cost, carbon dioxide emissions, and risk. We solve the problem using an augmented epsilon-constraint min-max fuzzy method that can produce optimal solutions that balance the different objectives and the decision maker's preferences. We present three case studies to show the benefits of the proposed strategy and to compare it with other methods. We also discuss using GAMS software to model and solve the scheduling problem. Two objective functions are addressed for this multi-objective optimization problem, first operation cost and second carbon emission reduction. The argument epsilon constraint method is implemented to solve multi-objective problems and obtain the optimal Pareto solutions. The epsilon constraint method offers significant advantages over other methods, such as the weighted sum method. The epsilon constraint method provides a more comprehensive explanation of the solutions on the Pareto front. Different methods are employed to select an optimal solution from the Pareto front, ensuring a balanced tradeoff between objectives. The max-min fuzzy technique is particularly effective for this purpose. Additionally, two distinct DR programs, real-time pricing (RTP) and Time-of-Use (TOU), are implemented to optimize operational costs and reduce carbon emissions [27].

The paper's contributions are succinctly summarized as follows:

- Establishment of a Comprehensive Framework: Integration of WT, PV, and CCHP systems, alongside electric heat pumps (EHP) and CAES units within an EH system.
- Optimal multi-objective model: development of a model addressing both economic and environmental challenges.
- Epsilon constraint method: the application of the epsilon constraint method addresses the multi-objective optimization problem effectively.
- Max-min fuzzy technique: the max-min fuzzy technique is utilized to derive a compromise solution.
- Reduction of operation costs and carbon emissions: implementing RTP and TOU-DR programs leads to the reduction of operational costs and carbon emissions, achieving simultaneous cost savings and environmental benefits.
- Mixed-integer linear programming: The application of mixed-integer linear programming techniques guarantees the derivation of the most efficient solution for the specified problem.

2. Problem formulation

2.1. Mathematical formulation for an energy hub system

Operation cost minimization is considered the first objective of the model as shown in Equation (1):

$$F(\mathrm{Cos}t) = \sum_{t=1}^{T} (C_{pg}(t) + C_{pe}(t) + SUC_{CHP}(t) + SDC_{CHP}(t)) \quad (1)$$

The second objective function is minimizing carbon emissions as shown in Equation (2).

$$F(Emission)=\sum_{t=1}^{T}(E_{pg}(t)+E_{pe}(t)) \tag{2}$$

where:

$$C_{pg}^{t}=P_{g}\times(P_{ge}^{t}+P_{gh}^{t}+P_{gchp}^{t}+P_{gcaes}^{t}) \tag{3}$$

$$C_{pe}^{t}=P_{e}^{t}\times(P_{buy}^{t}-P_{sell}^{t}) \tag{4}$$

$$E_{pg}^{t}=P_{g}\times\beta_{g}\times(P_{ge}^{t}+P_{gh}^{t}+P_{gchp}^{t}+P_{gcaes}^{t}) \tag{5}$$

$$E_{pe}^{t}=\eta_{t}\times P_{buy}^{t} \tag{6}$$

The power hub is capable of bi-directional energy transfer with the electrical grid, allowing for both the absorption and distribution of power. Exchanging power between the grid and EH is modeled as Equation (7):

$$P_{grid}^{t}\eta_{t}=P_{sell}^{t}+P_{buy}^{t} \tag{7}$$

The gas turbine model indicates that it comprises the GT power supply heat exchanger and the power hub. The representation of the GT model is as Equation (8):

$$P_{ge}^{t}\eta_{ge}=P_{gt}^{t} \tag{8}$$

The capacity limitations of different devices are presented in Equation (9)-(16).

$$0\le P_{pv}^{t}\le P_{pv}^{\max} \tag{9}$$

$$0\le P_{wt}^{t}\le P_{wt}^{\max} \tag{10}$$

$$0\le P_{gas}^{t}\le P_{gas}^{\max} \tag{11}$$

$$0\le P_{gt}^{t}\le P_{gt}^{\max} \tag{12}$$

$$P_{chp}^{\min}\le P_{chp}^{t}\le P_{chp}^{\max} \tag{13}$$

$$-P_{grid}^{\max}\le P_{grid}^{t}\le P_{pv}^{\max} \tag{14}$$

$$T_{EHP}^{\min}\le T_{EHP}^{t}\le T_{EHP}^{nax} \tag{15}$$

$$PS^{\min}\le PS^{t}\le PS^{\max} \tag{16}$$

The cooling section's energy conversion model outlines technical constraints, including the unidirectional reception of cooling energy from both electric and absorption chillers. The absorption chiller utilizes heat, while the electric chiller uses electricity to produce cooling.

The mathematical models for the electric and absorption chillers are outlined in Equation (17) and (18), respectively [27].

$$P_{ec}^{t}COP_{ec}=C_{ec}^{t} \tag{17}$$

$$H_{ac}^{t}COP_{ac}=H_{ac}^{t} \tag{18}$$

The ice storage air conditioning system, a critical element of the cooling infrastructure, is composed of a chiller unit and an ice storage tank. The chiller's role is to produce ice, while the tank is responsible for its storage and subsequent melting during peak demand periods. The implementation of intelligent storage co1000ntrol enables the efficient redistribution of electrical loads, shifting them from peak to off-peak periods, as documented in [28]. This shift in consumption patterns leads to a reduction in load variations, ensuring a more stable and balanced energy demand. Additionally, Reference [29] explores the optimization of ice storage tank efficiency and life cycle costs, providing valuable insights that enhance the system's overall effectiveness and economic viability.

The balance of cooling energy produced is detailed in Equation (19). The inequalities presented in Equation (20) and Equation (21) delineate the capacity limitations of the ice storage air conditioner and the electrical chiller, respectively.

$$P_{ice}^{t}COP_{ice}=P_{cs,c}^{t} \tag{19}$$

$$0\le P_{ice}^{t}\le P_{ice}^{\max} \tag{20}$$

$$0\le P_{ac}^{t}\le P_{ec}^{\max} \tag{21}$$

2.2. The thermal section energy conversion model

The Equation (22) illustrates the equilibrium of gas input within the EH system.

$$P_{gas}^{t}=P_{ge}^{t}+P_{chp}^{t}+P_{gh}^{t}+P_{caes}^{t} \tag{22}$$

The energy conversion process of the GB is delineated in Equation (23), where the output heat is transferred to the heating hub.

$$\eta_{gh,gb}P_{gh}^{t}=H_{gb}^{t} \tag{23}$$

The energy conversion of the GT is detailed in Equation (24), with the resultant heat being directed to the heat exchanger.

$$\eta_{gh,gt} P_{ge}^{t} = H_{gt}^{t} \tag{24}$$

The heat exchanger's output is then utilized by the heating hub. Equation (25) outlines the operational constraints of the GB, ensuring it operates at no less than 25% of its maximum capacity throughout all time horizon periods. Additionally, Equation (26) describes the limitations of the air conditioner (AC), where a deliberately reduced AC capacity results in a correspondingly lower cooling output.

$$0.25 \times H_{gb}^{\max} \le H_{gb}^{t} \le H_{gb}^{\max} \tag{25}$$

$$0 \le H_{ac}^{t} \le H_{ac}^{\max} \tag{26}$$

Equation (27) establishes the principle of energy parity within the power hub, stipulating that the sum of energy inputs must equate to the sum of energy outputs, with the left side of the equation representing the input power and the right side detailing the output power.

$$P_{buy}^{t} + P_{pv}^{t} + P_{wt}^{t} + P_{gt}^{t} + P_{es,d}^{t} + P_{chp}^{t} + P_{gen.}^{t} = P_{ec}^{t} + P_{es,c}^{t} + P_{ice}^{t} + P_{echp}^{t} + P_{con.}^{t} + PL^{t} \tag{27}$$

For the cooling hub, Equation (28) articulates the interplay between the absorption chiller, electric chiller, and the cold energy discharge from the intelligent storage control, which collectively meets the cooling demand detailed on the right side of the equation.

$$C_{ac}^{t} + C_{ec}^{t} + P_{cs,d}^{t} = CL^{t} \tag{28}$$

Additionally, Equation (29) defines the balance of heat exchange within the heating hub.

$$\eta_{he} H_{gt}^{t} + H_{gb}^{t} + P_{hs,d}^{t} + T_{chp}^{t} + T_{ehp}^{t} + T_{tr}^{t} = H_{ac}^{t} + P_{hs,c}^{t} + HL^{t} \tag{29}$$

2.3. Energy storage model

System inefficiencies often stem from elevated energy prices during peak load times. Integrating storage devices into the EH system can mitigate this issue by leveraging off-peak charging and peak-hour discharging to lower operational costs and CO_2 emissions. The utility of electric vehicles as energy storage solutions is examined in [30]. Reference [31] proposes a comprehensive model encompassing electricity, heating, and cooling energy storage systems. The operational parameters for electrical storage devices are formulated in Equation (30)-(34) [27].

$$E_{es}^{t+1} = E_{es}^{t}(1-\delta_{es}) + \left(P_{es,c}^{t}\eta_{es,c} - \frac{P_{es,d}^{t}}{\eta_{es,d}} \right) \tag{30}$$

$$0 \le P_{es,c}^{t} \le u_{es}.P_{es,c}^{\max} \tag{31}$$

$$0 \le P_{es,d}^{t} \le (1-u_{es}).P_{es,d}^{\max} \tag{32}$$

$$E_{es}^{\min} \le E_{es}^{t} \le E_{es}^{\max} \tag{33}$$

$$E_{es}^{24} = E_{es}^{0} \tag{34}$$

Equation (30) represents the stored energy in the electrical storage (ES) system based on its charging and discharging modes. The charging and discharging modes of electrical storage, along with their limitations, are expressed in Equation (31) and (32), respectively. A binary variable is introduced to prevent simultaneous charging and discharging. Equation (33) defines the limitation of stored energy. Additionally, Equation (34) ensures that the energy amounts in the first and last hours of the time horizon are equal [27]. For cooling storage devices, the equations are expressed in Equation (35)-(39).

$$E_{cs}^{t+1} = E_{cs}^{t}(1-\delta_{cs}) + \left(P_{cs,c}^{t}\eta_{cs,c} - \frac{P_{cs,d}^{t}}{\eta_{cs,d}} \right) \tag{35}$$

$$0 \le P_{cs,c}^{t} \le u_{cs}.P_{cs,c}^{\max} \tag{36}$$

$$0 \le P_{cs,d}^{t} \le (1-u_{cs}).P_{cs,d}^{\max} \tag{37}$$

$$E_{cs}^{\min} \le E_{cs}^{t} \le E_{cs}^{\max} \tag{38}$$

$$E_{cs}^{24} = E_{cs}^{0} \tag{39}$$

Equation (35) represents the stored energy in CS based on its charging and discharging mode. Charging and discharging modes of electrical storage and their limitations are expressed in Equation (36) and (37) respectively. Incorporating the binary variable can ensure that the processes of charging and discharging are mutually exclusive. Equation (38) defines the constraints on the amount of energy that can be stored. To balance the energy levels at the beginning and end of the planning horizon, Equation (39) is introduced. For electrical storage devices, the equations are expressed in Equation (40)-(44).

$$E_{hs}^{t+1} = E_{hs}^{t}(1-\delta_{hs}) + \left(P_{hs,c}^{t}\eta_{hs,c} - \frac{P_{hs,d}^{t}}{\eta_{hs,d}} \right) \tag{40}$$

$$0 \le P_{hs,c}^{t} \le u_{hs}.P_{hs,c}^{\max} \tag{41}$$

$$0 \le P_{hs,d}^{t} \le (1-u_{hs}).P_{hs,d}^{\max} \tag{42}$$

$$E_{hs}^{\min} \le E_{hs}^{t} \le E_{hs}^{\max} \tag{43}$$

$$E_{hs}^{24} = E_{hs}^{0} \tag{44}$$

Equation (40) represents the stored energy in the heat storage (HS) system based on its charging and discharging modes. The charging and discharging modes of electrical storage, along with their limitations, are expressed in Equation (41) and (42), respectively. A binary variable is introduced to prevent simultaneous charging and discharging. Equation (43) defines the limitation of stored energy. Additionally, Equation (44) ensures that the energy amounts in the first and last hours of the time horizon are equal.

2.4. Operation cost and constraints for CHP unit

CHP technologies are one of the most used units in smart and multi-carrier systems [9]. CHP units are recovering thermal to gain more performance and use wasted thermal energy for local heating. Power and thermal outputs in CHPs depend on each other and cannot change separately. CHP energy conversion is shown in Equation (45) and Equation (46).

$$\eta_{chp} \times P_{gchp}^{t}(t) = P_{chp}(t) \tag{45}$$

$$T_{chp}(t) = P_{chp}(t) \times HPR \times \eta_{He} \tag{46}$$

Equation (47) and (48) represent CHP power and thermal ramp-up and ramp-down constraints, respectively.

$$P_{chp}(t) - P_{chp}(t-1) \le P^{Ramp-up} \times \gamma_{t-1} \times i_t \times P_{chp}^{\min} \tag{47}$$

$$P_{chp}(t) - P_{chp}(t-1) \le P^{Ramp-up} \times \gamma_{t-1} \times i_t \times P_{chp}^{\min} \tag{48}$$

The CHP start-up and shut-down costs are shown in Equations (49) and (50), respectively. Equation (51)-(55) are employed to model CHP on and off mode [9].

$$SUC(t) = SU \times i(t) \tag{49}$$

$$SDC(t) = SD \times j(t) \tag{50}$$

$$0 \le i(t) \le \gamma(t) \tag{51}$$

$$\gamma(t) - \gamma(t-1) \le i(t) \le 1 - \gamma(t-1) \tag{52}$$

$$0 \le j(t) \le \gamma(t-1) \tag{53}$$

$$\gamma(t-1) - \gamma(t) \le j(t) \le 1 - \gamma(t) \tag{54}$$

$$\gamma(t-1) - \gamma(t) + i(t) - j(t) = 0 \tag{55}$$

2.5. Electrical heat pump constraints

Equation (56) represents the EHP system constrains.

$$T_{EHP}^{t} = P_{EHP}^{t} \times COP_{EHP} \tag{56}$$

2.6. CAES system constraints

Conventional natural GT generators serve as the foundation of the CAES technology. Within the CAES system, high-pressure compressed air is utilized as a form of stored energy, which can be converted into various types of energy. During off-peak periods, compressors in the CAES system compress air to high-pressure levels, which is then used during peak periods to drive an expander for electricity generation to meet high electrical demands. The injection of air into the CAES system is proposed in Equation (57) in [27]. Equation (57) and Equation (59) demonstrate the power produced by the CAES system based on the pumping of air and gas consumption, respectively. The constraints on pumping air into a chamber and injecting air into storage are formulated in Equation (60) and Equation (61), respectively. To prevent simultaneous injection and pumping in the CAES system, binary variables are introduced in Equation (62). It represents the thermal recovery of the CAES unit.

$$V_{injected}^{t} = e^{i} \times P_{cons.}^{t} \tag{57}$$

$$P_{gen.}^{t} = e^{p} \times V_{pumped}^{t} \tag{58}$$

$$P_{gen}^{t} = P_{caes}^{t} / \eta_{pcaes} \tag{59}$$

$$V_{pumped}^{\min} \times h^{t} \le V_{pumped}^{t} \le V_{pumped}^{\max} \times h^{t} \tag{60}$$

$$V_{ingected}^{\min} \times f^t \le V_{ingected}^t \le V_{ingected}^{\max} \times f^t \quad (61)$$

$$f^t + h^t \le 1 \quad (62)$$

$$P_{gen.}^t \times \eta_{tr} = T_{tr}^t \quad (63)$$

The distribution of air stored within specific time intervals is influenced by the inflow and outflow of air, a relationship which can be mathematically represented as Equation (64).

$$PS^{t+1} = PS^t + V_{injected}^t - V_{pumped}^t \quad (64)$$

The heat rate is a measure of the quantity of natural gas utilized for each unit of peak electrical energy produced by the expander [32].

2.7. Electric load with demand response

DR methods are used to prevent unnecessary capacity investment by shifting loads from peak and expensive periods to off-peak and inexpensive periods [30]. In this article, TOU and RTP methods are used to implement DR programs as follows:

2.8. TOU-DR formulation

The TOU demand response (TOU-DR) and the respective models are expressed by Equation (65) and Equation (66).

$$Pl_{DR}^t = Pl_D^t + ldr^t \quad (65)$$

$$ldr_t = DR_t \times Pl_t^d \quad (66)$$

Where Pl_t^{DR} is representing new power demand of hour t by applying TOU-DR and ldr_t is the amount of shifted load in hour t and the total amount of shifted load over a daily period should be equal to zero. This is expressed in Equation (67) and at each time period shifted load is limited by Equation (68).

$$\sum_{t=1}^{24} ldr_t = 0 \quad (67)$$

$$DR_t^{\min} \le DR_t \le DR_t^{\max} \quad (68)$$

2.9. RTP-DR programming

An RTP model, constructed from electricity load demand data, facilitates the implementation of the DR program in this sector. The application of RTP-based DR encourages the shifting of loads from peak to off-peak periods, resulting in a more uniform load demand curve.

Equation (69) represents the total electrical load demand of the EH and in Equation (70), P_{av}, is the average electricity demand.

$$W_d = \sum_{t=1}^{24} PL_t \quad (69)$$

$$P_{av} = \frac{W_d}{24} \quad (70)$$

The RTP float factor is considered as Equation (71).

$$\gamma_t = \frac{Pl_t}{Pl_{av}} \quad (71)$$

The RTP model is expressed in Equation (72) and Equation (73) as follows:

$$\lambda_{RTP}^t = \gamma_t \times \lambda_{TOU}^t \quad (72)$$

$$\lambda_{RTP}^{\min} \le \lambda_{RTP}^t \le \lambda_{RTP}^{\max} \quad (73)$$

In Reference [33], the effects of employing various DR methods based on price and incentive are investigated within the EH system. References [34,35] propose a mathematical formulation for demand response, which is encapsulated in Equation (74).

$$Pl_{RTP}^t = Pl^t + E \times Pl^t \left(\frac{\lambda_{RTP}^t - \lambda_{TOU}^t}{\lambda_{TOU}^t} \right) \quad (74)$$

3. Methodology

3.1. Augmented Epsilon-constraint method

The Augmented Epsilon-constraint method has been employed to achieve more precise results in the energy management problem. The advantages of this method can be summarized as follows:

1. The original feasible region will not be altering
2. non-inferior solutions are produced, and solutions will be independent of the scaling of the objective functions.

To implement the Epsilon method, the objective function is defined as Equation (75):

$$\begin{aligned} &\max\left(f_1(x)+\delta\left(s_1+\ldots+s_p\right)\right)\\ &subject\ to\\ &f_2(x)-s_2=e_2\\ &f_3(x)-s_3=e_3\\ &\ldots\\ &f_p(x)-s_p=e_p\\ &x\in s\ \ and\ \ s_i\in R^+ \end{aligned} \tag{75}$$

Equation (75) provides efficient solutions, while the proposed method has other alternative solutions. On the other hand, there is an answer like x, that dominates other answers. As a result, this issue is defined as Equation (76):

$$\begin{cases} e_2+s_2\le e_2+s_2'\\ e_3+s_3\le e_3+s_3'\\ \ldots\\ e_p+s_p\le e_p+s_p' \end{cases} \tag{76}$$

Equation (76) can be achieved considering at least one strict inequality regarding Equation (77).

$$\sum_{i=2}^{p} S_i \le \sum_{i=2}^{p} S_i' \tag{77}$$

In order to circumvent potential scaling complications, it is better to replace s_i with s_i/r_i. As a result, the objective function converts to Equation (78).

$$\max\left(f_1(x)+eps\times(s_2/r_2+\ldots+s_p/r_p)\right) \tag{78}$$

Equation (78) is the final equation used to solve a multi-objective problem. X, $f_p(x)$, s, r_i, and are a vector of decision variables, p objective functions, feasible region, and range of its objective function, respectively.

3.2. Decision-making

Reference [27], examines various methodologies for resolving multi-objective models, including the epsilon constraint method, the weighted sum approach, and evolutionary algorithms. This paper employs the epsilon constraint argument to address the multi-objective model. Additionally, the max-min fuzzy satisfying technique is utilized (Equation (79)) to standardize the dimensions across all objective function values, as detailed subsequently.

$$\mu_k^n=\begin{cases} 1 & f_k^n\le f_k^{\min}\\ \dfrac{f_k^{\max}-f_k^n}{f_k^{\max}-f_k^{\min}} & f_k^{\min}\le f_k^n\le f_k^{\max}\\ 0 & f_k^n\ge f_k^{\max} \end{cases} \tag{79}$$

$$\mu^n=\min(\mu_1^n,\ldots,\mu_n^n) \tag{80}$$

$$\mu^{\max}=\max(\mu^1,\ldots,\mu^{np}) \tag{81}$$

The selection of the minimum quantities of the Pareto solution is described by Equation (80), whereas Equation (81) expresses the attainment of the maximum value among the minimum solutions, signifying the compromise solution.

4. Numerical results

In this section, the initial part presents the input data and parameters for the EH. Then, the min-max fuzzy method is employed to identify the optimal solution for each case study. This method is applied after utilizing the argument epsilon constraint method to obtain a set of potential solutions. By comparing these solutions, the most suitable one is selected as the optimal solution for each of the three case studies. The first case study does not incorporate any DR program. However, the second case study examines the impact of TOU programs. Similarly, the third case study focuses on the effects of RTP DR programs. Within this section, the input parameters for the model components and energy carriers are presented. The output power generated by the PV and WT systems over 24 hours is depicted in Figure 1. Figure 2 illustrates the power, cooling, and heating energy demand during the optimization time horizon on a typical hot day. Figure 3 represents the Power load with and without DRPs. Figure 4 represents the electricity

tariff of TOU, RTP use, and gas prices. Tables 1-3 provide an overview of the parameters of coefficients, including those for CCHP, EHP, CAES, WT, PV, and carbon emissions. Additionally, Table 4 presents parameters for cooling, heating, and power storage devices. Lastly, Table 5 outlines the DR parameters. It is worth noting that the CHP unit is initially considered off.

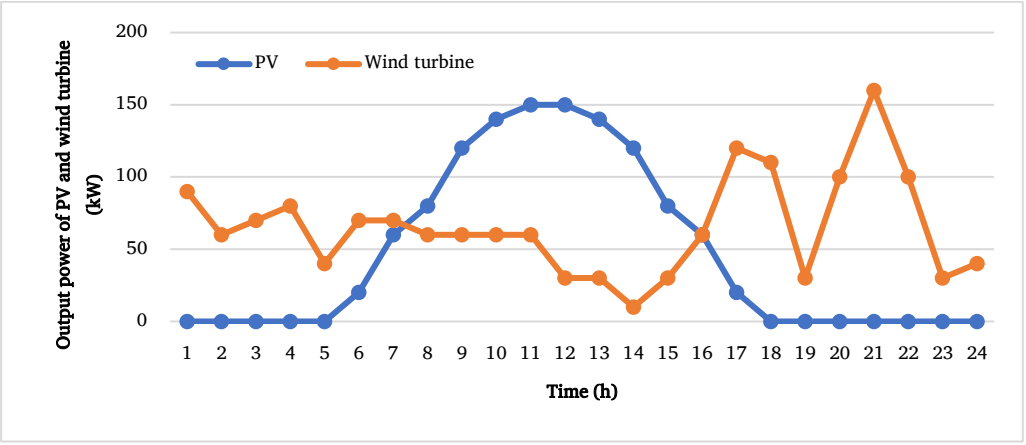

Figure 1. The output powers of WT and PV.

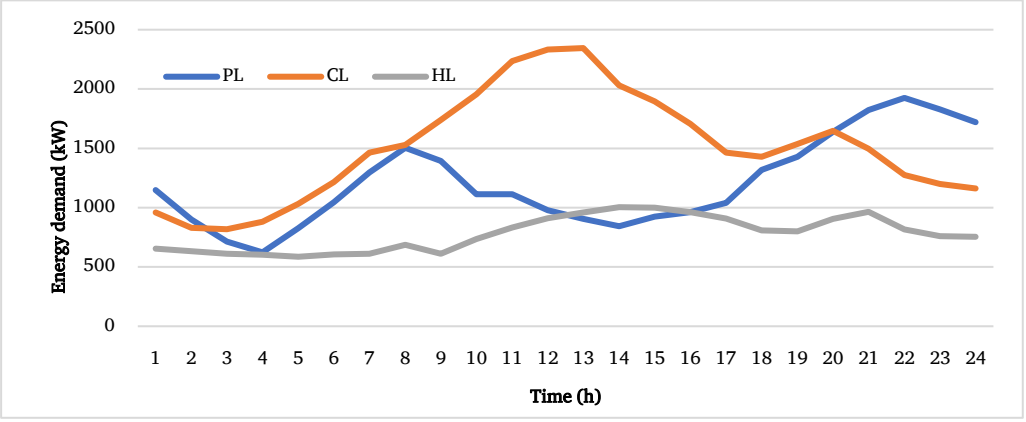

Figure 2. The power, cooling, and heating demands of the microgrid on a typical summer day.

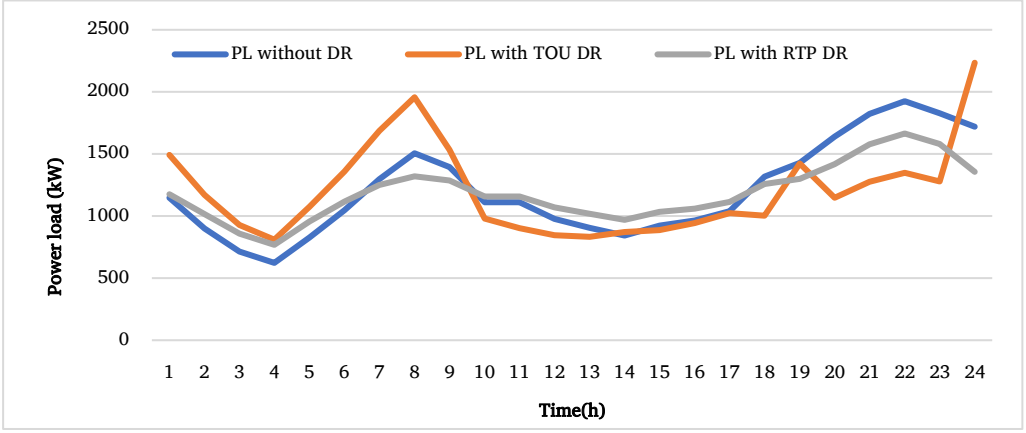

Figure 3. Power load with and without DRP.

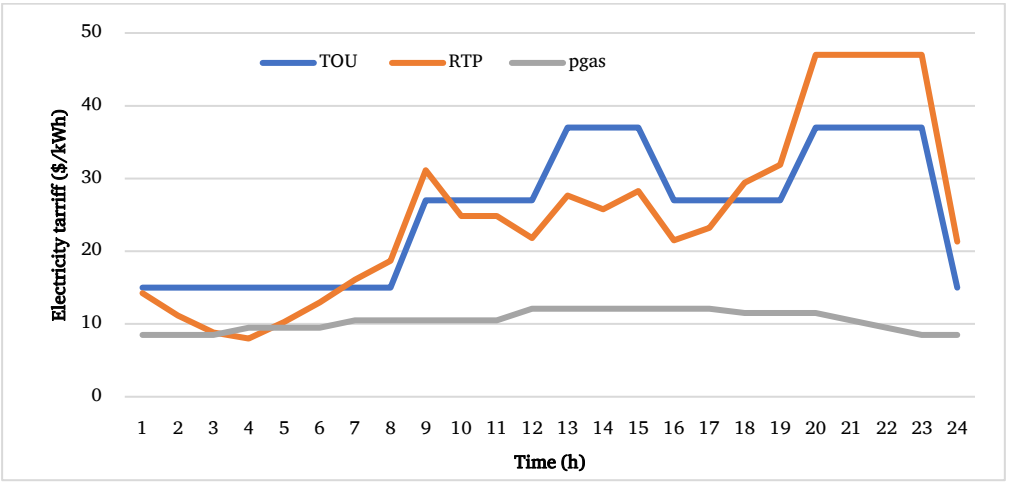

Figure 4. Electricity tariff of TOU, RTP, and gas price.

Table 1. Parameters of coefficients of CCHP, WT, PV, and Carbon emission

Parameter	Unit	Value	parameter	Unit	Value	parameter	Unit	Value
$P_{gt}^{\max}$	kW	1000	$P_{grid}^{\max}$	kW	1500	COP_{ec}	-	4
$H_{gb}^{\max}$	kW	800	$P_{gas}^{\max}$	kW	3400	COP_{ice}	-	3.5
$H_{ac}^{\max}$	kW	500	η_{ge}	-	0.3	COP_{ac}	-	1.2
$P_{ec}^{\max}$	kW	500	$\eta_{gh,gb}$	-	0.9	β_e	Kg/kWh	0.972
$P_{ice}^{\max}$	kW	100	$\eta_{gh,gt}$	-	0.4	β_g	Kg/kWh	0.23
$P_{pv}^{\max}$	kW	180	η_t	-	0.98	E	-	-0.5
$P_{wt}^{\max}$	kW	200	η_{he}	-	0.7		-	

Table 2. Parameters of CHP unit and CAES system.

CHP UNIT		CAES SYSTEM	
Capacity (kW)	1000	Maximum/ minimum level (kWh)	500/50
Electrical ramp-up/ramp-down (kW/h)	150	Maximum level of injected air (kW/h)	150
Startup/ shutdown cost ($)	65	Minimum level of injected air (kW/h)	5
Electrical/thermal conversion efficiency (%)	45/48	Maximum level of pumped air (kW/h)	150
		Minimum level of pumped air (kW/h)	5
		Efficiency of injected/produced power (%)	90/90

Table 3. Parameters of the EHP system.

Coefficient of performance	2.5
Maximum capacity (kW)	250
Minimum capacity (kW	0

Table 4. Parameters of storage devices.

Electrical storage parameters			Heat storage parameters			Cool storage parameter		
Parameter	Unit	Value	Parameter	Unit	Value	Parameter	Unit	Value
$P_{es,c}^{\max}$	kW	500	$P_{hs,c}^{\max}$	kW	800	$P_{cs,c}^{\max}$	kW	700
$P_{es,d}^{\max}$	kW	700	$P_{hs,d}^{\max}$	kW	800	$P_{cs,d}^{\max}$	kW	800
$E_{es}^{\min}$	kW	400	$E_{hs}^{\min}$	kW	400	$E_{cs}^{\min}$	kW	400
$E_{es}^{\max}$	kW	1800	$E_{hs}^{\max}$	kW	1800	$E_{cs}^{\max}$	kW	1800
$\eta_{es,c}$	-	0.96	$\eta_{hs,c}$	-	0.98	$\eta_{cs,c}$	-	0.97
$\eta_{es,d}$	-	0.96	$\eta_{hs,d}$	-	0.98	$\eta_{cs,d}$	-	0.95
δ_{es}	-	0.01	δ_{hs}	-	0.02	δ_{cs}	-	0.02

Table 5. TOU and RTP DR parameters.

$\lambda_{RTP}^{\min}$	8
$\lambda_{RTP}^{\max}$	47
E	-0.5
$DR_t^{\min}$	-30%
$DR_t^{\max}$	30%

4.1. A comparative analysis of Pareto results and the trade-off solution across three cases

In this section, an examination is conducted of the EH system model through three distinct case studies. The objective is to address the problem using the augmented epsilon constraint method, thereby showcasing the benefits and effectiveness of the proposed model as a solving technique. Figure 5 shows the Pareto solutions for scenarios with and without DRPs.

The first case study focuses on minimizing both the total cost and emissions in the EH System without any DR programs. Analyzing the system under this scenario allows for a comprehensive understanding of the baseline performance and serves as a benchmark for comparison with the subsequent cases. Moving on to the second case study, the aim remains the same to minimize the total cost and emissions in the EH system.

However, this time, the analysis considers the presence of RTP DR programs. These programs introduce a dynamic element to the system, as the pricing varies based on real-time demand. By considering this factor, the model can optimize the system's performance under these conditions. Lastly, the third case study delves into the optimization of the EH System by considering the time of use pricing DR programs. This means that the model considers the specific time periods during which the DR programs are active. By incorporating this temporal aspect, the model can further refine its optimization strategy and achieve even greater efficiency in minimizing both the total cost and emissions. Overall, these three case studies provide a comprehensive analysis of the EH system model and its solving method. Examining the system under different scenarios allows for a thorough evaluation of its advantages and efficiency in optimizing the total cost and emissions.

In case one, each component of the EH and energy carriers possesses distinct specifications in terms of cost and emissions, resulting in diverse behaviors within each Pareto front optimal solution. To derive the Pareto-optimal solutions, the epsilon constraint method is applied. Subsequently, the max-min fuzzy technique is employed to determine an optimal trade-off solution among the derived solutions. The outcomes are depicted in Figure 5. In the EH model for case study one, the operation cost is determined to be 9835.762 $, while the carbon emission amounts to 26481.681 kg. The selected solution is highlighted in red in Figure 5 and corresponds to entry number 14 in Table 6. Similar techniques are employed to obtain optimal solutions in other case studies. In case study two, the TOU-DR program is applied, resulting in an operation cost of 9297.363 $ and an emission of 26339.917 kg. On the other hand, case study three involves the implementation of the RTP DR program, which leads to an operation cost of 9610.959 $ and an emission of 25919.747 kg.

The comparative analysis between Case 1 and Case 2 underscores the benefits of the TOU-DR program. In Case 2, the operational costs are curtailed by 5.47%, marking a notable enhancement in the EH system's economic efficiency. Moreover, the model advocates environmental sustainability by registering a 0.53% reduction in emissions, equivalent to 141.764 kg. The outcomes of this case are represented in Table 7. Similarly, a comparison between the results of the first case and the third case demonstrates the benefits of implementing the RTP DR program. In case three, the operation cost experiences a reduction of 2.285%, signifying a noteworthy advancement in the economic aspect of the EH system. Moreover, the proposed model achieves a 2.12% (561.934 kg) decrease in carbon emission, further supporting environmental objectives. The outcomes of this case are represented in Table 8.

4.2. The comparison of the energy flow of the hub in three cases

This section presents a detailed discussion of the optimized EH's outcomes across different scenarios, focusing on power flow, cooling, and heating efficiencies. Case 2 demonstrates the efficacy of the TOU-DRP. The strategic implementation of TOU-DRP not only leads to a decrease in operational costs but also contributes to a reduction in carbon emissions. Figure 6-8 illustrate the energy balance of the power hub in each case, as well as the energy production of each device. The negative values in the diagram are input energy and positive values show output energy for each time period. Figure 6 shows the energy flow in the power hub without DR programs, while Figure 7 shows the energy flow with TOU. By implementing TOU, the gas purchased costs increased from $7382.294 to $7456.332, while the electricity purchased costs decreased from $2388.467 to $1776.031. The GT, when TOU is applied, operates in hour 1 and produces more power in hours 2 and 24 compared to the base case. The DR program and load shifting to off-peak and cheaper hours reduce the number of hours energy needs to be purchased from the main grid from 20 to 10 in case two.

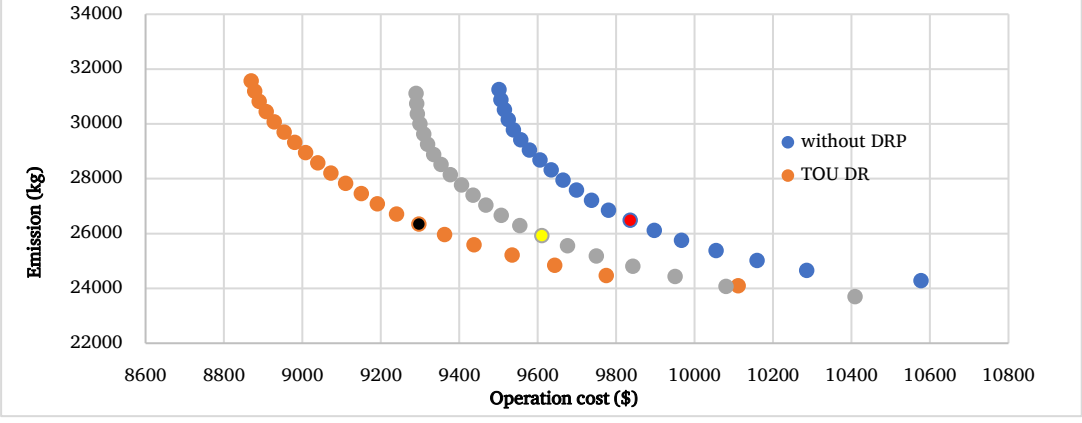

Figure 5. Pareto solutions for scenarios with and without DRP.

Table 6. Pareto results of scenario one (without DRP).

#	Operation cost ($)	Carbon emission (kg	$\psi_1(pu)$	$\psi_2(pu)$	$Min(\psi_1(pu),\psi_2(pu))$
1	9500.732	31247.116	1.00000000	0	0
2	9505.730	30880.544	0.99535629	0.05263159	0.053
3	9514.838	30513.972	0.98689392	0.10526319	0.105
4	9524.622	30147.400	0.97780346	0.15789478	0.158
5	9537.937	29780.828	0.96543231	0.21052638	0.211
6	9556.125	29414.256	0.94853358	0.26315797	0.263
7	9578.279	29047.685	0.92794998	0.31578942	0.316
8	9605.599	28681.113	0.90256658	0.36842101	0.368
9	9633.715	28314.541	0.87644361	0.42105261	0.421
10	9664.468	27947.969	0.84787056	0.47368420	0.474
11	9698.066	27581.397	0.81665419	0.52631580	0.526
12	9736.392	27214.825	0.78104496	0.57894739	0.579
13	9779.835	26848.253	0.74068145	0.63157899	0.632
14	**9835.762**	**26481.681**	**0.68871888**	**0.68421058**	**0.684**
15	9897.165	26115.109	0.63166848	0.73684217	0.632
16	9966.216	25748.537	0.56751222	0.78947377	0.568
17	10054.092	25381.965	0.48586539	0.84210536	0.486
18	10158.776	25015.393	0.38860200	0.89473696	0.389
19	10285.229	24648.821	0.27111273	0.94736855	0.271
20	10577.026	24282.250	0	1	0

Table 7. Pareto results of scenario two (with TOU DRP).

#	Operation cost ($)	Carbon emission (kg	$\psi_1(pu)$	$\psi_2(pu)$	$Min(\psi_1(pu),\psi_2(pu))$
1	8868.649	31569.164	1	0	0
2	8877.768	31195.647	0.99265842	0.04999991	0.050
3	8889.097	30822.129	0.98353761	0.09999996	0.100
4	8907.255	30448.611	0.96891887	0.15000001	0.150
5	8927.953	30075.094	0.95225521	0.19999992	0.200
6	8953.215	29701.576	0.93191713	0.24999997	0.250
7	8979.806	29328.058	0.91050910	0.30000001	0.300
8	9008.038	28954.541	0.88777993	0.34999993	0.350
9	9038.469	28581.023	0.86328037	0.39999997	0.400
10	9072.187	28207.505	0.83613449	0.45000002	0.450
11	9109.833	27833.987	0.80582624	0.50000007	0.500
12	9150.126	27460.470	0.77338693	0.54999998	0.550
13	9190.938	27086.952	0.74052978	0.60000003	0.600
14	9239.505	26713.434	0.70142919	0.65000007	0.650
15	**9297.363**	**26339.917**	**0.65484855**	**0.69999999**	**0.655**
16	9362.414	25966.399	0.60247693	0.75000003	0.602
17	9437.403	25592.881	0.54210436	0.80000008	0.542
18	9533.991	25219.364	0.46434276	0.84999999	0.464
19	9643.077	24845.846	0.37651920	0.90000004	0.377
20	9774.472	24472.328	0.27073498	0.95000009	0.271
21	10110.753	24098.811	0	1	0

Table 8. Pareto results of scenario three (with RTP DRP).

#	Operation cost ($)	Carbon emission (kg	$\psi_1(pu)$	$\psi_2(pu)$	$Min(\psi_1(pu),\psi_2(pu))$
1	9289.634	31107.707	1	0	0
2	9291.128	30737.139	0.99866527	0.04999993	0.050
3	9292.891	30366.570	0.99709022	0.09999999	0.100
4	9299.352	29996.002	0.99131800	0.14999991	0.150
5	9308.657	29625.433	0.98300497	0.19999997	0.200
6	9318.809	29254.864	0.97393523	0.25000003	0.250
7	9334.122	28884.296	0.96025469	0.29999996	0.300
8	9353.085	28513.727	0.94331326	0.35000002	0.350
9	9377.076	28143.159	0.92187984	0.39999995	0.400
10	9405.361	27772.590	0.89661020	0.45000001	0.450
11	9434.747	27402.021	0.87035692	0.50000007	0.500
12	9467.307	27031.453	0.84126801	0.54999999	0.550
13	9506.700	26660.884	0.80607454	0.60000005	0.600
14	9553.922	26290.316	0.76388669	0.64999998	0.650
15	**9610.959**	**25919.747**	**0.71293018**	**0.70000004**	**0.700**
16	9675.206	25549.179	0.65553230	0.74999997	0.656
17	9748.998	25178.610	0.58960697	0.80000003	0.590
18	9841.912	24808.041	0.50659816	0.85000009	0.507
19	9950.031	24437.473	0.41000530	0.90000001	0.410
20	10079.544	24066.904	0.29429916	0.95000007	0.294
21	10408.961	23696.336	0	1	0

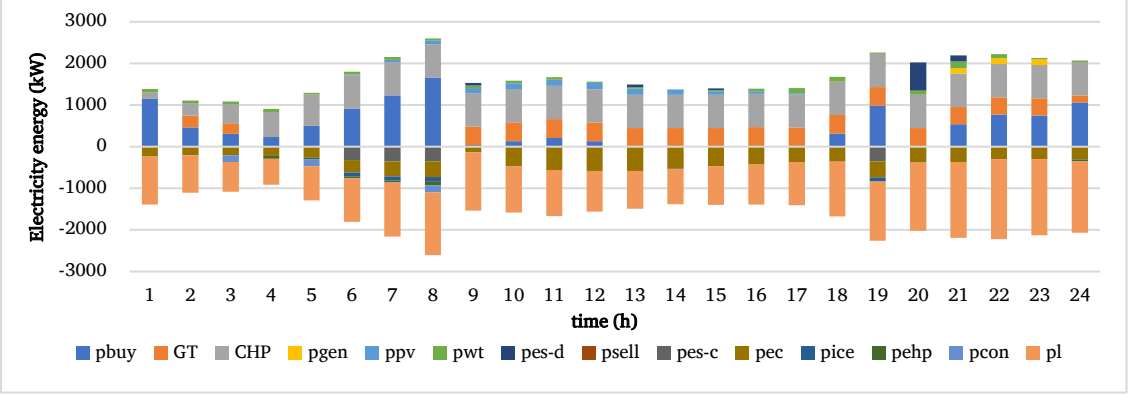

Figure 6. The energy balance of the power hub without DRP.

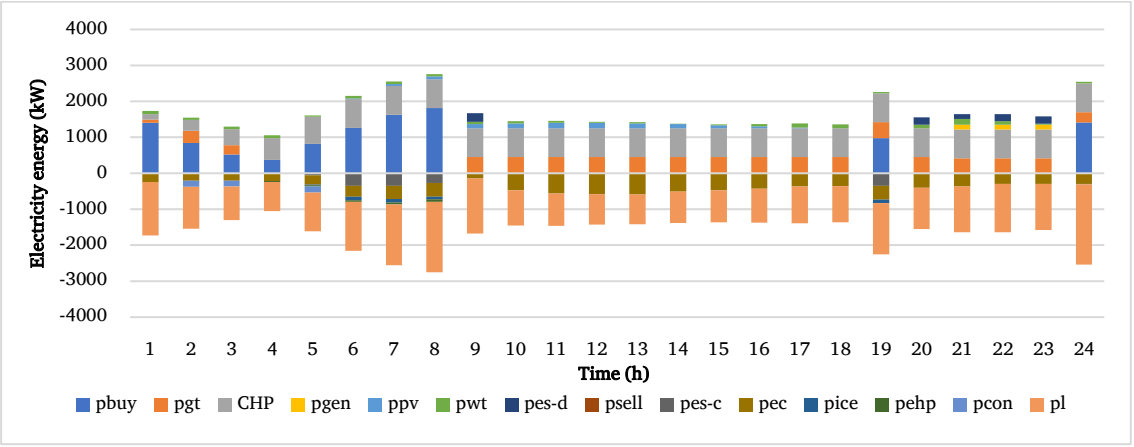

Figure 7. The energy balance of the power hub with TOU-DR.

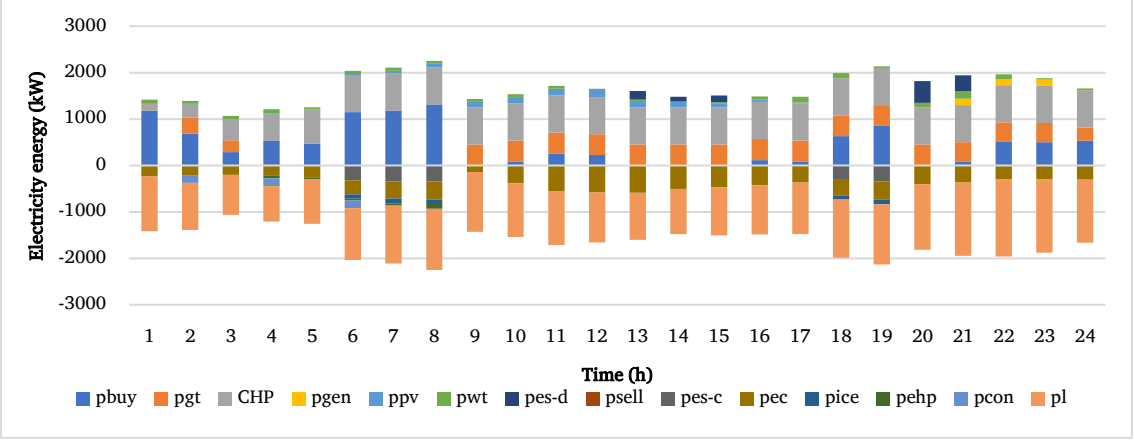

Figure 8. The energy balance of the power hub with RTP DR.

This reduction is due to the multi-objective feature of the model. The power output by the CAES unit remains similar in both cases, but the power consumed by CAES varies based on the imported energy to the EH and the shifted load in hours such as (2:00-8:00). The TOU DRP effectively shifts the load from peak to off-peak and cheaper periods, resulting in lower purchased power costs in case two and a slight decrease in emissions. Additionally, the load is distributed more efficiently. The operational modes of the energy storage (ES) system oscillate between charging and discharging, contingent upon the time of day. For instance, at 16:00, the ES engages in charging mode, whereas it switches to discharging mode during the 13:00-15:00 interval.

In scenarios devoid of a DR Program, the energy discharge rates escalate during peak hours, such as 9:00-21:00, and diminish at 20:00, in response to TOU pricing dynamics. Conversely, in Case 2, with the DRP active, the ES system experiences increased utilization. As a result, the operation time and energy consumed by the EH power are decreased in case two. Figure 8 illustrates the energy flow through the power hub, without and with the RTP DR Program. Upon implementing RTP-DR, the cost of purchased gas rose from $7,382.294 to $7,432.484, while the cost of purchased electricity decreased from $2,388.467 to $2,113.474.

Additionally, the GT generates more power during hours 2, 3, and 24 when RTP DR is applied, as opposed to the base case. In case three time periods in which energy is needed to buy from the main grid are reduced by 1 hour and less power is bought in expensive hours which is caused by the DR program and load shifting to off-peak and cheaper hours. The power output by the CAES unit is similar in both cases which are related to lower gas prices in this time period, but power consumed by CAES is changed based on import energy to the EH and shifted load in hours such as (2:00-4:00-6:00) in RTP DR case. RTP and DRP facilitate the redistribution of loads from peak to more economical off-peak periods. Consequently, in Case 3, the cost of purchased power is marginally reduced, and carbon emissions are decreased by the energy storage system (ES) operating in a charging mode during specific hours, such as 14:00, and switches to a discharging mode during other hours, such as 9:00, in cases where there is no DR program in effect. Additionally, the amount of energy discharged during hours like 13:00, 15:00, 21:00, and 20:00 is increased and decreased, respectively, by RTP-DRP.

The energy flow of the cooling hub is illustrated in Figure 9-11, without and with DRPs, respectively. The primary supplier in the cooling hub is the electric chiller (EC), while the air conditioner (AC) and ice storage chiller (ISC) serve as secondary options during critical hours such as 9:00-20:00 when electricity prices are high. The operation pattern of the absorption chiller remains mostly the same in both case one and case two, except for hour 10, where the cooling output is significantly reduced due to the

implementation of DR. The ISC behaves similarly in both cases, indicating that DRPs have a minimal effect on cooling energy suppliers.

The energy flow of the heating hub is depicted in Figures 12 and 13, without and with TOU DRP, respectively. The main heat suppliers in both cases are the GT, CHP, and EHP. The utilization of heat storage, GT, and CHP remains almost the same in both cases, with only the behavior of EHP differing in each operation hour, particularly at 24:00. The GB produces a minimal amount of adjustment heat, which is similar in both cases one and two.

In the third scenario, the implementation of the RTP DR program yields a reduction in operational costs and a marginal increase in carbon emissions. Figure 8, 11, and 14 depict the power, cooling, and heating energy flows within the EHs, as well as the energy production from each device for Case 3, respectively.

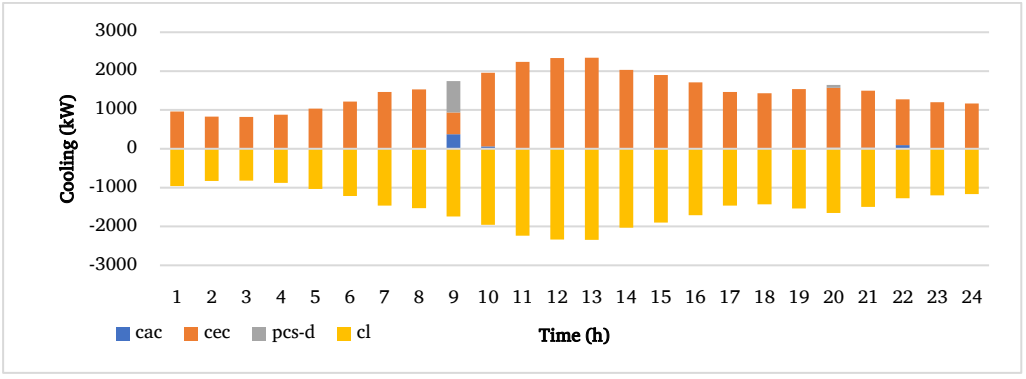

Figure 9. The energy balance of the cooling hub without DRP.

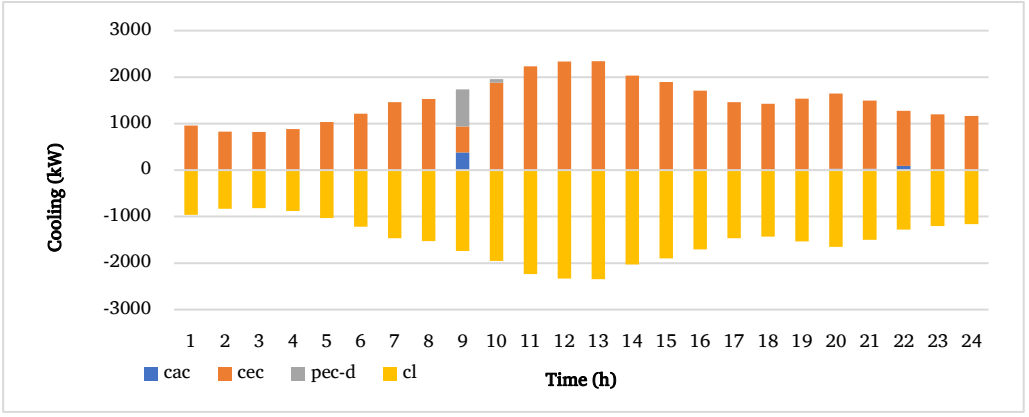

Figure 10. The energy balance of the cooling hub with TOU DR.

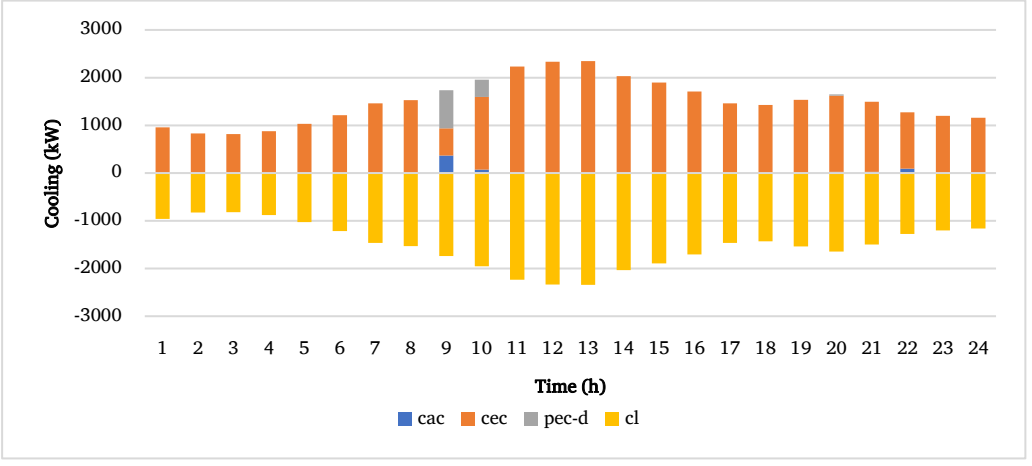

Figure 11. The energy balance of the cooling hub with RTP DR.

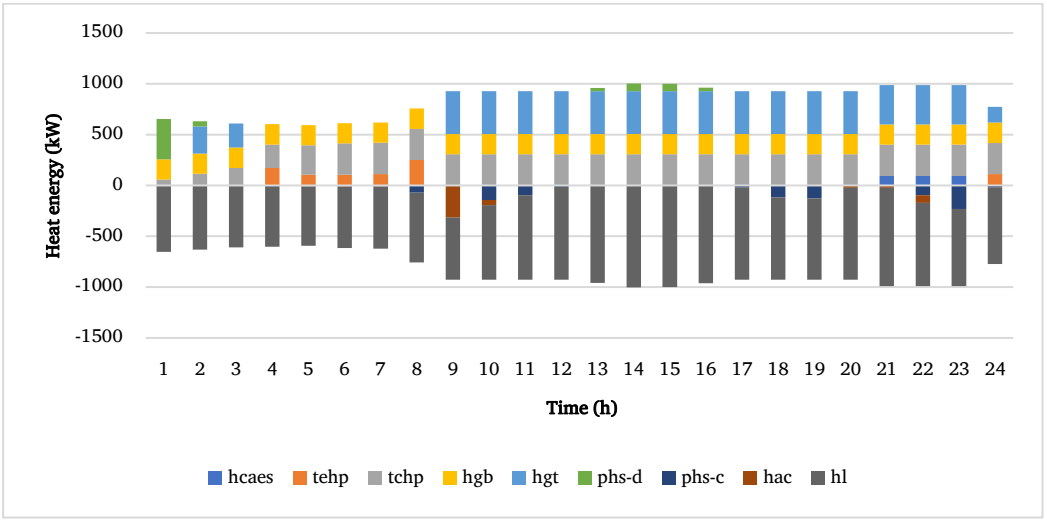

Figure 12. The energy balance of the heat hub without DRP.

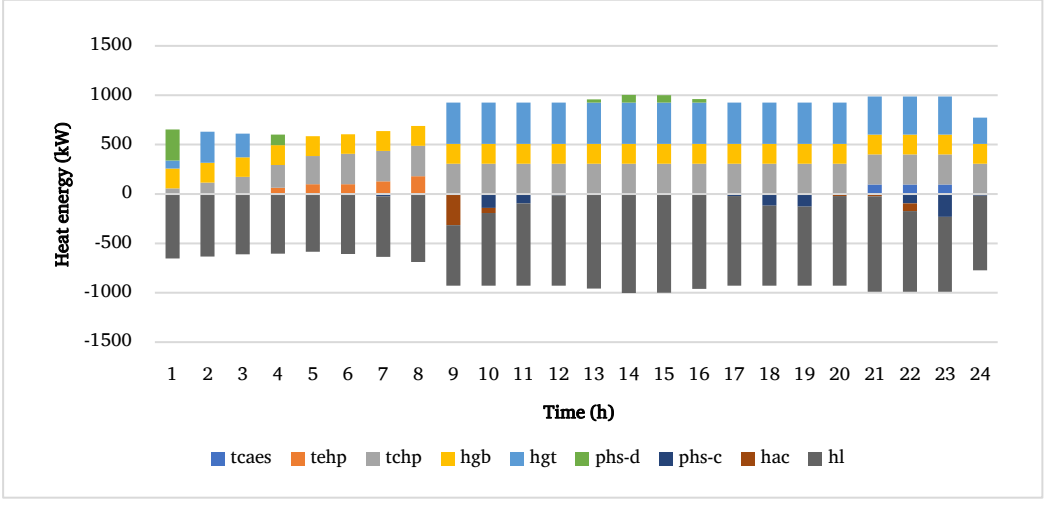

Figure 13. The energy balance of the heat hub with TOU-DR.

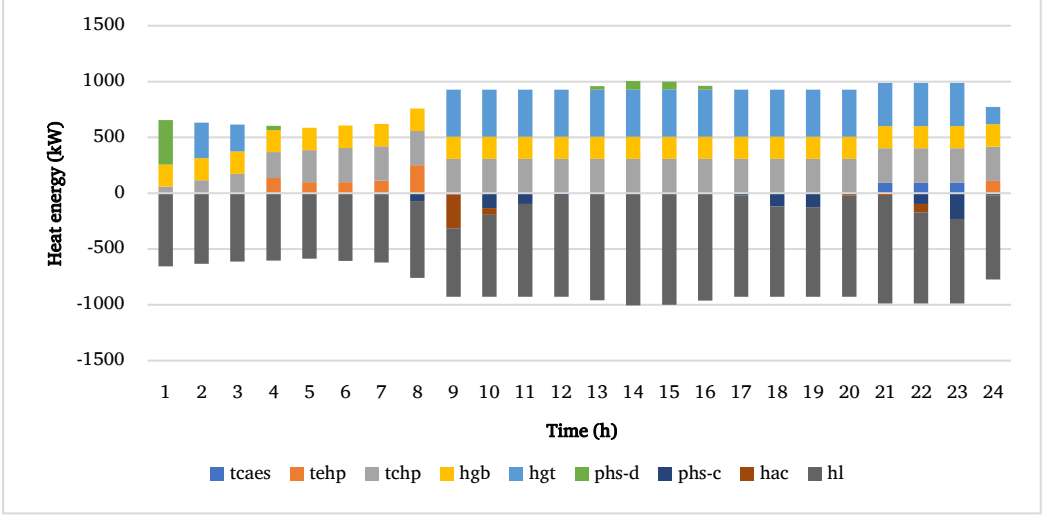

Figure 14. The energy balance of the heat hub with RTP-DR.

Figure 14 represents the energy balance of the cooling hub in the third case. The primary source of cooling is provided by the EC, while AC and ISC serve as alternative options during peak hours, specifically from 9:00 to 10:00, when electricity costs are elevated. The absorption chiller operation pattern is mainly the same in case 1 and case 3 except in hour 10 when the cooling output is increased to 71.290 with applying DR. The ISC works in more hours and produces more cooling in case 3, which proves RTP DR has more effects on cooling energy suppliants compared with RTP DR.

The energy balance of the heating hub for the third case is demonstrated in Figure 14. The use of CHP is almost the same in both cases. The CHP unit's behavior is the same in all three cases, but it is acting very differently in Pareto front solutions with higher priority for operation costs. EHP behavior is different in each of its operation hours especially in (24:00) in DRP. GB produced a minimum amount of its adjustment heat which is similar in all cases. The ES charging and discharge are the same in both cases. The reduction in operation cost and carbon emissions in an EH system can be attributed to two main factors: the decrease in electricity consumption and the increased utilization of storage devices in conjunction with DR programs. Additionally, Figure 15-20 illustrate the charging and discharging of storage devices and the state of ES, CS, and HS in three EHs. It is worth noting that the utilization of storage devices is more prominent in DRP.

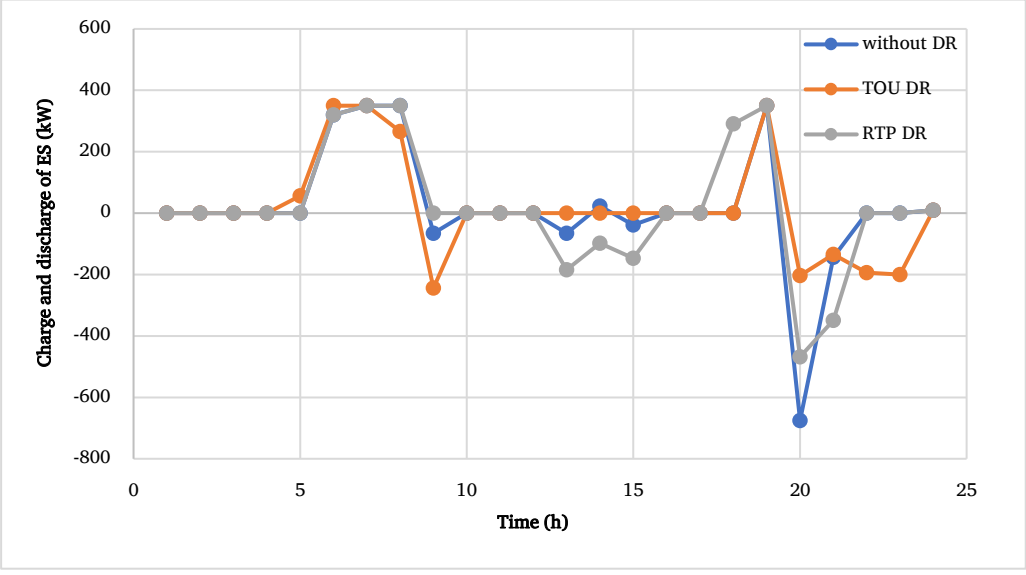

Figure 15. The charging and discharging of electrical storage.

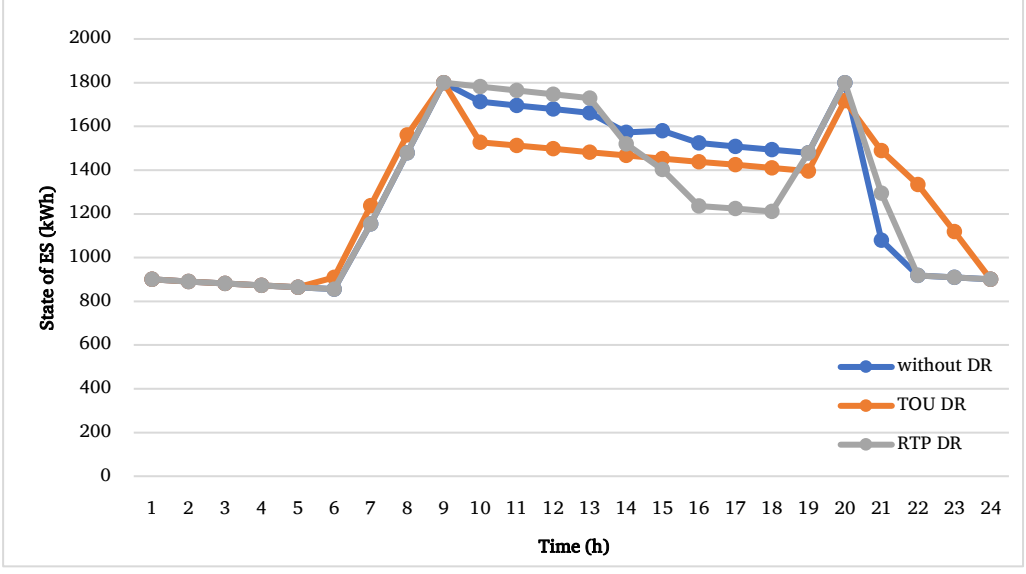

Figure 16. The state of ES.

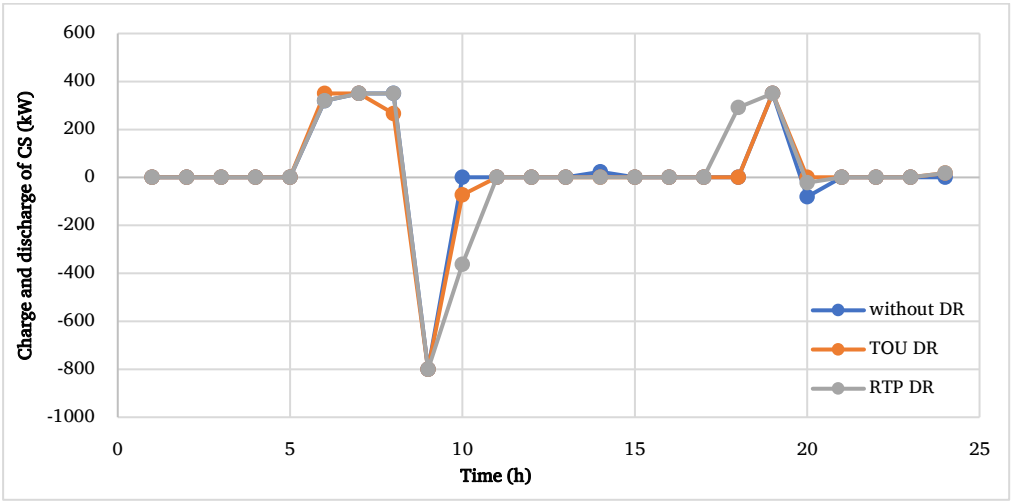

Figure 17. The charging and discharging of cooling storage.

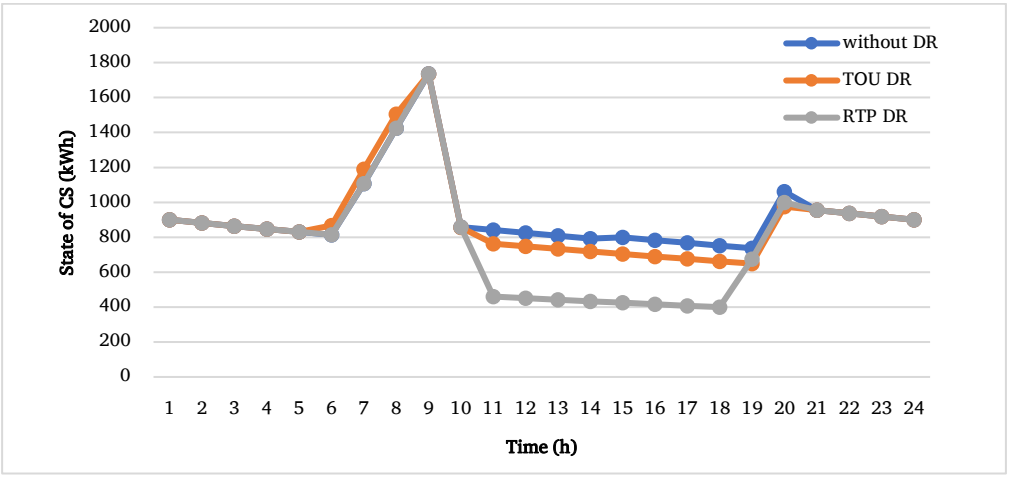

Figure 18. The state of CS.

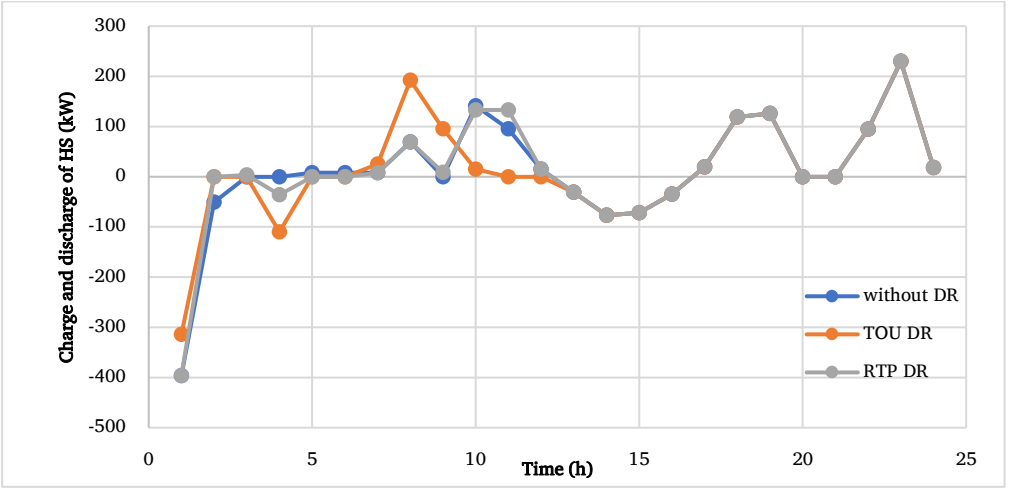

Figure 19. The charging and discharging of heating storage.

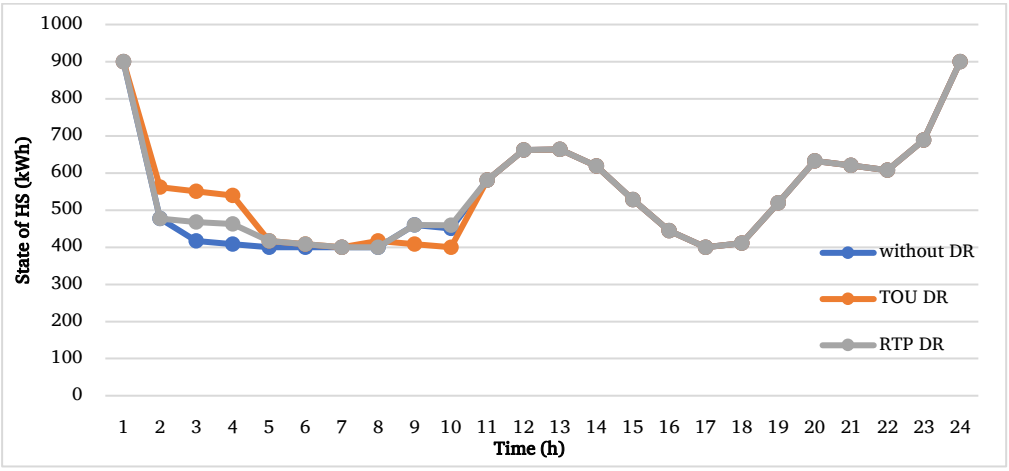

Figure 20. The state of HS.

4.3. The comparison of different CAES storage capacities on objective functions

This section aims to investigate the CAES storage capacity effect on objective functions. For this manner, 6 different levels of capacity are considered for the CAES unit in the model. As shown in Table 9, without considering the CAES unit in the model, operation cost and CO_2 emission are 9879.419 $ and 26407.91 kg, respectively.

Considering the CAES unit in the model with a capacity of 500 kW, operation costs and CO_2 emission are reduced to 9835.76 $ and increased to 26481.7 kg, respectively. As shown in Table 9 and Figure 21 and 22, by increasing CAES unit capacity, operation cost is reduced, and CO_2 emission is increased. For 800 kW and 900kW capacity, operation cost and CO_2 emissions are almost the same, which shows that increasing the capacity of the CAES unit has no benefit for the system. As shown in Figure 21 optimal solution for a minimum amount of emission (number 20 or 21 solution in the Pareto chart) for different CAES capacities are the same. This is due to the CAES unit's CO_2 emission which leads the CAES unit not to operate in these solutions. 500kW CAES capacity is the only capacity that can lead to operation cost and CO_2 emission reduction at the same time compared with 0 capacities for CAES in lower number optimal solutions (number 1 to 13 solutions in Pareto chart) . for example, in a minimum amount of operation cost and emission for 0kW capacity CAES are 9560.456$ and 31367.59kg, and for the 500kW capacity CAES are 9500.732$ and 31247.12kg.

Table 9. Sensitivity analysis of the proposed planning.

CAES capacity (kW)	Objective functions	
	Cost ($)	Pollution (kg)
0	9879.419	26407.91
500	9835.76	26481.7
600	9827.219	26494.1
700	9816.6	26536.52
800	9811.667	26564.52
900	9811.545	26564.86

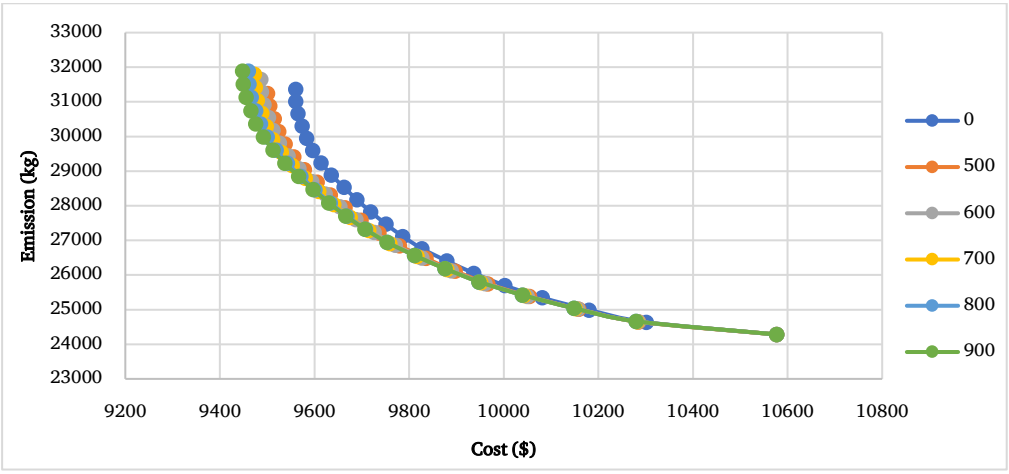

Figure 21. Pareto solutions for different CAES capacity.

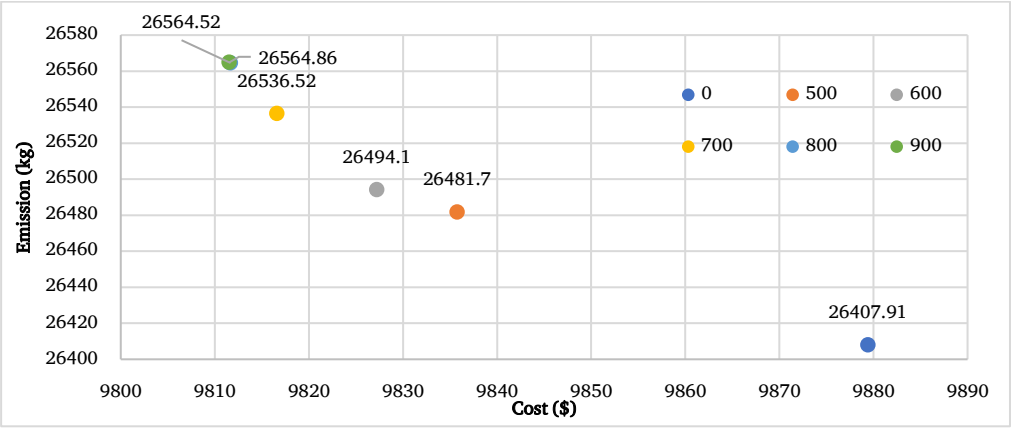

Figure 22. CAES sensitivity analyzed.

5. Conclusion

This paper proposes a comprehensive model of the microenergy grid as an EH system that can provide electricity, heating, and cooling from various sources. The system includes renewable energies, storage devices, and CAES systems. Reduction of operation costs and CO2 emission are investigated in three different cases for the proposed model. Multi-objective model is solved by the augmented epsilon constraint method to obtain Pareto solutions, and the optimal solution is chosen by the max-min fuzzy technique. A good trade-off solution is obtained by the augmented epsilon constraint method in comparison with other methods. TOU and RTP DRs are used to improve the economic and environmental aspects of the proposed EH. Optimal objective functions for the proposed EH are investigated in three cases which are the first case without DRP, the second case with TOU DR, and the third case with RTP DR. In the EH model for case study one without considering any DRP, results for operation cost and carbon emission are 9835.762 $ and 26481.681 kg, respectively. Comparing the results of cases one and two shows that employing TOU-DR causes a 5.47% reduction in operation cost and a 0.53% (141.764kg) decrease in carbon emission. Furthermore, significant improvement has been made by the implementation of TOU-DR for operation costs and a small reduction in CO2 emission. Comparing the results of cases one and three shows that employing RTP DR causes a 2.285% reduction in operation cost and a 2.12% (561.934kg) decrease in carbon emission. Implementation of RTP DR has gained good operation cost and CO2 emission reduction for the proposed model objective functions. Different CAES capacities are applied in the model which shows using a CAES unit mainly will improve operation cost and increase CO2 emission in the proposed model. However, employing a CAES unit with 500kW capacity in some solutions can improve operation cost and CO2 emission, simultaneously.

Nomenclature

t	Time index (h)
C_{ec}^{t}	Output cooling of electrical chiller (kW)
C_{ac}^{t}	Output cooling of absorption chiller (kW)
Pl_{RTP}^{t}	Load demand considering real-time DRP (kW)
Pl_{DR}^{t}	Load demand with considering time of use DRP (kW)
E_{es}^{t}	Stored energy of electricity storage (kWh)
E_{hs}^{t}	Stored energy of heat storage (kWh)
E_{cs}^{t}	The stored energy of the ice storage tank (kWh)
H_{gb}^{t}	Output heat of gas boiler (kW)
H_{gt}^{t}	Waste Heat of gas turbine (kW)

H_{ac}^{t}	Input heat of absorption chiller (kW)
M_{pg}	Gas purchased cost ($)
M_{pe}	Electricity purchased cost ($)
P_{gas}^{t}	Input gas from gas grid (kW) t
P_{ge}^{t}	Input gas of gas turbine (kW)
P_{pv}^{t}	Generated power by PV (kW)
P_{wt}^{t}	Generated power by WT (kW)
P_{gh}^{t}	Input gas of gas boiler (kW)
P_{gt}^{t}	Generated power from gas turbine (kW)
P_{gcaes}^{t}	Input gas of gas CAES (kW)
P_{gchp}^{t}	Input gas of gas CHP (kW)
P_{grid}^{t}	Exchange power between the electricity grid and energy hub system (kW)
P_{buy}^{t}	Import electricity power from the grid (kW)
P_{sell}^{t}	export electricity power to the grid (kW)
P_{grid}^{t}	Input power of chiller (kW)
P_{ice}^{t}	Input power of the ISC's chiller (kW)
$P_{cs,c}^{t}$	Charging cool of ice storage conditioner (kW)
$P_{cs,d}^{t}$	Discharging cool of ice storage conditioner (kW)
$P_{hs,c}^{t}$	Charging heat of heat storage (kW)
$P_{hs,d}^{t}$	Discharging heat of heat storage (kW)
$P_{es,c}^{t}$	Charging power of electricity storage (kW)
$P_{es,d}^{t}$	Discharging power of electricity storage (kW)
SUC	Startup cost of the CHP unit
SDC	shutdown cost of the CHP unit
P_{chp}^{t}, T_{chp}^{t}	Electricity/thermal generation of the CHP
$V_{injected}^{t}$	The energy equivalent of injected air to CAES/combustion chamber
V_{pumped}^{t}	The energy equivalent of pumped air to CAES/combustion chamber

$P^t_{cons.}$, $P^t_{gen.}$	The power consumed/output by/of CAES.
PS^t	The amount of stored energy in the CAES.
T^t_{tr}	Thermal output of the CAES
T^t_{EHP}	Thermal output of the EHP
P^t_{EHP}	Electrical input of the EHP
u^t_{es}	The binary variable of electrical storage is 1 in charging mode otherwise 0
u^t_{hs}	Binary variable of heat storage,1 in charging mode otherwise 0
u^t_{cs}	Binary variable of ISC, 1 in charging mode otherwise 0
COP_{ec}	Coefficient for the performance of electrical chiller
COP_{ice}	Coefficient for the performance of ice storage conditioner (ISC)
COP_{ac}	Coefficient for the performance of absorption chiller
Pl^t	Initial electricity demand (kW)
$E^{\min}_{es}$	Minimum stored energy of electricity storage (kWh)
$E^{\max}_{es}$	Maximum stored energy of electricity storage (kWh)
$E^{\min}_{hs}$	Minimum stored energy of heat storage (kWh)
$E^{\max}_{hs}$	Maximum stored energy of heat storage (kWh)
$E^{\min}_{cs}$	Minimum stored energy of ice storage tank (kWh)
$E^{\max}_{cs}$	Maximum stored energy of ice storage tank (kWh)
E	Elasticity coefficient of RTP demand price
$H^{\max}_{gb}$	Maximum output heat of gas boiler (kW)
$H^{\max}_{ac}$	Maximum input heat of absorption chiller (kW)
$P^{\max}_{es,c}$	Maximum charging power of electricity storage (kW)
$P^{\max}_{hs,c}$	Maximum charging heat of heat storage (kW)
$P^{\max}_{cs,c}$	Maximum charging cool of ISC (kW)
$P^{\max}_{es,d}$	Maximum discharging power of electricity storage (kW)
$P^{\max}_{hs,d}$	Maximum discharging heat of heat storage (kW)
$P^{\max}_{cs,d}$	Maximum discharging cool of ISC (kW)

$P_{gt}^{\max}$	Maximum generated power from gas turbine (kW)
$P_{wt}^{\max}$	Maximum generated power by wind turbine (kW)
$P_{grid}^{\max}$	Maximum exchange power between the electricity grid and energy hub system (kW)
$P_{gas}^{\max}$	Maximum of input gas from gas grid (kW)
$P_{ec}^{\max}$	Maximum input power of chiller (kW)
$P_{ice}^{\max}$	Maximum input power of the ISC's chiller (kW)
$P_{pv}^{\max}$	Maximum generated power by photovoltaic system (kW)
P_g^t	Gas price ($/kWh)
P_{av}	Average electricity demand (kW)
Dn_i , Up_i	Auxiliary variable for modeling MDT and MUT constraints
$\lambda_{RTP}^{\min}$	Minimum amount of RTP ($)
$\lambda_{RTP}^{\max}$	Maximum amount of RTP ($)
λ_{RTP}^t	Real-time pricing ($)
γ^t	Float factor of RTP
W_d	Integrated of all energy demand (kW)
β_e	Equivalent emission coefficient of electricity (kg/kWh)
β_g	Equivalent emission coefficient of natural gas (kg/kWh)
$\eta_{es,c}$	Charging efficiency of electrical storage
$\eta_{hs,c}$	Charging efficiency of heating storage
$\eta_{cs,c}$	Charging efficiency of cooling storage
$\eta_{es,d}$	Discharging efficiency of electrical storage
$\eta_{hs,d}$	Discharging efficiency of heating storage
$\eta_{cs,d}$	Discharging efficiency of cooling storage
η_{ge}	Gas turbine efficiency for generating power
$\eta_{gh,gb}$	Gas boiler efficiency for generating heat
$\eta_{gh,gt}$	Gas turbine efficiency for generating heat
η_t	Transformer efficiency

η_{he}	Efficiency of heat exchanger
δ_{es}	Energy loss ratio of electrical storage
δ_{hs}	Energy loss ratio of heat storage
δ_{cs}	Energy loss ratio of ISC
$P_{chp}^{\max}$, $P_{chp}^{\min}$	Upper/lower limits of the CHP units outputs.
HV	Heat value of the natural gas
SU, SD	The start-up and shut-down cost of CHP
η_{He}	Efficiency of the CHP heat exchanger
HPR	Heat to power ratio of the CHP unit.
$P^{Ramp-up}$	Ramp-up rate of the CHP
$P^{Ramp-down}$	Ramp-down rate of the CHP
η_{chp}	Electrical efficiency of the CHP unit.
e^{i}, e^{p}	The efficiency of injected/produced power of the CAES system.
$V_{pumped}^{\max}$	Maximum level of pumped air from storage to combustion chamber
$V_{pumped}^{\min}$	Minimum level of pumped air from storage to combustion chamber
$V_{ingected}^{\max}$	Maximum level of injected air into the CAES system
$V_{ingected}^{\min}$	Minimum level of injected air into the CAES system
$PS^{\min}$	Minimum level CAES
$PS^{\max}$	Maximum level CAES
COP_{EHP}	Coefficient of performance of the EHP.

References

[1] T. Ding, W. Jia, et al., "Review of Optimization Methods for Energy Hub Planning, Operation, Trading, and Control," *IEEE Transactions on Sustainable Energy*, vol. 13, no. 3, pp. 1802–1818, 2022.

[2] P. Hajiamoosha, A. Rastgou, S. Bahramara, and S. M. Bagher Sadati, "Stochastic Energy Management in a Renewable Energy-Based Microgrid Considering Demand Response Program," *International Journal of Electrical Power & Energy Systems*, vol. 129, 106791, 2021.

[3] A. Rastgou, "Distribution Network Expansion Planning: An Updated Review of Current Methods and New Challenges," *Renewable and Sustainable Energy Reviews*, vol. 189, 114062, 2024.

[4] K. Gholami, S. Karimi, and A. Rastgou, "Fuzzy Risk-Based Framework for Scheduling of Energy Storage Systems in Photovoltaic-Rich Networks," *Journal of Energy Storage*, vol. 52, 104902, 2022.

[5] A. A. Eladl, M. I. El-Afifi, M. M. El-Saadawi, and B. E. Sedhom, "A Review on Energy Hubs: Models, Methods, Classification, Applications, and Future Trends," *Alexandria Engineering Journal*, vol. 68, pp. 315–342, 2023.

[6] T. Ha, Y. Xue, et al., "Optimal Operation of Energy Hub Based Micro-Energy Network with Integration of Renewables and Energy Storages," *Journal of Modern Power Systems and Clean Energy*, vol. 10, no. 1, pp. 100–108, 2022.

[7] X. Zhou, Z. Ma, S. Zou, J. Zhang, and Y. Guo, "Distributed Energy Management of Double-Side Multienergy Systems Via Sub-Gradient Averaging Consensus," *IEEE Transactions on Smart Grid*, vol. 14, no. 2, pp. 979–995, 2023.

[8] A. Rastgou, J. Moshtagh, and S. Bahramara, "Probabilistic Power Distribution Planning Using Multi-Objective Harmony Search Algorithm," *Journal of Operation and Automation in Power Engineering*, vol. 6, no. 1, pp. 111-125, 2018.

[9] M. Jadidbonab, E. Babaei, and B. Mohammadi-ivatloo, "CVaR-Constrained Scheduling Strategy for Smart Multi Carrier Energy Hub Considering Demand Response and Compressed Air Energy Storage," *Energy*, vol. 174, pp. 1238–1250, 2019.

[10] M. Rastegar, M. Fotuhi-Firuzabad, and M. Lehtonen, "Home Load Management in a Residential Energy Hub," *Electric Power Systems Research*, vol. 119, pp. 322–328, 2015.

[11] A. Hussain, S. M. Arif, M. Aslam, and S. D. A. Shah, "Optimal Siting and Sizing of Tri-Generation Equipment for Developing an Autonomous Community Microgrid Considering Uncertainties," *Sustainable Cities and Society*, vol. 32, pp. 318–330, 2017.

[12] F. Jabari, S. Nojavan, and B. Mohammadi Ivatloo, "Designing and Optimizing a Novel Advanced Adiabatic Compressed Air Energy Storage and Air Source Heat Pump Based M-Combined Cooling, Heating and Power System," *Energy*, vol. 116, pp. 64–77, 2016.

[13] X. Chen, G. Gong, Z. Wan, C. Zhang, and Z. Tu, "Performance Study of a Dual Power Source Residential CCHP System Based on PEMFC and PTSC," *Energy Conversion and Management*, vol. 119, pp. 163–176, 2016.

[14] M. Geidl, G. Koeppel, et al., "Energy Hubs for the Future," *IEEE Power and Energy Magazine*, vol. 5, no. 1, pp. 24–30, 2007.

[15] M. Geidl, and G. Andersson, "Optimal Coupling of Energy Infrastructures," *2007 IEEE Lausanne Power Tech*, 2007.

[16] S. Bahrami, and F. Safe, "A Financial Approach to Evaluate an Optimized Combined Cooling, Heat and Power System," *Energy and Power Engineering*, vol. 05, no. 05, pp. 352–362, 2013.

[17] D. Xu, Q. Wu, et al., "Distributed Multi-Energy Operation of Coupled Electricity, Heating, and Natural Gas Networks," *IEEE Transactions on Sustainable Energy*, vol. 11, no. 4, pp. 2457–2469, 2020.

[18] M. Rastegar, and M. Fotuhi-Firuzabad, "Load Management in a Residential Energy Hub with Renewable Distributed Energy Resources," *Energy and Buildings*, vol. 107, pp. 234–242, 2015.

[19] M. C. Bozchalui, S. A. Hashmi, H. Hassen, C. A. Canizares, and K. Bhattacharya, "Optimal Operation of Residential Energy Hubs in Smart Grids," *IEEE Transactions on Smart Grid*, vol. 3, no. 4, pp. 1755–1766, 2012.

[20] M. Moeini-Aghtaie, A. Abbaspour, M. Fotuhi-Firuzabad, and P. Dehghanian, "Optimized Probabilistic PHEVs Demand Management in the Context of Energy Hubs," *IEEE Transactions on Power Delivery*, vol. 30, no. 2, pp. 996–1006, 2015.

[21] S. Zheng, Y. Sun, et al., "Incentive-Based Integrated Demand Response for Multiple Energy Carriers Considering Behavioral Coupling Effect of Consumers," *IEEE Transactions on Smart Grid*, vol. 11, no. 4, pp. 3231–3245, 2020.

[22] M. Majidi, and K. Zare, "Integration of Smart Energy Hubs in Distribution Networks Under Uncertainties and Demand Response Concept," *IEEE Transactions on Power Systems*, vol. 34, no. 1, pp. 566–574, 2019.

[23] M. Mazidi, A. Zakariazadeh, S. Jadid, and P. Siano, "Integrated Scheduling of Renewable Generation and Demand Response Programs in a Microgrid," *Energy Conversion and Management*, vol. 86, pp. 1118–1127, 2014.

[24] S. Nojavan, and H. A. Aalami, "Stochastic Energy Procurement of Large Electricity Consumer Considering Photovoltaic, Wind-Turbine, Micro-Turbines, Energy Storage System in the Presence of Demand Response Program," *Energy Conversion and Management*, vol. 103, pp. 1008–1018, 2015.

[25] P. Mancarella, and G. Chicco, "Real-Time Demand Response from Energy Shifting in Distributed Multi-Generation," *IEEE Transactions on Smart Grid*, vol. 4, no. 4, pp. 1928–1938, 2013.

[26] B. Yan, S. Xue, Y. Li, J. Duan, and M. Zeng, "Gas-Fired Combined Cooling, Heating and Power (CCHP) in Beijing: A Techno-Economic Analysis," *Renewable and Sustainable Energy Reviews*, vol. 63, pp. 118–131, 2016.

[27] K. Saberi, H. Pashaei-Didani, R. Nourollahi, K. Zare, and S. Nojavan, "Optimal Performance of CCHP Based Microgrid Considering Environmental Issue in the Presence of Real Time Demand Response," *Sustainable Cities and Society*, vol. 45, pp. 596–606, 2019.

[28] D. K. Critz, S. Busche, and S. Connors, "Power Systems Balancing with High Penetration Renewables: The Potential of Demand Response in Hawaii," *Energy Conversion and Management*, vol. 76, pp. 609–619, 2013.

[29] L. Guo, W. Liu, J. Cai, B. Hong, and C. Wang, "A Two-Stage Optimal Planning and Design Method for Combined Cooling, Heat and Power Microgrid System," *Energy Conversion and Management*, vol. 74, pp. 433–445, 2013.

[30] Z. Tan, L. Ju, et al., "The Optimization Model for Multi-Type Customers Assisting Wind Power Consumptive Considering Uncertainty and Demand Response Based on Robust Stochastic Theory," *Energy Conversion and Management*, vol. 105, pp. 1070–1081, 2015.

[31] H. Aalami, M. P. Moghaddam, and G. Yousefi, "Demand Response Modeling Considering Interruptible/Curtailable Loads and Capacity Market Programs," *Applied Energy*, vol. 87, no. 1, pp. 243–250, 2010.

[32] E. Drury, P. Denholm, and R. Sioshansi, "The Value of Compressed Air Energy Storage in Energy and Reserve Markets," *Energy*, vol. 36, no. 8, pp. 4959–4973, 2011.

[33] R. Rezaeipour, and A. Zahedi, "Multi-Objective Based Economic Operation and Environmental Performance of PV-Based Large Industrial Consumer," *Solar Energy*, vol. 157, pp. 227–235, 2017.

[34] S. Nojavan, M. Majidi, and N. N. Esfetanaj, "An Efficient Cost-Reliability Optimization Model for Optimal Siting and Sizing of Energy Storage System in a Microgrid in the Presence of Responsible Load Management," *Energy*, vol. 139, pp. 89–97, 2017.

[35] S. Nojavan, M. Majidi, A. Najafi-Ghalelou, M. Ghahramani, and K. Zare, "A Cost-Emission Model for Fuel Cell/PV/Battery Hybrid Energy System in the Presence of Demand Response Program: E-Constraint Method and Fuzzy Satisfying Approach," *Energy Conversion and Management*, vol. 138, pp. 383–392, 2017.

Declaration of competing interest

The authors declare that they have no known competing financial interests or personal relationships that could have appeared to influence the work reported in this paper. The ethical issues, including plagiarism, informed consent, misconduct, data fabrication and/or falsification, double publication and/or submission, redundancy, have been completely observed by the authors.

Bibliography

Pouria Hajiamoosha is a dedicated researcher in the field of electrical power engineering, with a focus on optimization and the management of microgrids and energy systems. He holds a Master's degree in Electrical Power Engineering from the Islamic Azad University, Science and Research Branch of Kermanshah, as well as a Bachelor's degree in Electrical and Electronics Engineering from the Islamic Azad University.
Email: poorya.php@gmail.com
ORCID: 0009-0009-3345-8986
Contribution Statement: Formal analysis, Methodology, Software, Roles/Writing - original draft, Writing-review & editing.

Abdollah Rastgou holds a Bachelor's, Master's, and Ph.D. degree in Power Electrical Engineering. He completed his Bachelor's degree at Tabriz University and went on to earn both his Master's and Ph.D. degrees with honors from Kurdistan University in Sanandaj. Dr. Rastgou has a keen interest in power system planning, bi-level planning, and renewable resource planning. His academic journey reflects a strong commitment to advancing the field of electrical engineering, particularly in optimizing power systems for sustainability and efficiency.
Email: abdollah.rastgou@iau.ac.ir
ORCID: 0000-0002-8620-2185
Contribution Statement: Conceptualization, Data curation, Formal analysis, Funding acquisition, Investigation, Methodology, Project administration, Resources, Software, Supervision, Validation, Visualization,

Hadi Afshar received the B.Sc. and the M.Sc. degrees in electrical engineering from the Semnan University, Semnan, Iran, in 2010 and 2013, respectively. His research interests include smart grids, renewable energy systems, energy management, power system operation, optimization, and planning.
Email: Haaf963@gmail.com
ORCID: 0009-0000-2799-367X
Contribution Statement: Formal analysis, Software, Writing-review & editing.

Journal of Green Energy Research and Innovation

Assessing Wind Energy Potential in Markazi Province, Iran: A Data-Driven Approach with AI Algorithms

Amir Hossein Karamali, Abolghasem Daeichian, Saber Rezaei, Ali Reihanian

Highlights

- **Suggesting suitable locations for wind power plants in Markazi Province by analyzing real wind speed data**
- **Analyzing wind patterns using a combination of statistical approaches and artificial intelligence techniques**
- **Conducting statistical analysis using the Weibull distribution and wind rose diagrams**
- **Employing Long Short-Term Memory network to predict wind speeds and temporal trends.**

Graphical Abstract

Use your device to scan and read the article online

Citation

A. H. Karamali, A. Daeichian, S. Rezaei, and A. Reihanian," Assessing Wind Energy Potential in Markazi Province, Iran: A Data-Driven Approach with AI Algorithms," *Journal of Green Energy Research and Innovation*, vol. 2, no. 2, pp. 26-35, 2025.

https://doi.org/10.61186/jgeri.2.2.26

Journal of Green Energy Research and Innovation 2.2 (2025) 26-35

Online ISSN: 3041-9018

Journal of Green Energy Research and Innovation

Journal Homepage: www.jgeri.araku.ac.ir

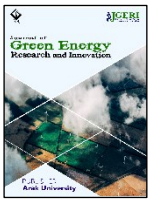

Assessing Wind Energy Potential in Markazi Province, Iran: A Data-Driven Approach with AI Algorithms

Amir Hossein Karamali [1] , Abolghasem Daeichian [2,3], Saber Rezaei [1], Ali Reihanian [3,4,*]

[1] *Department of Electrical Engineering, Iran University of Science and Technology, Tehran, Iran.*

[2] *Department of Electrical Engineering, Faculty of Engineering, Arak University, Arak, 38156-8-8349, Iran.*

[3] *Research Institute of Artificial Intelligence, Arak University, Arak, 38156-8-8349, Iran.*

[4] *Department of Computer Engineering, Faculty of Engineering, Arak University, Arak, 38156-8-8349, Iran.*

A R T I C L E I N F O

Keywords:
Wind Energy Potential,
Wind rose,
Weibull Function,
Long Short-Term Memory,
Renewable energy.

Article History:
Received: 12 December 2024;
Revised: 06 January 2025;
Accepted: 18 January 2025.

Article type:
Research Article

* ***Corresponding author***
E-mail address
a-reihanian@araku.ac.ir (A. Reihanian)

A B S T R A C T

This paper investigates the wind energy potential in Markazi Province, Iran, focusing on three cities: Tafresh, Khomein, and Saveh. The primary objective of this study is to provide a comprehensive analysis of wind patterns using a combination of statistical approaches and artificial intelligence techniques. Wind data was collected from advanced meteorological stations in these cities over two years (2018–2020), including detailed measurements of wind speed and direction at 10-minute intervals. This high-resolution dataset facilitated an in-depth examination of wind behavior and its suitability for energy production. Statistical analysis was conducted using the Weibull distribution and wind rose diagrams, which provided insights into the wind characteristics and their spatial variations. Additionally, Long Short-Term Memory (LSTM) networks were employed to predict wind speeds and temporal trends. These models effectively captured the complex relationships within the wind data and produced highly accurate forecasts. The comparison of actual and predicted wind rose diagrams demonstrated a strong alignment, validating the reliability of the LSTM-based predictions in reflecting real-world wind patterns. The results of this study demonstrate that combining traditional statistical methods with modern machine learning techniques provides a robust framework for analyzing wind energy potential. By leveraging these tools, the study offers valuable insights for sustainable energy planning and supports informed decision-making for renewable energy investments in Markazi Province.

1. Introduction

The study of wind speed patterns and the assessment of wind energy potential are critical in renewable energy planning [1]. Numerous studies have employed various techniques to analyze wind characteristics and evaluate wind energy potential across diverse regions. For example, the variability of wind speeds and power potential has been frequently examined using the Weibull distribution [2]. However, while the Weibull distribution remains a popular tool for modeling wind speed, its limitations in capturing multimodal and highly variable wind speed distributions are often overlooked.

In [3], the performance of three probability distributions, Weibull, Logistic, and Lognormal, was compared for wind speed modeling. The study highlighted that the Logistic distribution outperformed Weibull and Lognormal in certain cases, offering better accuracy for specific datasets. Nonetheless, these approaches heavily rely on static assumptions and often fail to adapt to rapidly changing meteorological conditions or seasonal variability.

The assessment of wind energy potential in Turkey, as discussed in [4], provides valuable insights into high-potential regions such as Marmara, Aegean, and Southeastern Anatolia, emphasizing favorable wind speeds and densities. Despite this, the study relies on historical averages and static probability distributions, which might not fully reflect short-term variations or long-term trends in wind speed data. Additionally, regional assessments often lack integration with predictive frameworks that could dynamically evaluate wind speed fluctuations for better resource planning.

The use of statistical tools like probability density functions (PDFs) for wind speed modeling is well-established. For instance, combining the Weibull function with wind rose diagrams allows a more comprehensive understanding of wind patterns throughout the year [3]. Wind rose diagrams provide critical information about wind direction and frequency, aiding in the assessment of wind regimes for energy projects [5]. However, these methods predominantly offer descriptive insights and do not inherently account for predictive or real-time applications.

Machine learning algorithms, such as support vector regression, random forests, and ensemble methods, have shown promise in predictive modeling of renewable energy systems [6,7]. Moreover, GIS-based multi-criteria decision-making has been explored for optimal site selection of renewable energy installations like solar power plants [8]. Despite these advancements, the application of machine learning models in wind energy often suffers from insufficient integration with statistical frameworks, leading to limited accuracy in capturing long-term wind speed trends.

In [9], the impact of wind direction on the power output and income of wind farms was explored. This research proposed a modified quadratic power curve to account for wind direction variability, offering a novel method for predicting wind turbine output. However, the study heavily relies on historical data to complete the wind datasets.

In [10], the feasibility of wind energy potential along the coastline of Pakistan is analyzed using predictive models and artificial neural networks (ANN) for forecasting wind data. While the study highlights Karachi as the most suitable location for wind farms, the ANN employed lacks sufficient precision in capturing long-term wind variability, limiting its reliability for accurate forecasting.

Long Short-Term Memory (LSTM) neural networks, in particular, have gained recognition for their effectiveness in time series analysis, making them ideal for wind speed prediction over extended periods [11]. However, past studies employing LSTM networks often overlook the incorporation of domain-specific statistical insights, such as Weibull or wind rose analysis, which could enhance model interpretability and robustness. This highlights the need for hybrid approaches that combine statistical methods with machine learning techniques to address gaps in adaptability, accuracy, and contextual understanding of wind speed variations.

Iran has made significant strides in the development of wind power plants, with notable projects scattered across the country. One of the earliest and most influential wind farms is the Manjil Wind Power Plant situated in Gilan. This pioneering onshore wind farm was commissioned in 1994 and boasts a capacity of around 90 MW. It played a pivotal role in jumpstarting wind energy production in Iran. Another remarkable wind farm in Iran is the Kahak Wind Farm located in Qazvin. It was commissioned in 2017 and has been inaugurated in two phases, ultimately reaching a final capacity of 100 MW. This sizable wind farm stands as one of the largest in the country. Similarly, in Qazvin, the Siahpoosh Wind Farm was commissioned in 2018 and has a capacity of 61.2 MW, contributing to the renewable energy landscape of the region. In addition to these larger wind farms, there are also smaller-scale installations that deserve recognition. One such example is the Khaf Wind Turbine in Khorasan Razavi, installed by Aria Razi Company. With a capacity of 2.5 MW, it was commissioned in 2015. Furthermore, the Aoun Ben Ali Wind Power Plant in Tabriz and the Safa Wind Power Plant in Isfahan each have capacities of 0.66 MW. Overall, wind power in Iran has made noteworthy progress, with a daily electricity generation capacity of approximately 600 MW from wind sources alone. However, considering the country's total electricity generation capacity of around 90,000 MW, there is ample scope for further growth and the establishment of new wind power plants in regions like Markazi Province to meet the growing energy demand [2].

While wind power plants have been successfully developed in various regions of Iran, including Gilan, Qazvin, Neyshabur, Khorasan Razavi, and Isfahan, there remains ample potential for further expansion. One such region that could greatly benefit from the establishment of a wind power plant is Markazi Province. This province boasts favorable conditions for wind energy production due to its strong and consistent winds. Furthermore, its central location within Iran, proximity to major population centers, and high electricity demand make it an ideal candidate for the development of a wind power plant. Such a project in Markazi Province could significantly contribute to Iran's overall electricity generation capacity. The efforts and dedication of Iran's Renewable Energy and Electricity Efficiency Organization have contributed to the acquisition of valuable insights through their website. By examining the map provided on the website, we observe the regions prone to wind, visualized through distinctive red dots. These areas signify immense potential for the harnessing of wind energy and serve as promising locations for future renewable energy projects in Markazi Province. Considering the rich data available from the meteorological stations and the continued efforts in renewable energy development, Markazi Province stands as a promising hub for advancing sustainable energy solutions within Iran's broader energy landscape [12].

This study offers an in-depth analysis of wind patterns in Markazi Province, Iran, with a focus on three towns in the province, Tafresh, Khomein, and Saveh, using a hybrid approach. This information is crucial for the assessment of wind power potential and the development of wind energy projects in the region. To facilitate the analysis of wind patterns in the region, comprehensive meteorological stations have been established in these cities. The Tafresh, Saveh, and Khomein meteorological stations, renowned for their cutting-edge technology and reliable data, serve as invaluable sources of information for wind energy enthusiasts and researchers alike. However, Weibull distribution and wind rose visualization are combined with LSTM networks for advanced wind resource assessment. The use of LSTM networks is expected to capture complex spatiotemporal dependencies in wind data for accurate forecasting of wind speeds at different altitudes. By leveraging the strengths of statistical tools and modern machine learning, the proposed approach provides superior insights into wind speed variability. The innovation of this study lies in its hybrid methodology, which combines traditional statistical techniques with state-of-the-art machine learning algorithms. This approach not only enhances the accuracy of wind energy potential assessments but also facilitates a deeper understanding of spatiotemporal wind behavior. Moreover, this research highlights the potential of Markazi Province as a hub for renewable energy development, addressing a critical gap in the literature. By demonstrating the utility of LSTM models in wind resource assessment, the study sets a precedent for future applications of AI-driven techniques in renewable energy planning.

This study has been folded as follows. In Section 2, we give some preliminaries. Section 3 analyses the wind data. LSTM is used to predict the wind speed in Section 4. Finally, the paper is concluded in Section 5.

2. Preliminaries

2.1. Dataset

In this study, we collected wind data from three meteorological stations Tafresh, Khomein, and Saveh for a period of two years, from 2018 to 2020. Tafresh, Khomein, and Saveh meteorological stations were chosen due to their strategic locations and availability of reliable wind data. These stations are equipped with advanced anemometers and meteorological instruments that accurately measure wind speed and direction. The data sampling was conducted at regular intervals of every 10 minutes, providing us with a comprehensive dataset to analyze wind patterns and assess wind power potential in the region. By collecting data at such high frequency, we were able to capture the fine-scale variations in wind behavior over two years. This level of temporal resolution allows for a detailed analysis of wind patterns and the identification of important trends and variations throughout different seasons and years.

The wind data collected from these stations serves as a valuable resource for understanding the wind characteristics in the region and determining the wind energy potential. It provides insights into the prevailing wind directions, average wind speeds and wind speed fluctuations at different times of the day.

Wind speed typically rises as altitude increases. Within the boundary layer, this rise occurs because friction diminishes at greater heights. In wind turbine engineering, the change in wind speed with elevation is often expressed relative to a standard measurement taken at 10 meters. This relationship can be modeled using a power law Equation, as shown below [13]:

$$V(h) = v(10)(\frac{h}{10})^{\alpha} \quad (1)$$

Here, $V(h)$ represents the wind speed at a given height h, $V(10)$ is the wind speed recorded at the reference height of 10 meters by an anemometer, and α is an exponent that fluctuates between 0.11 and 0.40, depending on factors like surface roughness and atmospheric conditions. For a smooth, open landscape under neutral stability, α is commonly set at 0.14. Vallero demonstrated this power law approach using an exponent of $\frac{1}{7}$, which is roughly equivalent to 0.14. This value is suitable for low-roughness, exposed locations and has been widely adopted in research to map the vertical wind speed profile within the boundary layer. Accordingly, in our analysis, we applied an α value of 0.14 to compute wind speeds at heights of 50 meters, 80 meters, 100 meters, and 120 meters, based on wind speed data measured at the 10-meter anemometer level [14].

2.2. 2.1. Weibull parameters and probability assessment of wind power density

Generally, wind speed data well matches the Weibull shape. Many studies have used the Weibull distribution and the following equations to assess the properties of wind speed and the corresponding wind power densities at various places around the world [13]. The Weibull wind speed probability density function can be represented as Equation (2):

$$f(v) = \left(\frac{k}{c}\right)\left(\frac{v}{c}\right)^{k-1} exp\left[-\left(\frac{v}{c}\right)^{k}\right] \quad (2)$$

Where $f(v)$ is the probability of observing wind speed v. Also, k is the dimensionless Weibull shape parameter, and c is the Weibull scale-parameter in m/s. The shape parameter determines the shape of the distribution curve, indicating whether the wind speed data is skewed or bell-shaped. On the other hand, the scale parameter represents the wind speed at which the distribution reaches its maximum value, also known as the most probable wind speed. The Weibull shape and scale parameters k and c are related to the mean wind speed v_m as Equation (3):

$$v_m = c\Gamma\left(1 + \frac{1}{k}\right) \quad (3)$$

where Γ is the gamma function. After estimating the mean and the variance of the wind speed data, Weibull parameters, k and c, can be calculated as Equations (4) and (5):

$$k = (\frac{\sigma}{v_m})^{-1.086} \quad (4)$$

$$c = \frac{v_m}{\Gamma\left(1 + \frac{1}{k}\right)} \quad (5)$$

The most probable wind speed, $v_{mp}(m/s)$, defined as the most common wind speed for a given wind speed probability distribution function, can be expressed as Equation (6):

$$v_{mp} = c\left(\frac{k-1}{k}\right)^{1/k} \quad (6)$$

Wind speed corresponding to the maximum energy $v_{max}(m/s)$ can be calculated by using the Weibull parameters k and c as Equation (7):

$$v_{\max} = C\left(\frac{k+2}{k}\right)^{\frac{1}{k}} \quad (7)$$

Wind power density $P_d(W/m^2)$ can be determined as Equation (8):

$$P_d = \frac{1}{2}\rho c^3 \Gamma(1+\frac{3}{k}) \quad (8)$$

where ρ is the density of air in kg/m^3 [14,15].

2.3. LSTM neural network

LSTM is a type of artificial recurrent neural network (RNN) architecture that has gained significant popularity in the field of deep learning. It is designed to effectively capture and process long-term dependencies in sequential data, making it particularly suitable for tasks such as natural language processing, speech recognition, and time series analysis. Traditional RNNs suffer from the "vanishing gradient" problem, where the gradients diminish exponentially over time, making it difficult for the network to learn long-term dependencies. LSTM addresses this issue by introducing a memory cell and several gates that regulate the flow of information within the network [16]. So, the key component of an LSTM cell is the memory cell, which stores information over long sequences (see Figure 1). The cell has an internal state that can be selectively updated or forgotten based on the inputs and the current state. This makes LSTMs capable of retaining relevant information over extended periods, enabling them to handle sequences with long gaps between important events.

In addition to the memory cell, LSTMs contain three types of gates: the input gate, the forget gate, and the output gate. These gates are responsible for controlling the flow of information into and out of the memory cell [16,17]. The input gate determines which values from the input should be stored in the memory cell. It takes into account the current input and the previous hidden state. By applying a sigmoid activation function, it outputs values between 0 and 1, indicating how much of each input component should be stored [18]. The forget gate decides which information should be erased from the memory cell. It considers the current input and the previous hidden state and applies a sigmoid function to determine which parts of the memory cell should be forgotten. The output gate regulates the output of the LSTM cell. It combines the current input and the previous hidden state, passes them through a sigmoid function, and then applies the hyperbolic tangent function to the cell's current state to produce the final output.

During the training process, the parameters of the LSTM network, including the weights and biases, are learned using backpropagation through time. This involves computing the gradients of the loss function with respect to the network's parameters and updating them using optimization algorithms such as stochastic gradient descent [17,19]. By incorporating memory cells and gating mechanisms, LSTMs excel at learning from and predicting sequences, making them valuable tools in a wide range of applications [17-20].

Based on the connections shown in Figure 1, the mathematical expressions can be expressed as follows:

Forget gate: $$f_t = \sigma(W_{fh}h_{t-1} + W_{fx}x_t + b_f) \quad (9)$$

Input gate: $$i_t = \sigma(W_{ih}h_{t-1} + W_{ix}x_t + b_i) \quad (10)$$

Candidate Cell State: $$\tilde{c}_t = tanh(W_{\tilde{c}h}h_{t-1} + W_{\tilde{c}x}x_t + b_{\tilde{c}}) \quad (11)$$

Cell State Update: $$c_t = f_t.c_{t-1} + i_t.\tilde{c}_t \quad (12)$$

Output Gate: $$o_t = \sigma(W_{oh}h_{t-1} + W_{ox}x_t + b_o) \quad (13)$$

Hidden State: $$h_t = o_t.tanh(c_t) \quad (14)$$

Where W_{fh}, W_{fx}, W_{ih}, W_{ix}, $W_{\tilde{c}h}$, $W_{\tilde{c}x}$, W_{oh}, and W_{ox} represent the weight matrices associated with different gates and transformations in the LSTM architecture. W_{fh} and W_{fx} are weighted for the forget gate, W_{ih} and W_{ix} for the input gate, $W_{\tilde{c}h}$ and $W_{\tilde{c}x}$ for the candidate cell state, W_{oh} and W_{ox} for the output gate. They determine how much influence the previous hidden state h and current input x have on the computation of each gate or transformation. h_{t-1} represents the previous hidden state at time $(t-1)$ while x_t denotes the input at time t. These are the main sources of information that LSTM cells use to update their internal states and produce outputs. b_f, b_i, $b_{\tilde{c}}$, and b_o are bias terms associated with the forget gate b_f, input gate b_i, candidate cell state$b_{\tilde{c}}$, and output gate b_o. Bias terms allow the LSTM to introduce shifts in the activation functions, aiding in learning and capturing relevant patterns in the data. c_t represents the cell state at time t, capturing and preserving long-term information. h_t denotes the hidden state or output of the LSTM cell at time t, which may be passed to subsequent layers or used for further processing. o_t represents the output gate activation, determining which parts of the cell state should be transmitted to subsequent stages. $\tilde{c}(t)$ denotes the candidate cell state, offering potential updates to the cell state. i_t represents the input gate activation, controlling the flow of new information into the cell state. f_t denotes the forget gate activation, determining what information from the previous cell state should be retained or discarded. Finally, c_{t-1} is the previous cell state, providing context for the update of the current cell state [17].

3. Analysis of wind data

The distribution of wind speeds plays a crucial role in the assessment of wind power potential for the installation of a wind power plant. In this study, the Weibull distribution function was utilized to analyze the wind distribution characteristics at three different wind stations in Tafaresh, Khomein and Saveh. To better visualize the wind distribution patterns, Figure 2 presents the Weibull distribution graphs for the three wind stations. The x-axis represents wind speed, while the y-axis represents the probability density function (PDF).

Table 1 displays the scale and shape parameters obtained for each of the three wind stations. This distribution effectively models the statistical characteristics and variability of wind speed using two main parameters:

- Shape parameter (k): Represents the concentration or uniformity of the wind speed distribution. Higher values of (k) indicate a more uniform and narrower distribution of wind speeds.
- Scale parameter (c): Reflects the average wind speed, and has a significant impact on the amount of energy that can be extracted from the wind.
- Tafresh: Indicates low wind speeds and relatively wide variability.
- Khomein: Suggests higher wind speeds and more uniformity compared to Tafresh.
- Saveh: Represents the most uniform wind distribution and the highest average wind speed among the three regions.

The wind power density (WPD) is the measure of the amount of energy available in the wind at a specific location [19, 21-23]. It is calculated by multiplying the air density by the cube of the wind speed. WPD is usually expressed in watts per square meter (W/m^2). The higher the WPD, the more suitable the location is for wind energy generation. In this study, we calculated the WPD for three meteorological stations in Iran: Tafresh, Khomein, and Saveh. We assumed a standard air density of 1.225 kg^3 and a wind turbine height of 80 m.

The calculation of wind power density at an altitude of 80 meters indicates that Saveh, with 38.85 W/m^2 has the highest potential for wind energy exploitation. This value highlights the favorable wind conditions in the region for installing high-performance wind turbines. Khomein, with a wind power density of 16.17 W/m^2 also shows considerable potential for developing wind energy projects, particularly for medium-scale applications. In contrast, the wind power density in Tafresh, at 2.27 W/m^2 is very low, indicating that the wind conditions in this region are not economically viable for wind energy exploitation. This analysis underscores the importance of selecting suitable locations based on local wind data for designing and operating wind farms.

3.1. Applications of the Data

Estimating Wind Uniformity: Saveh, with the highest (k) value (5.45), has the most uniform wind distribution, meaning wind speeds in this region are concentrated within a specific range, and are more stable. This can contribute to more consistent turbine performance.

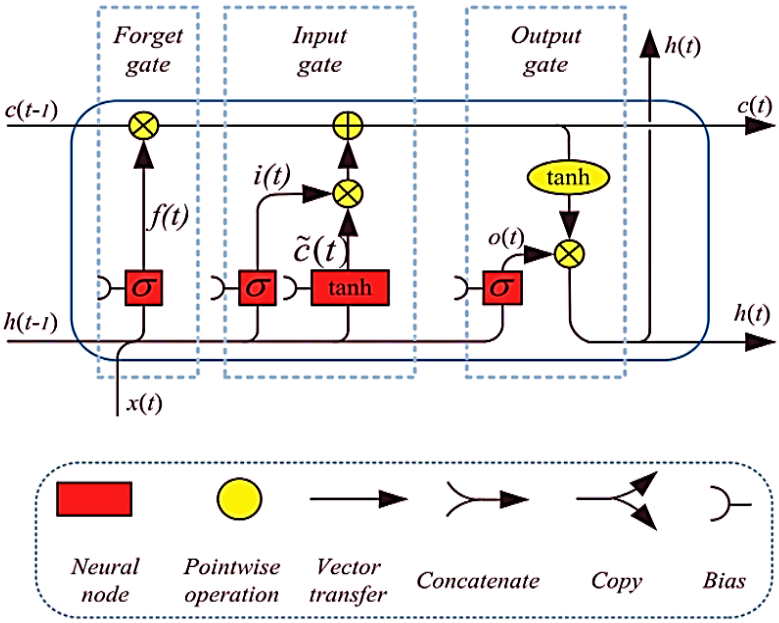

Figure 1. Architecture of LSTM with a forget gate [15].

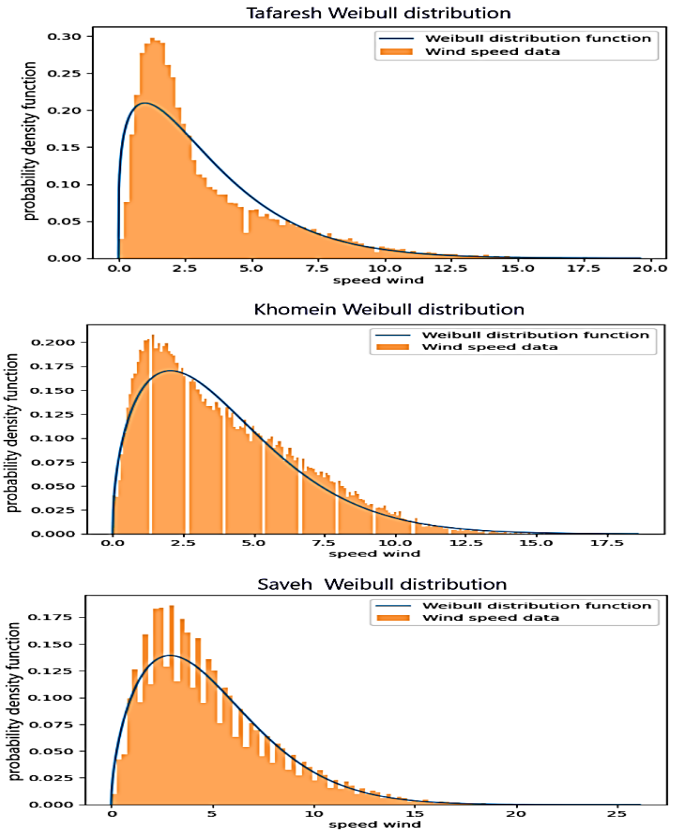

Figure 2. Weibull distribution graphs for the three wind stations.

Table 1. Shape parameters k (m/s) and scale parameters c (m/s) in the 2018-2020 period.

Parameters	Tafresh	Khomein	Saveh
K	4.06	4.37	5.45
C	1.19	2.3	3.1

Evaluating Energy Production Potential: The (c) parameter in Saveh (3.1) and Khomein (2.3) indicates higher average wind speeds compared to Tafresh (1.19), suggesting greater potential for wind energy production in these regions.

Designing Suitable Turbines: Using the Weibull distribution data, turbines can be selected to match the wind speed distribution of each region. For example, turbines for Khomein and Saveh should be designed for higher wind speeds.

Prediction with LSTM Models: Weibull parameters are key inputs for LSTM models to predict the temporal trends and variations in wind speed over different periods.

Economic and Engineering Analysis: Weibull data indicates that Saveh, with higher uniformity and greater average wind speed, is a suitable option for wind energy investment. In contrast, Tafresh, due to its lower wind speeds, may not be economically viable for wind energy projects.

4. Wind Data Analysis Using LSTM

Modeling the wind data in the previous section and calculating the scale and shape parameters can help us in analyzing the wind speed in the area. Using these parameters obtained by artificial intelligence, which uses a two-layer LSTM network, the speed can be predicted, and the generated power will help in the future, in this way, we achieved very good accuracy. Figure 3 showcases a comparison between the actual and predicted wind speeds at the Khomein, Tafaresh, and Saveh wind stations in the central province of Iran. The x-axis represents the sample index, while the y-axis represents the wind speed in meters per second. In Figure 3, the blue line represents the actual wind speeds recorded at the respective stations. These values serve as the ground truth for evaluating the accuracy of the wind forecasting model. The orange line, on the other hand, represents the predicted wind speeds generated by the two-layer algorithm of artificial intelligence. Upon visual inspection, it is evident that the predicted wind speeds closely align with the actual wind speeds. The model successfully captures the underlying patterns and trends in the wind data, resulting in accurate predictions. The closeness of the red line to the blue line indicates the model's ability to capture the dynamics of wind

behavior in the central province of Iran. The figure provides valuable insights into the performance of the two-layer algorithm in wind forecasting. It demonstrates the algorithm's effectiveness in capturing the complex relationships and dependencies in the wind data, enabling accurate predictions.

Figure 4 shows the wind roses derived from the actual measured data. The LSTM-based predictions were compared, and they demonstrated a remarkably close resemblance. The wind direction distribution and wind speed frequencies exhibited a strong alignment, indicating the effectiveness of the LSTM algorithm in capturing the underlying patterns and characteristics of the wind behavior in the study areas. The level of approximation between the real and predicted wind roses suggests the reliability and potential utility of the LSTM model for wind forecasting in the Markazi Province of Iran.

In this study, wind forecasting was performed in three stations, namely Tafarsh, Khomein, and Saveh, located in the Markazi Province of Iran. The wind patterns observed at these stations were compared with the predictions generated by the double-layer LSTM (Long Short-Term Memory) algorithm. To evaluate the performance and accuracy of the algorithm, three important evaluation metrics were utilized: Mean Squared Error (MSE), Mean Absolute Error (MAE), and R-squared coefficient.

MSE represents the average squared difference between the predicted wind values and the observed wind values at each station. It provides a measure of the model's ability to minimize prediction errors. Similarly, MAE indicates the average absolute difference between the predicted and observed wind values, giving insights into the magnitude of errors. Additionally, the R-squared coefficient, also known as the coefficient of determination, assesses the goodness-of-fit of the predicted wind values against the actual wind values. It represents the proportion of variance in the observed wind patterns that can be explained by the LSTM model. A higher R-squared value indicates a better fit and higher predictive accuracy.

To present a comprehensive analysis, these evaluation metrics were calculated for all three stations, and the results are tabulated in Table 2. The table provides a concise summary of the model's performance, allowing for a direct comparison of MSE, MAE, and R-squared values across the stations. The inclusion of this table enhances the clarity and transparency of our findings, enabling readers to easily interpret and assess the predictive capabilities of the double-layer LSTM algorithm in wind forecasting.

Table 2. Three parameters to measure the accuracy of the obtained model for three stations.

	Tafresh	Khomein	Saveh
MSE	0.0017	0.0029	0.0012
MAE	0.0292	0.0377	0.0256
R-squared	0.8838	0.8719	0.9183

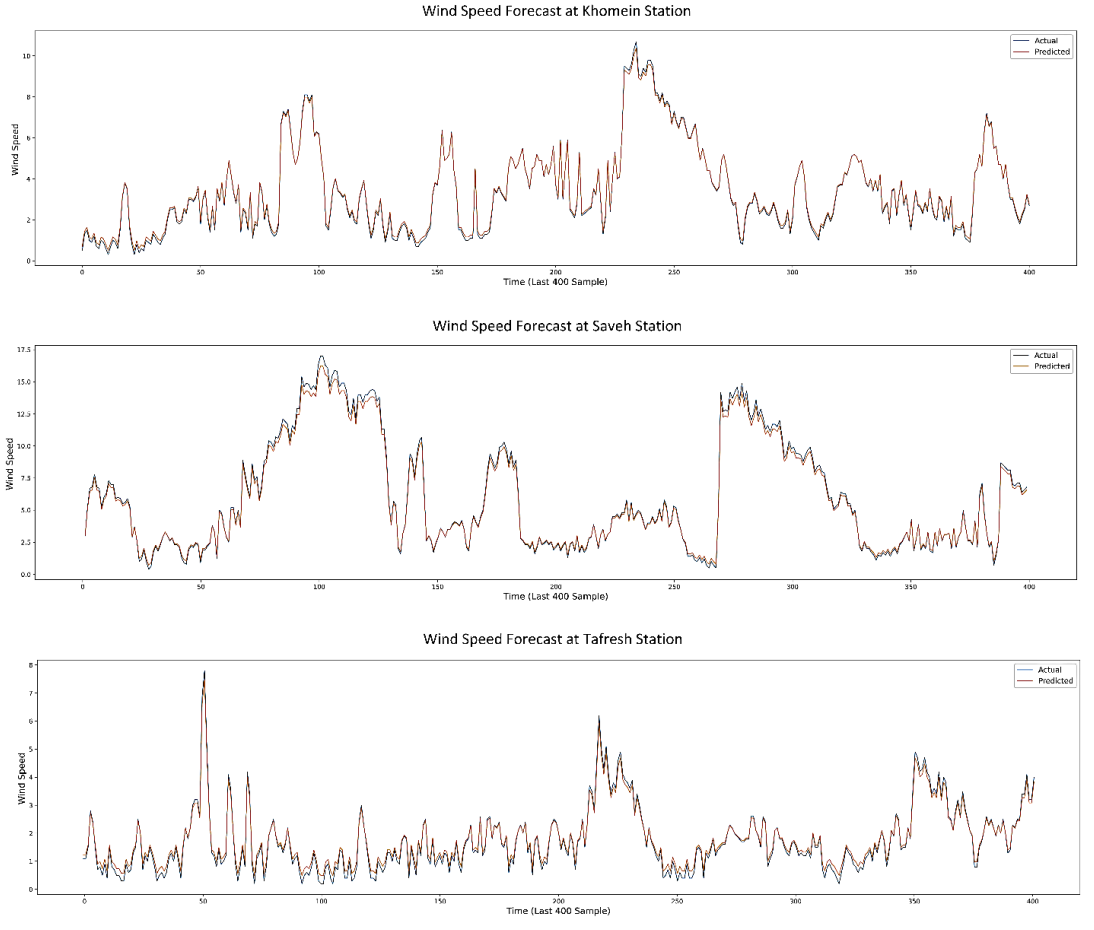

Figure 3. Comparison between the actual and predicted wind speeds at Khomein, Tafaresh and Saveh.

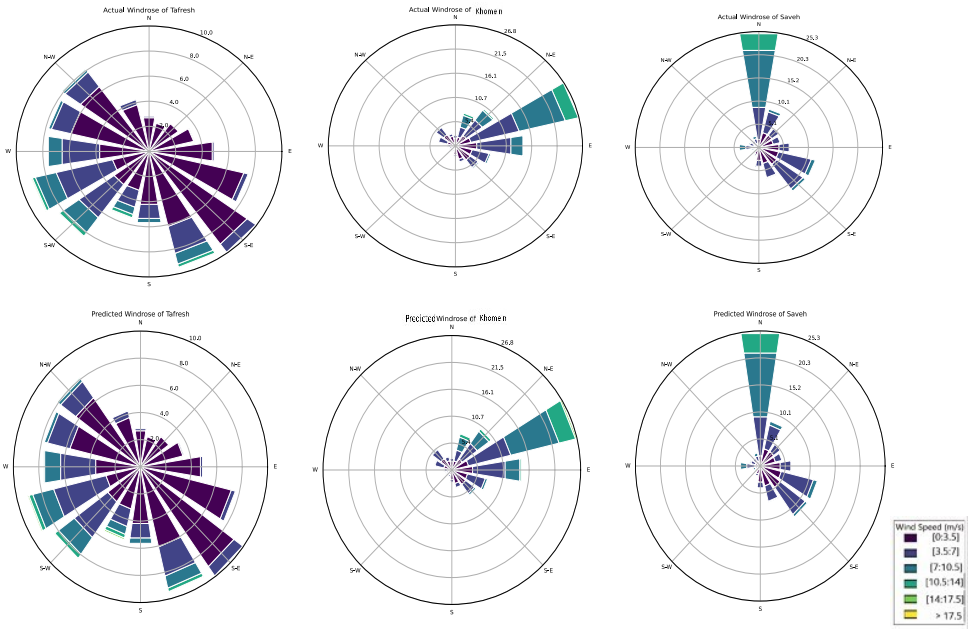

Figure 4. Comparison between actual and predicted wind roses of three stations in the two years of 2018-2020.

5. Conclusion

This study provides a detailed assessment of wind energy potential in Markazi Province, Iran, focusing on the cities of Tafresh, Khomein, and Saveh. Using a combination of statistical methods and artificial intelligence techniques, it evaluates wind patterns, temporal variations, and energy potential in these regions. Data collected over a two-year period from advanced meteorological stations formed the basis for analyzing wind speed and direction, enabling a comprehensive understanding of wind behavior.

The Weibull distribution and wind rose diagrams revealed significant variations in wind characteristics across the three locations. Saveh emerged as the most suitable area for wind energy development, given its consistent and higher wind speeds, while Khomein showed moderate potential for medium-scale projects. Conversely, Tafresh exhibited limited wind energy potential, making it economically unsuitable for large-scale wind farm investments.

The use of Long Short-Term Memory (LSTM) neural networks added value by predicting wind speeds and temporal patterns with high accuracy. The alignment between the actual and predicted data validated the model's reliability in capturing wind dynamics, including direction and frequency. This predictive capability is crucial for planning future wind energy projects and optimizing energy production strategies.

The calculation of wind power density (WPD) further supported these findings, with Saveh showing the highest potential for efficient wind energy exploitation. These insights underline the importance of site-specific data in designing wind farms and selecting appropriate technologies for maximum efficiency.

This research demonstrates the effectiveness of combining statistical and machine learning techniques in wind resource assessment. By leveraging these approaches, decision-makers can make informed choices about renewable energy investments, enhancing sustainability in energy production. Additionally, the study emphasizes the role of wind energy in reducing dependence on fossil fuels, mitigating environmental impacts, and supporting Iran's goals for sustainable development.

References

[1] T. V. Ramachandra, and B. V. Shruthi, "Spatial Mapping of Renewable Energy Potential," *Renewable and Sustainable Energy Reviews*, vol. 11, no. 7, pp. 1460–1480, 2007.

[2] M. Bahrami, and P. Abbaszadeh, "An Overview of Renewable Energies in Iran," *Renewable and Sustainable Energy Reviews*, vol. 24, pp. 198–208, 2013.

[3] J. Wu, J. Wang, and D. Chi, "Wind Energy Potential Assessment for the Site of Inner Mongolia in China," *Renewable and Sustainable Energy Reviews*, vol. 21, pp. 215–228, 2013.

[4] C. İlkiliç, "Wind Energy and Assessment of Wind Energy Potential in Turkey," *Renewable and Sustainable Energy Reviews*, vol. 16, no. 2, pp. 1165–1173, 2012.

[5] M. D. Farahani, S. Sharafi, and A. Farahani " Application of Remote Sensing in Wind Power Plant Location," *Journal of Green Energy Research and Innovation*, vol. 2, no. 1, pp. 57-65, 2025.

[6] L. Roubeyrie, and S. Celles, "Windrose: A Python Matplotlib, Numpy Library to Manage Wind and Pollution Data, Draw Windrose," *Journal of Open Source Software*, vol. 3, no. 29, 268, 2018.

[7] M. W. Ahmad, J. Reynolds, and Y. Rezgui, "Predictive Modelling for Solar Thermal Energy Systems: A Comparison of Support Vector Regression, Random Forest, Extra Trees and Regression Trees," *Journal of Cleaner Production*, vol. 203, pp. 810–821, 2018.

[8] R. Pandit, D. Infield, and M. Santos, "Accounting for Environmental Conditions in Data-Driven Wind Turbine Power Models," *IEEE Transactions on Sustainable Energy*, vol. 14, no. 1, pp. 168–177, 2023.

[9] A. A. Karimi Taleb, H. Makvandi, and A. Oraee, "The Impact of Wind Direction on Wind Farms' Output Power and Income," *Journal of Green Energy Research and Innovation*, vol. 1, no. 1, pp. 34–47, 2024.

[10] S. S. Ahmad, A. Al Rashid, et al., "Feasibility Analysis of Wind Energy Potential Along the Coastline of Pakistan," *Ain Shams Engineering Journal*, vol. 13, no. 1, 101542, 2022.
[11] A. Karamali, A. Daeichian, and S. Rezaei, "Using Long Short-Term Memory Networks as Virtual Wind Direction Sensors for Improved Wind Farm Turbines Orientation," *2024 9th International Conference on Technology and Energy Management (ICTEM)*, pp. 1–5, 2024.
[12] H. Yousefi, H. Hafeznia, and A. Yousefi-Sahzabi, "Spatial Site Selection for Solar Power Plants Using a GIS-Based Boolean-Fuzzy Logic Model: A Case Study of Markazi Province, Iran," *Energies*, vol. 11, no. 7, 1648, 2018.
[13] E. Kavak Akpinar, and S. Akpinar, "A Statistical Analysis of Wind Speed Data Used in Installation of Wind Energy Conversion Systems," *Energy Conversion and Management*, vol. 46, no. 4, pp. 515–532, 2005.
[14] A. Mayhoub, and A. Azzam, "A Survey on the Assessment of Wind Energy Potential in Egypt," *Renewable Energy*, vol. 11, no. 2, pp. 235–247, 1997.
[15] H. Bagiorgas, M. Assimakopoulos, D. Theoharopoulos, D. Matthopoulos, and G. Mihalakakou, "Electricity Generation Using Wind Energy Conversion Systems in the Area of Western Greece," *Energy Conversion and Management*, vol. 48, no. 5, pp. 1640–1655, 2007.
[16] H. Arslan, H. Baltaci, B. O. Akkoyunlu, S. Karanfil, and M. Tayanc, "Wind Speed Variability and Wind Power Potential Over Turkey: Case Studies for Çanakkale and İstanbul," *Renewable Energy*, vol. 145, pp. 1020–1032, 2020.
[17] A. Sherstinsky, "Fundamentals of Recurrent Neural Network (RNN) and Long Short-Term Memory (LSTM) Network," *Physica D: Nonlinear Phenomena*, vol. 404, 132306, 2020.
[18] X. Le, H. V. Ho, G. Lee, and S. Jung, "Application of Long Short-Term Memory (LSTM) Neural Network for Flood Forecasting," *Water*, vol. 11, no. 7, p. 1387, 2019.
[19] X. Song, Y. Liu, et al., "Time-Series Well Performance Prediction Based on Long Short-Term Memory (LSTM) Neural Network Model," *Journal of Petroleum Science and Engineering*, vol. 186, 106682, 2020.
[20] G. Van Houdt, C. Mosquera, and G. Nápoles, "A Review on the Long Short-Term Memory Model," *Artificial Intelligence Review*, vol. 53, no. 8, pp. 5929–5955, 2020.
[21] M. Ghouchani, M. Taji, A. S. Cheheltani, and M. S. Chehr, "Developing a Perspective on the Use of Renewable Energy in Iran," *Technological Forecasting and Social Change*, vol. 172, 121049, 2021.
[22] M. G. N. M. Abad, A. A. Ghadimi, M. Ebadi, and A. Daeichian, "Lyapunov-Based Model Predictive Control for a Single-Phase Grid-Connected Cascaded Multilevel Asymmetrical Inverter," *International Journal of Electrical Power & Energy Systems*, vol. 147, 108789, 2023.
[23] M. Pirzadi, A. A. Ghadimi, and A. Daeichian, "Distributed Multi-Agent Transmission System Restoration Using Dynamic Programming in an Uncertain Environment," *Electric Power Systems Research*, vol. 196, 107270, 2021.

Declaration of competing interest

The authors declare that they have no known competing financial interests or personal relationships that could have appeared to influence the work reported in this paper. The ethical issues, including plagiarism, informed consent, misconduct, data fabrication and/or falsification, double publication and/or submission, redundancy, have been completely observed by the authors.

Bibliography

Amir Hossein Karamali was born in 2000 in Mahallat, Iran. He completed his bachelor's degree in Electrical Engineering at Arak University in 2022, and is currently pursuing a master's degree in Power Electronics and Electric Machines at Iran University of Science and Technology (IUST). His research focuses on power electronics and the application of artificial intelligence in power systems, aiming to contribute to the development of advanced technologies for a sustainable future.
Email: amirhosseinkaramali@gmail.com
ORCID: 0009-0008-2320-9719
Contribution Statement: Data curation, Formal analysis, Software, Validation, Visualization, Roles/Writing-original draft.

Abolghasem Daeichian was born in Iran, in 1982. He received the Bachelor's degree in electrical engineering from the Isfahan University of Technology in 2003, and the M.Sc. and Ph.D. degree in control engineering from Shiraz University and Isfahan University of Technology in 2006 and 2014, respectively. He visited Australian National University in 2012. Since 2017, he has been with the Department of Electrical Engineering, Faculty of Engineering, Arak University, where he is currently an Associate Professor. He was the head of Research Institute of Renewable Energy, Arak University, Arak, Iran from 2021 to 2023 and the IT manager at Arak University from 2023 to 2024. His research interests include estimation & filtering, stochastic control, quantum control, and cyber-physical systems. Dr. Daeichian is a fellow of the Iranian Society of Instrumentation and Control Engineers.
Email: a-daeichian@araku.ac.ir
ORCID: 0000-0002-6318-579X
Contribution Statement: Conceptualization, Methodology, Project administration, Supervision, Writing-review & editing.

Saber Rezaei was born in 1996 in Tehran, Iran. He completed his bachelor's degree in Electrical Engineering with a focus on Control Engineering at Semnan University in 2020. Currently, he is pursuing a Master's degree in Neurocognitive Engineering at Iran University of Science and Technology (IUST). His expertise lies in signal processing, artificial intelligence and machine learning, with a particular interest in deep learning and its applications in biomedical engineering.
Email: s-rezaei@elec.iust.ac.ir
ORCID: 0009-0002-3733-2108
Contribution Statement: Data curation, Formal analysis, Software, Validation, Visualization, Roles/Writing-original draft.

Ali Reihanian received his B.Sc. degree in Information Technology (IT) from Mazandaran University of Science and Technology, Iran, in 2011. He received his M.Sc. degree in Information Technology (IT), with special focus on Artificial Intelligence, from Mazandaran University of Science and Technology, Iran, in 2014. He also received his Ph.D. degree in Artificial Intelligence and Robotics from University of Tabriz, Iran, in 2018. Since 2021, he has been with the Department of Computer Engineering, Faculty of Engineering, Arak University, where he is currently an Assistant Professor. Also, he has been the head of Research Institute of Artificial Intelligence, Arak University, Arak, Iran, since 2023. His research interests include machine learning and pattern recognition, social network analysis, natural language processing and data mining.

Email: a-reihanian@araku.ac.ir

ORCID: 0000-0001-6668-3535

Contribution Statement: Methodology, Supervision, Writing-review & editing.

Journal of Green Energy Research and Innovation

Improving the Absorption Bandwidth in Carbon-Based Perovskite Cells with A Combined Light Trapping Structure

Bahareh Boroomandnasab, Salem Doreghi

Highlights

- **Combines silver-silica nanoparticles and PMMA anti-reflective coating to boost absorption in carbon-based perovskite solar cells.**
- **Uses 100 nm radius nanoparticles, 280 nm period, 2 nm silica shell, and 60 nm PMMA for near-total light absorption.**
- **Achieves 25.264 mA/cm^2 short-circuit current, 22% better than reference cells.**
- **Enables 600 nm perovskite layers to match thicker ones, reducing lead use despite fabrication challenges.**

Graphical Abstract

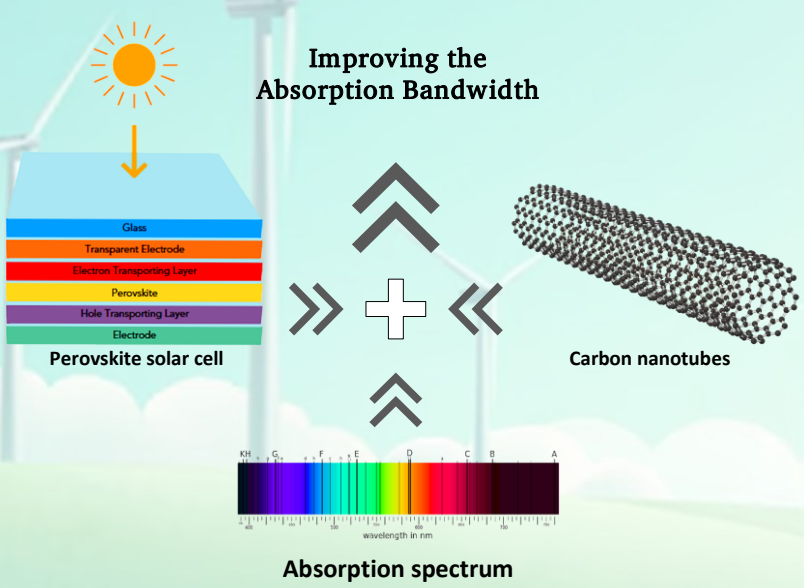

Use your device to scan and read the article online

Citation

B. Boroomandnasab, and S. Doreghi," Improving the Absorption Bandwidth in Carbon-Based Perovskite Cells with A Combined Light Trapping Structure," *Journal of Green Energy Research and Innovation*, vol. 2, no. 2, pp. 36-47, 2025.

https://doi.org/10.61186/jgeri.2.2.36

Journal of Green Energy Research and Innovation 2.2 (2025) 36-47

Online ISSN: 3041-9018

Journal of Green Energy Research and Innovation

Journal Homepage: www.jgeri.araku.ac.ir

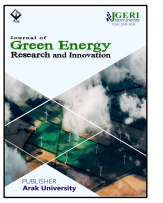

Improving the Absorption Bandwidth in Carbon-Based Perovskite Cells with A Combined Light Trapping Structure

Bahareh Boroomandnasab [*] , Salem Doreghi

Department of Electrical and ICT, Faculty of Technical Engineering, Institute for Higher Education, ACECR, Khouzestan, IRAN.

A R T I C L E I N F O

Keywords:
Perovskite solar cells,
Nanoparticles,
Absorption enhancement,
Light trapping.

Article History:
Received: 26 February 2025;
Revised: 15 March 2025;
Accepted: 18 March 2025.

Article type:
Research Article

* ***Corresponding author***
E-mail address
boroomand@acecr.ac.ir (B. Boroomandnasab)

A B S T R A C T

The research introduces a hybrid light trapping structure designed to enhance the absorption bandwidth in carbon-based perovskite solar cells. Silver nanoparticles coated with silica are included within the active layer of this structure. An anti-reflective coating is applied to the upper surface to enhance the absorption of additional wavelengths. The influence of geometric parameters, such as the radius and period of silver nanoparticles, the thickness of the silica protective shell, and the thickness of the anti-reflection coating, on light absorption is examined. The finite difference time domain technique in Lumerical software is employed to examine the specified parameters. A carbon-based perovskite solar cell was first introduced as a reference, followed by an examination of the proposed structure utilizing various geometric light absorption factors. The simulation findings indicate that nearly total light absorption may be attained using the ideal structural parameters for a 600 nm thick perovskite layer utilizing this configuration. A short-circuit current density of 25.264 mA/cm^2 can be attained utilizing silver-silica nanoparticles with a radius of 100 nm, a period of 280 nm, and a 60 nm thick PMMA anti-reflection coating over a 600 nm thick perovskite layer. This metric indicates a 22% enhancement relative to carbon-based perovskite solar cells lacking light control. The suggested hybrid light-trapping architecture enhances light usage and reduces material consumption in carbon-based perovskite solar cells.

1. Introduction

Improving the absorption bandwidth in carbon-based perovskite solar cells (CBPSCs) can significantly enhance their efficiency by allowing them to capture a broader spectrum of sunlight. A combined light trapping structure is one approach to achieve this. Here are some key aspects and strategies involved:

1. Concept of Light Trapping:
- Light Trapping Structures: Implementing structures such as textured surfaces, photonic crystals, or nanostructures can increase the effective path length of light within the active layer of the solar cell, resulting in more absorption.
- Multiple Scattering: Light trapping techniques can lead to multiple scattering events that allow light to be absorbed more effectively, particularly in thinner films.

2. Carbon-based Perovskites:
- Advantages: Carbon-based perovskites, such as MAPbI3 (where MA is methylammonium) or FAPbI3 (formamidinium), are known for their stability and non-toxicity compared to traditional lead-based perovskites.
- Higher Bandgap Tuning: These materials can be engineered to have a bandgap that is better suited for light absorption in the visible and near-infrared regions.

3. Strategies for Enhancing Absorption Bandwidth:
- Use of Nanostructures: Incorporating nanoparticles or nanowires into the perovskite layer can scatter light and enhance absorption over a wider range of wavelengths.
- Hybrid Structures: Combining organic materials with perovskites or using layered structures can help in optimizing the light absorption characteristics.

- Optimizing Thickness: Adjusting the thickness of the perovskite layer can also play a crucial role, as an optimal thickness can maximize light absorption while maintaining charge transport efficiency.

4. Simulation and Modeling:

- Optical Simulations: Computational techniques, such as finite-difference time-domain (FDTD) simulations or transfer matrix methods, can be utilized to model light interaction with the device and optimize the design of the light-trapping structures.

5. Experimental Validation:

- Device Fabrication: Fabricating devices using the proposed light trapping structures and testing them under standard solar conditions can help in evaluating their performance and absorption characteristics.
- Characterization Techniques: Employing techniques such as UV-Vis spectroscopy can help in measuring the absorption spectra and understanding how effectively the device captures light across different wavelengths.

Recently, perovskite solar cells (PSCs) have attracted the attention of many researchers in electronics because of lower manufacturing cost and good optical features [1-3]. The efficiency of these cells has increased from 3.8% in 2009 to 25.5% in 2020 [4,5]. Most high-efficiency perovskite cells use a metal electrode such as gold or silver as the back electrode because these electrodes act as a reflector for light that is not absorbed in the initial passage through the cell and by reflecting this light, they increase the light path in the active layer, thus improving absorption [6]. Of course, in addition to numerous advantages, the metal electrode also has disadvantages such as increased manufacturing cost and low stability. Carbon is used as a substitute for the metal electrode in carbon-based perovskite cells (CBPSCs) due to its low price, excellent stability, abundance of materials, and effective operability. Despite these advantages, carbon, due to its non-reflective nature, limits the optical gain of the cell, especially at long wavelengths that are not absorbed in the primary path [7]. Therefore, the use of optical trapping approaches to raise the optical path in CBPSCs is crucial. The conventional light trapping methods cannot be adopted for PSCs because of the large compound size compared to the thickness of the perovskite. Thus, nanometer-scaled light trapping structures, like plasmonic metal nanoparticles, photonic crystals, diffraction gratings, and anti-reflection layers, are preferred to reach larger light absorption in PSCs. With the same token, the plasmonic impacts of metal nanoparticles are extensively incorporated to improve the operation of solar cells thanks to their ease of manufacturing process. Surface plasmon resonance in PSCs have greatly been focused lately and many works have been presented in this realm [8]. Placing metal nanoparticles in the perovskite active layer (PAL) and exciting the surface resonances assists in improving the electric field around the nanoparticles and enhance the light absorption [9]. Meanwhile, silver nanoparticles are suitable for photovoltaic applications due to their strong plasmonic resonances. Nonetheless, because of their strong reactivity with halide ions, silver nanoparticles are easily corroded when directly contacted with perovskite. In addition, their direct contact creates electric charge recombination regions [10]. When silver nanoparticles are coated with silica materials to prevent direct contact with the active layer, more acceptable performance is achieved for photovoltaic systems. Up to this date, a majority of studies related to light trapping have focused on single structures, few of which have studied the combination of different light management schemes [11]. While prior studies have independently explored plasmonic nanoparticles (e.g., Ag) or anti-reflective coatings (e.g., PMMA) for light trapping, their synergistic integration in carbon-based perovskite solar cells (CBPSCs) has not been systematically investigated. Existing designs suffer from either narrow bandwidth (e.g., SiO_2-only coatings) or instability (e.g., Ag aggregation). This work introduces a hybrid Ag-SiO_2/PMMA structure that uniquely combines plasmonic resonance (400–800 nm) with graded refractive index matching, achieving a 25% enhancement in JSC compared to conventional configurations. The novelty lies in optimizing the nanoparticle core-shell ratio ($Ag:SiO_2$ = 3:1) to minimize parasitic absorption while ensuring compatibility with solution-processed carbon electrodes. In addition to providing silver nanoparticles with silica coating, an anti-reflective coating of polymethyl methacrylate (PMMA) has been placed on the front surface of the cell to absorb long wavelengths. This material is a synthetic polymer. It is a very hard, transparent material with excellent resistance to ultraviolet radiation and air. Its light-conducting property is the most prominent feature of this material, which are able to positively enhance the light absorption bandwidth in CBPSCs.

The paper is structured as follows: Section 2 details the simulation framework, including material parameters, boundary conditions, and optical models. Section 3 presents the optimization of Ag/SiO_2 nanoparticle geometry (radius, period) and PMMA coating thickness, evaluating electrical performance, highlighting trade-offs between JSC enhancement and voltage stability, discussing fabrication challenges and future experimental directions. Conclusions are summarized in Section 4.

2. Fundamentals and simulation details

The FDTD simulations were performed using Lumerical Suite 2022, with a mesh size of 1 nm to resolve nanoparticle geometries. Periodic boundaries conditions were applied along the x-y axes, and perfectly matched layers (PMLs) were used in the z-direction to suppress artificial reflections. A convergence test confirmed that a simulation time of 1,000 fs ensured numerical stability. The optical absorption was calculated using Equation (1), where the divergence of the Poynting vector ($\nabla \cdot S \nabla \cdot \mathbf{S}$) accounts for both absorption and scattering losses in the active layer. Figure 1 illustrates the schematic of the carbon-based perovskite cell, depicting both the suggested structure and the reference carbon-based perovskite cell, which comprises five layers: ITO, TiO2, CH3NH3PbI3, Spiro-OMeTAD, and a carbon electrode. The thicknesses of these five layers are 50 nm, 90 nm, 400 nm, 70 nm, and 100 nm, respectively. CH3NH3PbI3 was selected as the active layer because of its ease of production and appropriate energy bandgap. Spiro-OMeTAD was employed as the hole transport layer (HTL) because to its prevalent utilization in high-efficiency perovskite cells at the laboratory scale. The complicated refractive index of these materials, utilized to characterize their optical properties, is sourced from multiple databases and publications [12,13]. Key simulation parameters and assumptions are given in Table 1, during the simulation; we implemented periodic boundary conditions and a perfectly matched layer (PML) in the lateral and incidence directions of the light source, respectively. A plane wave light source with a wavelength range of 300 nm to 800 nm was examined, aligning with the

energy gap of the perovskite (1.55 eV).

The absorbed optical power per unit volume (Pabs) can be expressed as:

$$p_{abs} = -\frac{1}{2}\omega|E|^2 imag(\varepsilon) \quad (1)$$

Equation (1) assumes a linear optical response and neglects non-linear effects, as the incident light intensity is within the typical solar irradiance range (~100 mW/cm^2). The permittivity (ε) is treated as wavelength-dependent, derived from experimentally validated data [12,13], ensuring the model aligns with real material behavior. Carrier generation rates are presumed proportional to the local electric field intensity, a valid approximation under low-injection conditions.

In this context, imag(ε) denotes the imaginary component of the material's permittivity, ω signifies the angular frequency of the light, and |E| indicates the intensity of the electric field. To examine the variations in solar cell performance with and without light trapping structures, we computed the absorption enhancement factor (G), defined as follows [14].

$$G = \frac{\int \lambda P_{LT}(\lambda) I_{AM1.5}(\lambda)\, d\lambda}{\int \lambda P_{ref}(\lambda) I_{AM1.5}(\lambda) d\lambda} \quad (2)$$

Equation (2) quantifies absorption enhancement by comparing the integrated absorbed power (PLT) of the proposed structure to a reference cell. The AM1.5G spectrum weights each wavelength, ensuring relevance to real-world solar conditions. This metric excludes parasitic absorption in Ag nanoparticles, focusing solely on useful perovskite absorption a critical distinction from prior works [8,9].

P_{ref} (λ) and P_{LT} (λ) denote light absorption in the absence and presence of the light trapping structure, respectively. The undesired absorption of metal nanoparticles mostly transforms light energy into heat rather than enhancing the light flow; hence, we focused solely on the absorption of perovskite in our light flux calculations, omitting the light absorbed by plasmonic nanoparticles. $I_{AM1.5}$(λ) is the air mass of the solar spectrum radiation, quantified as 1.5. Assuming that all electron-hole pairs are captured by the electrodes, the short-circuit current density (J_{SC}) can be computed as follows in Equation (3) [15].

$$J_{SC} = e\int \frac{\lambda}{hc} P_{abs}(\lambda) I_{AM1.5}(\lambda) d\lambda \quad (3)$$

Note that h is Planck's constant, λ denote the wavelength, c represents the speed of light in free space, and e denotes the initial charge.

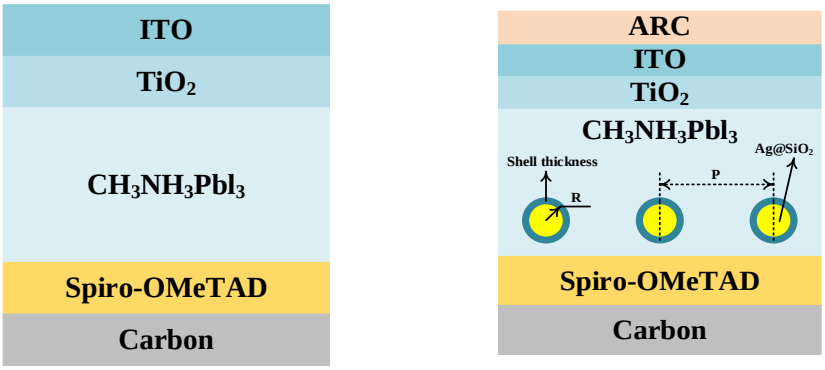

Figure 1. a) Reference perovskite cell, b) Proposed perovskite cell.

Table 1. Key simulation parameters and assumptions.

Parameter	Value/Range	Source
Perovskite thickness	200–1000 nm	Optimized in this work
Ag nanoparticle radius	20–140 nm	Section 3.1
PMMA coating thickness	0–100 nm	Section 3.4
Illumination spectrum	AM1.5G (300–800 nm)	ASTM G173-03
Mesh accuracy	2 nm	Lumerical default settings

3. Results and discussion

3.1. Optimization of nanoparticle radius

This section examines the influence of the core radius (R) of core-shell silver-silica (Ag/SiO2) nanoparticles on absorption enhancement. This is a significant area of study in nanotechnology and plasmonics, particularly in applications such as photothermal therapy, biosensing, and enhancing the photonic response in solar cells. Here are some key points regarding how the core radius affects absorption enhancement:

1. Plasmon Resonance:
- Localized Surface Plasmon Resonance (LSPR): Core-shell Ag/SiO2 nanoparticles exhibit plasmonic behavior due to the presence of silver. The plasmonic resonance is highly sensitive to the size, shape, and environment of the nanoparticles.
- Impact of Core Radius: The core radius directly affects the resonance frequency of the localized surface plasmons. Generally, as the core radius increases, the resonance shifts in wavelength and can lead to enhanced absorption at longer wavelengths (red shift).

2. Absorption Enhancement Mechanisms:
- Scattering and Absorption: Larger core radii can lead to increased scattering cross-sections. This results in a higher ratio of light scattered by the nanoparticles, which can enhance the effective absorption when these nanoparticles are illuminated.
- Near-Field Enhancement: The electromagnetic field near the surface of the nanoparticles amplifies the light intensity. This near-field effect can be more pronounced for larger nanoparticles, leading to higher absorption rates within adjacent materials, such as a perovskite layer in a solar cell.

3. Hybridization of Plasmon Modes:
- Multiple Modes of Resonance: Core radius can affect the hybridization of plasmon modes in the core and shell materials. When R increases, the interactions between these modes can lead to more complex resonance behaviors, which can be engineered to optimize absorption characteristics.
- Effect of Shell Thickness: The thickness of the silica shell also plays a role. A thicker shell may shield the core's plasmonic effect, while an optimal thickness can fine-tune the plasmonic resonance and enhance absorption capabilities.

4. Absorption Spectrum Tuning:
- Dependence on Composition: The material properties, including the dielectric constant of the shell (SiO2) and the core (Ag), affect how the absorption spectrum changes with varying R. This allows for fine-tuning the absorption spectrum according to application needs, such as targeting specific wavelengths for photothermal applications.

5. Applications in Enhancing Photovoltaics:
- In Solar Cells: Incorporating Ag/SiO2 nanoparticles into the active layer of solar cells can improve light absorption and efficiency. The ability to tune the core radius allows researchers to maximize the light-trapping effect, leading to better performance in energy conversion.

6. Experimental and Simulation Studies:
- Optimization Studies: Experimental studies and numerical simulations (e.g., FDTD methods) can be employed to investigate how varying the core radius influences absorption rates. These studies are crucial in determining the optimal design for specific applications.

In this particular study, the radius of the silver nanoparticles ranges from 20 to 140 nm, with a constant shell thickness of 2 nm and a fixed period of 300 nm. Figure 2 illustrates the absorption spectra within the PAL as a function of nanoparticle radius. Table 2 and Figure 2(b) illustrate that the absorbance enhancement coefficient (G) varies with nanoparticle radius. Initially, G increases with the nanoparticle radius, attaining a peak value of 1.106 at a radius of 100 nm, before thereafter declining with further increases in radius. Larger metal nanoparticles, as illustrated in Figure 3, are correlated with increased light scattering in their vicinity, resulting in greater absorption enhancement. Nonetheless, when the radius beyond a specific threshold, the advantageous optical impact of the nanoparticles fails to offset the depletion of active material, hence constraining the overall absorption. The simulation indicates that a core radius of 100 nm yields optimal enhancement in light absorption. Figure 2(b) demonstrates that the incorporation of silver-silica nanoparticles enhances light absorption at longer wavelengths, specifically from 600 to 800 nm, in contrast to light absorption without light trapping. This enhancement results from the activation of localized surface plasmon resonances inside the active layer. The electric field generated by plasmon excitation enhances light absorption in the active layer. Moreover, the nanoparticles serve as scattering centers for light emission, extending the route length for photons and consequently enhancing their absorption probability in the active layer. Consequently, the core radius of silver-silica nanoparticles is deemed to be 100 nm in the next calculations.

Table 2. G values as a function of nanoparticle radius.

Radius(nm)	20	40	60	80	100	120	140
G	1.0016	1.0176	1.0416	1.0783	1.1068	1.0802	1.0558

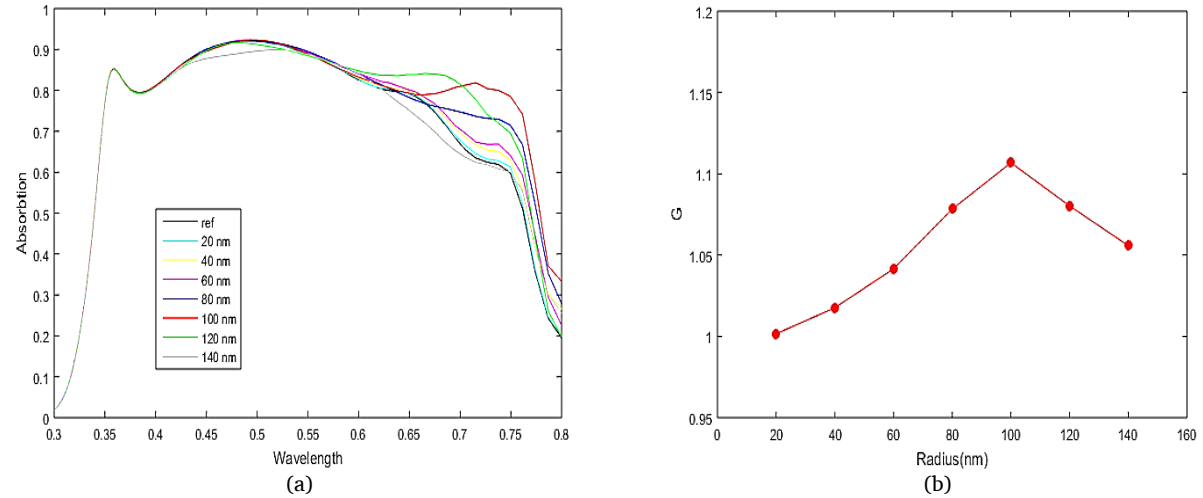

(a) (b)

Figure 2. Absorption spectrum (a) and absorption enhancement factor (b) of the active layer as a function of nanoparticle radius.

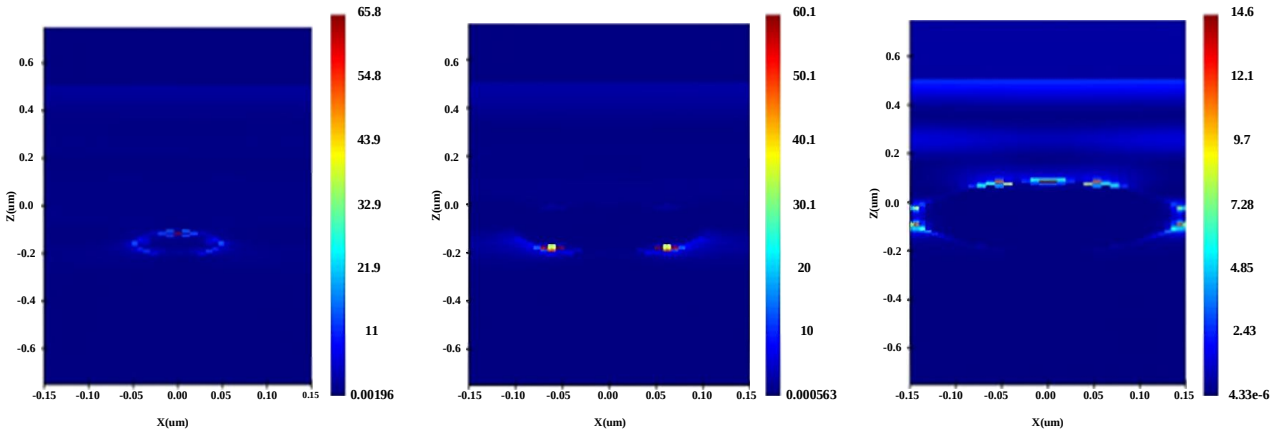

Figure 3. Electric field intensity profiles for radii of 40, 100, and 140 nm generated using Lumerical FDTD simulations.

3.2. Optimization of the period of nanoparticles

This section examines the influence of the period (P) of silver-silica nanoparticles by calculating the variations in G and the absorption spectra for various periods, maintaining a constant radius of 100 nm. The period (P) of silver-silica (Ag/SiO2) nanoparticles, particularly in a structured array or periodic arrangement, can significantly influence their optical properties, including absorption and scattering characteristics. Here are some key aspects regarding the influence of the period on the behavior and performance of these nanoparticles:

1. Periodic Structures and Plasmonic Effects:
- Plasmonic Coupling: When silver nanoparticles are arranged in a periodic manner, they can exhibit coupling effects due to their plasmonic resonances. The spacing (period) affects how these resonances interact, leading to collective behaviors that can modify the overall optical response.
- Bragg Diffraction: In periodic structures, the arrangement can lead to Bragg diffraction effects, where certain wavelengths of light are strongly reflected or transmitted based on the periodicity of the structure.

2. Absorption Enhancement:
- Tuning Absorption Peaks: The period of the nanoparticles can be engineered to tune the LSPR absorption peaks. Periodic arrangements can enhance the effective absorption of light by enabling constructive interference for specific wavelengths, thus amplifying absorption at those wavelengths.
- Enhanced Local Fields: As the period becomes comparable to the wavelength of light, the interactions among the nanoparticles can create enhanced localized electric fields, thereby increasing the absorption of light in the material interacting with the nanoparticles, such as a nearby semiconductor in solar cells.

3. Optical Band Structure:
- Photonic Band Gaps: The arrangement of nanoparticles can create a photonic band gap where certain wavelengths are prevented from propagating. This can be utilized to selectively enhance absorption at specific wavelengths, depending on

the design of the periodic structure.

- Modified Dispersion Relations: The period affects the dispersion relations of the plasmons, potentially leading to new modes that can absorb light more effectively.

4. Effect on Energy Transfer:

- Near-field Coupling: The distance between nanoparticles (i.e., the period) influences near-field interactions. A shorter period can enhance energy transfer between nanoparticles, allowing for efficient coupling to nearby materials or adjacent nanoparticles.
- Spatial Distribution: The geometrical arrangement provided by the period can impact how energy is transferred, absorbed, or scattered in a composite system, particularly in applications like photothermal therapy or in photovoltaics where energy distribution is critical.

5. Dependence on Polymer/Matrix Material:

- Matrix Interaction: The surrounding medium or matrix (e.g., SiO2) affects how the period influences the optical properties. The dielectric contrast between the silver core and the silica shell, along with the matrix material, can significantly alter how the period impacts the absorption and scattering.

6. Simulation and Experimental Validation:

- Computational Modeling: Numerical simulations, such as Finite Element Method (FEM) or FDTD methods, can provide insights into how changing the period influences the operational parameters of the nanoparticles.
- Experimental Measurements: Experimental techniques like UV-Vis spectroscopy, scattering measurements, and surface-enhanced Raman spectroscopy (SERS) can be used to confirm theoretical predictions on the effects of period on absorption and other optical characteristics.

The nanoparticle period ranges from 220 nm to 360 nm in 20 nm increments. Figure 4 and Table 3 indicate that the value of G enhances with an increasing period until the nanoparticle period attains its maximum at 280 nm. This enhancement is ascribed to the augmentation of the local field. When the nanoparticle period exceeds 280 nm, both G and absorption progressively diminish, as elucidated by the optical transmission spectrum in Figure 5. The transmission from the active layer initially diminishes as the nanoparticle period increases from 220 to 280 nm, subsequently rising with further increases in the nanoparticle period. This suggests that the incident light is not efficiently absorbed by the active layer; instead, it passes through the rear surface of the perovskite layer.

Table 3. G values are a function of nanoparticle period.

Period(nm)	220	240	260	280	300	320	340	360
G	1.101	1.107	1.124	1.134	1.123	1.110	1.108	1.100

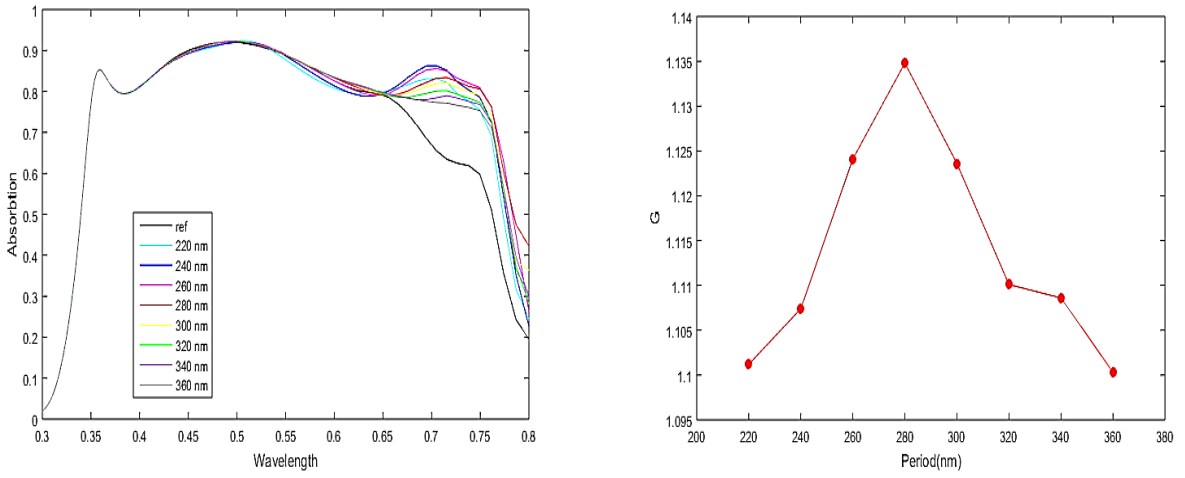

(a) (b)

Figure 4. a) Absorption spectrum, b) Active layer absorption enhancement factor as a function of nanoparticle period generated using Lumerical FDTD simulations.

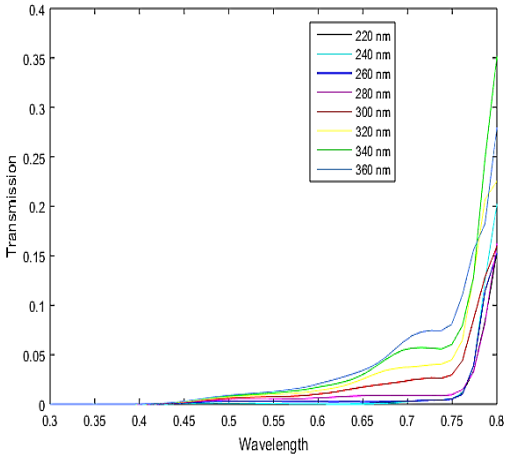

Figure 5. Transmission spectra vs nanoparticle period.

3.3. Effect of silica shell thickness

This section examines the impact of the shell thickness of core-shell silver-silica nanoparticles on absorption enhancement. The slender dielectric layer enveloping the silver nanoparticles not only inhibits direct metal-perovskite contact but also mitigates charge recombination at the semiconductor-metal interface and influences the optical performance of the nanoparticles; thus, simulating its impact on the electric field distribution is crucial. Figure 6 and Table 4 provide the impact of silica shell thickness on light absorption and short-circuit current. The silica shell's existence restricts absorption enhancement at wavelengths between 650 and 800 nm relative to silver nanoparticles lacking a shell. The absorption and short-circuit current progressively diminish with the increasing thickness of the silica shell. This phenomenon can be elucidated by contrasting the electric field intensity profile at 720 nm, both in the absence and presence of a 10 nm thick silica shell, as illustrated in Figure 7. The electric forces are focused around the silver nanoparticles, regardless of the presence of the silica shell. Nonetheless, the electric field is significantly more intense within the silica shell, which, due to its dielectric properties, does not absorb in this region and constrains the field around the nanoparticles, thereby diminishing the absorption improvement in the PAL; consequently, a reduced dielectric shell thickness is advised for optimal optical performance. In the current configuration, we select 2 nm as the ideal shell thickness to minimize current dissipation while preserving the protective efficacy of the corrosive halide in the perovskite layer.

Table 4. Short circuit current values for different shell thicknesses.

Shell Thickness(nm)	0	2	5	10	15	20
J_{sc}(ma/cm^2)	24.017	23.979	23.887	23.365	23.044	22.662

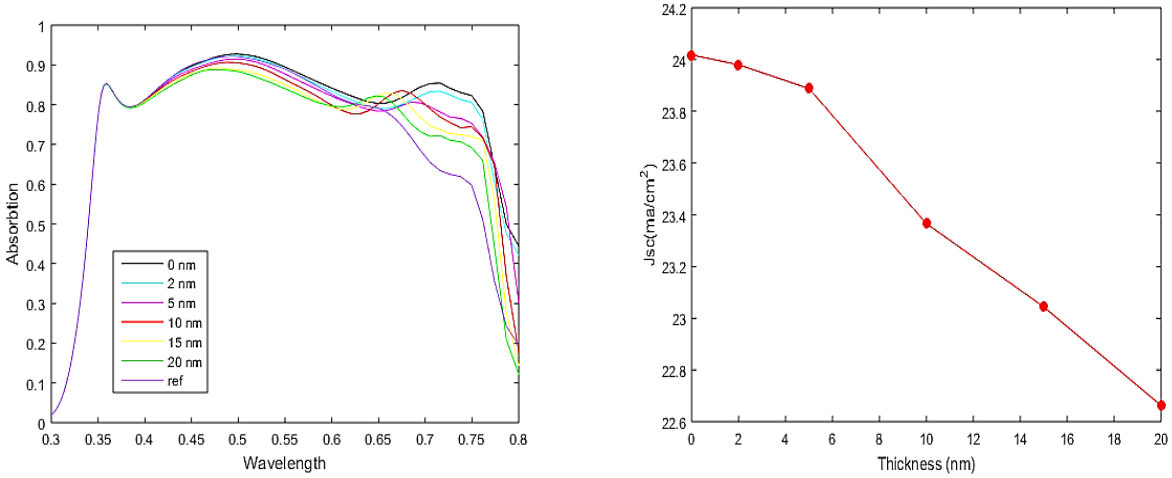

Figure 6. a) Short-circuit current as a function of shell thickness, b) Absorption spectrum.

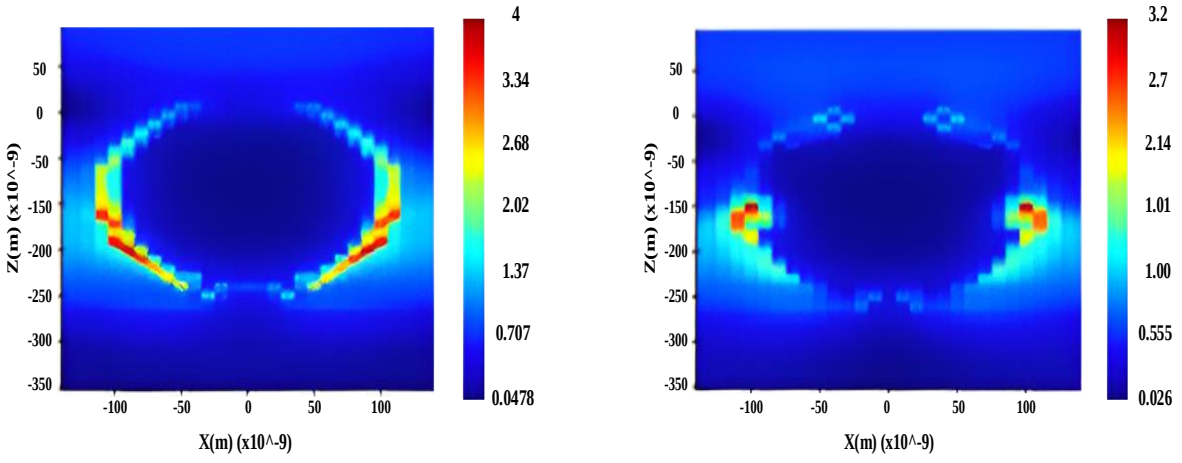

Figure 7. Electric field intensity at a wavelength of 720 nm, a) with a 10 nm thick silica shell, b) without shell.

3.4. Effect of anti-reflective coating on the front surface of the cell

The addition of silver-silica nanoparticles significantly enhances absorption at long wavelengths ranging from 600 to 800 nm due to the plasmon resonance. To optimize the absorption of the perovskite layer, we concentrate on the optical design of the front surface to minimize light loss from the incident direction. Anti-reflection coating (ARC) is extensively utilized in diverse solar cell kinds as an efficient means to diminish light reflection. Three-layer, two-layer, and single-layer anti-reflection coating configurations have all been evaluated to achieve the optimal anti-reflection performance. Here, to simplify real-work actions, a single-layer anti-reflection coating is adopted as the light trapping structure on the front surface of the optimized nanoparticles discussed previously. Previous investigations indicate that PMMA is utilized for anti-reflection coatings. Figure 8 examines the influence of the anti-reflection coating and its thickness on light absorption to achieve an optimal design. The 60 nm thick anti-reflection coating exhibits optimal efficiency. The absorption and reflection spectra for varying thicknesses of the anti-reflection coating, as illustrated in Figure 9, indicate that as the PMMA thickness rises from 0 to 60 nm, there is a corresponding enhancement in the bandwidth absorption within the 450-800 nm range, accompanied by a gradual elevation of the absorption peaks. This escalation results from the reduction in reflectance between 450 and 800 nm. In the case the PMMA thickness exceeds 60 nm, the reflection in the 400 to 550 nm range adversely affects absorption relative to the scenario without an anti-reflection coating; therefore, the optimal PMMA anti-reflection coating thickness in this design is 60 nm. Figure 10 illustrates the distribution of electric field intensity at 600 nm, both with and without anti-reflection coating. The electric field intensity beneath the anti-reflection coating markedly increases due to a substantial portion of the incident light being reflected back into the incident space, resulting in a pronounced interference effect within the structure that diminishes the loss of short wavelengths. Consequently, it enhances absorption in the active layer.

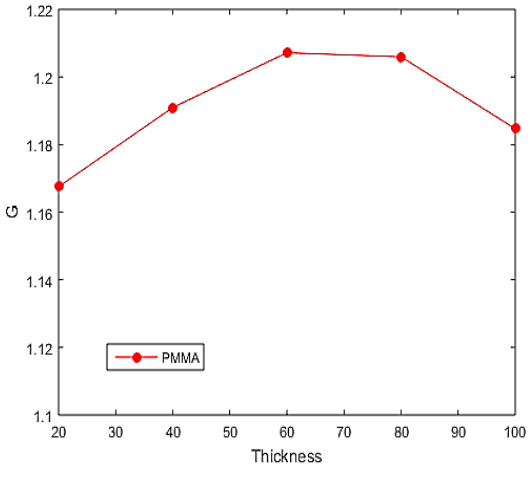

Figure 8. G values as a function of PMMA anti-reflective coating thickness.

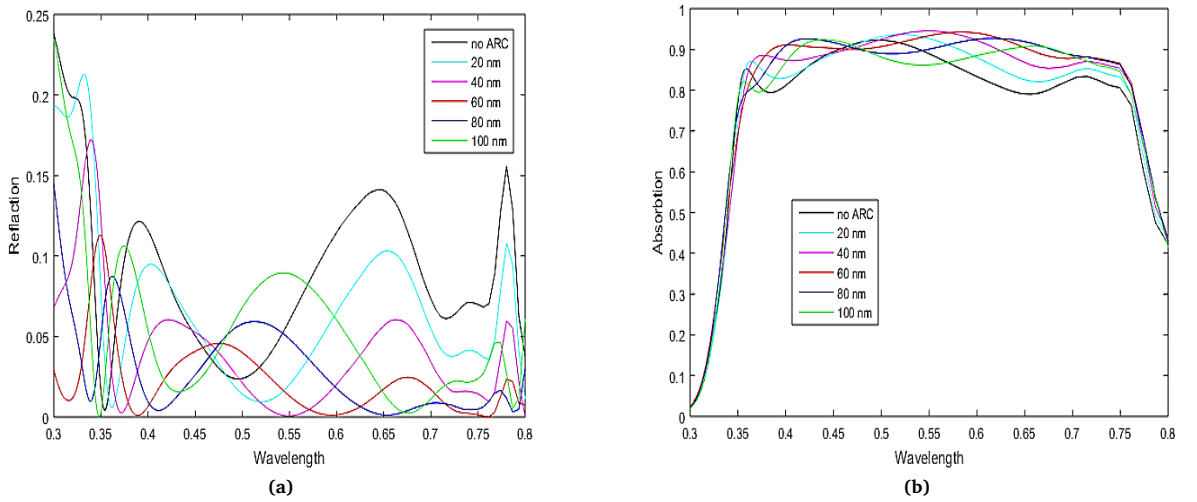

Figure 9. a) Reflectance, b) Absorption spectrum, as a function of anti-reflection coating thickness.

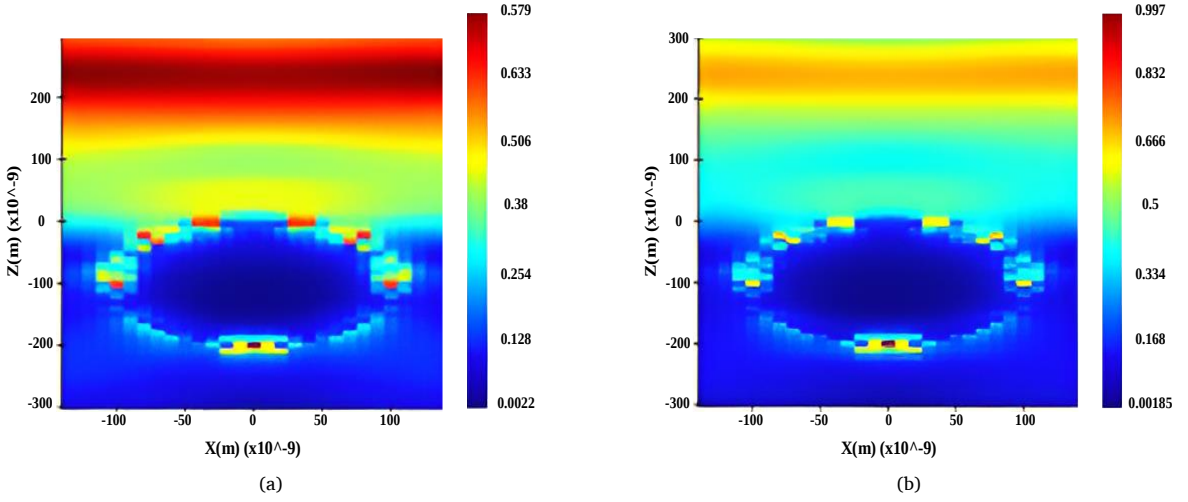

Figure 10. Electric field intensity distribution at a wavelength of 600 nm, a) with 60 nm anti-reflection coating, b) without coating.

3.5. Comparison of the reference and proposed perovskite cells

This part of the paper makes use of and conducts an analysis of the light-harvesting structure that CBPSCs possess. In addition to this, it is essential to investigate the manner in which the light absorption in the active layer varies over the solar spectrum in relation to the thickness of the perovskite. In Figure 11, the absorption spectrum of the 400 nm thick active layer is compared among various cases. These cases include the reference solar cell, solar cells with silver-silica nanoparticles embedded in the perovskite layer, solar cells with a PMMA anti-reflection coating on the top surface, and solar cells with a hybrid structure that traps light. It has been determined that the anti-reflection coating has a thickness of sixty nanometers, and the period and radius of the nanoparticles composed of silver and silica are, respectively, 280 and 100 nanometers. It has been shown that when the perovskite layer is comprised only of silver-silica nanoparticles, the device exhibits the same absorption characteristic as the reference cell when it is exposed to short wavelengths. The LSPR excitation and the scattering effect of the nanoparticles are responsible for the evident enhancement of the perovskite absorber's absorption at wavelengths longer than 550 nm. This comes about as a result of the perovskite absorber's ability to absorb light. The anti-reflection coating made of polymathic methacrylate (PMMA) is applied to the front surface, which results in an increase in absorption throughout a broad wavelength range, from 500 to 800 nm, and a modest rise from 350 to 400 nm. In addition, in order to quantify the enhancement of absorption in various light trapping structures, Table 5 displays the short-circuit current enhancement that was calculated for each of the various light trapping structures. By applying the combined light trapping structure to the carbon-based perovskite solar cell, a relative enhancement of 86.22% is obtained in comparison to the reference cell. This demonstrates the advantage of the proposed hybrid structure over the current enhancement of the independent structure of nanoparticles and anti-reflection coating which is currently being utilized. In comparison to the

reference cell, the combined light trapping structure has been shown to be capable of increasing the short-circuit current by 86.22 percent when the perovskite layer is 400 nanometers in thickness. It is essential to have a solid understanding of how this value shifts in relation to the perovskite thickness. The results of the simulation are displayed in Figure 12, and they demonstrate that the optimized light trapping composite structure has the potential to effectively improve the performance of CBPSCs throughout a spectrum of active layer thicknesses. In situations when the perovskite thickness falls within the range of 200–600 nm, the application of the light trapping composite structure demonstrates a significant improvement. It is possible to get a high short-circuit current of 25.264 mA/cm2 using a perovskite layer that is 600 nm thick. This is practically identical to the current that is produced by a perovskite layer that is 1000 nm thick. When the perovskite layer is 600 nm thick, this shows that the existing light trapping architecture is almost totally capable of absorbing the incident spectrum with its light trapping capabilities. The end solution makes it possible to create a perovskite absorber that is thinner, which in turn reduces the quantity of harmful lead that is utilized without negatively impacting the performance of the cell. As a result of insufficient light absorption after 600 nm, the short-circuit current continues to increase for reference CBPSCs that do not include light control. After utilizing a hybrid light-trapping structure, our findings indicate that thinner perovskite layers may be utilized in order to accomplish high-efficiency CBPSCs. While the hybrid structure improves absorption, potential drawbacks include: (1) Increased interfacial recombination at the SiO_2/Ag-perovskite boundaries, which could reduce charge collection efficiency. (2) Thermal degradation of PMMA at elevated temperatures (>80°C), necessitating alternative coatings for outdoor applications. (3) Complexity in scaling up the dual nanostructure-ARC fabrication process.

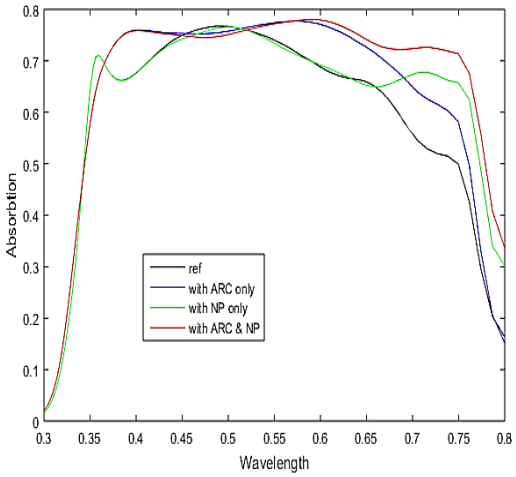

Figure 11. Absorption with different light trapping structures in a 400 nm thick perovskite monolayer.

Table 5. Short-circuit current values and relative gain for different light trapping structures.

Cell structure	J_{sc}(ma/cm^2)	Relative Enhancement of the Jsc (%)
Reference	20.7946	-
With ARC Only	22.4267	7.85
With NP Only	24.0148	15.49
With NP & ARC	25.5591	22.86

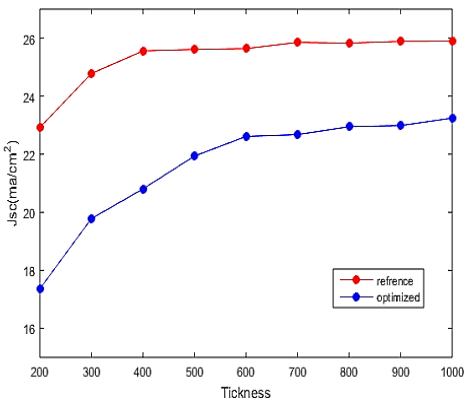

Figure 12. Short circuit current of the reference cell and the cell with light trapping structure for different thicknesses of the perovskite layer.

3.6. Power-voltage and current-voltage characteristics

This part examined electrical modeling utilizing the Device module. The Shockley-Read Hall and surface recombination models were employed for the recombination function, while the drift-diffusion model was utilized for the carrier transport equations. The optical properties of the reference perovskite cell were replicated, and its structure was simulated, with the results documented in Table 6. The carbon-based perovskite cell including the light trapping structure was simulated, resulting in the anticipated enhancement of all electrical parameters. Figure 13 illustrates the power-voltage and current-voltage characteristics of both the reference perovskite cell and the perovskite cell with the trapping structure. This simulation accounts for the light absorbed in the electron and hole transport layers. The negligible change in open-circuit voltage (Voc) and fill factor (FF) despite enhanced JSC can be attributed to two factors: (1) The Shockley-Read-Hall recombination model assumes defect-dominated recombination, which becomes more pronounced at higher carrier densities induced by light trapping. (2) The hybrid structure introduces additional interfaces (e.g., SiO_2/Ag, PMMA/perovskite), potentially creating localized trap states that limit Voc improvement. Future work should incorporate interface passivation strategies to mitigate this trade-off.

Table 6. Parameter values of the reference perovskite cell and the optimized perovskite cell.

Cell structure	Voc	Jsc	FF	η
Reference	0.51584	21.4346	0.806147	8.91342%
Optimized	0.52118	26.5031	0.807701	11.1567%

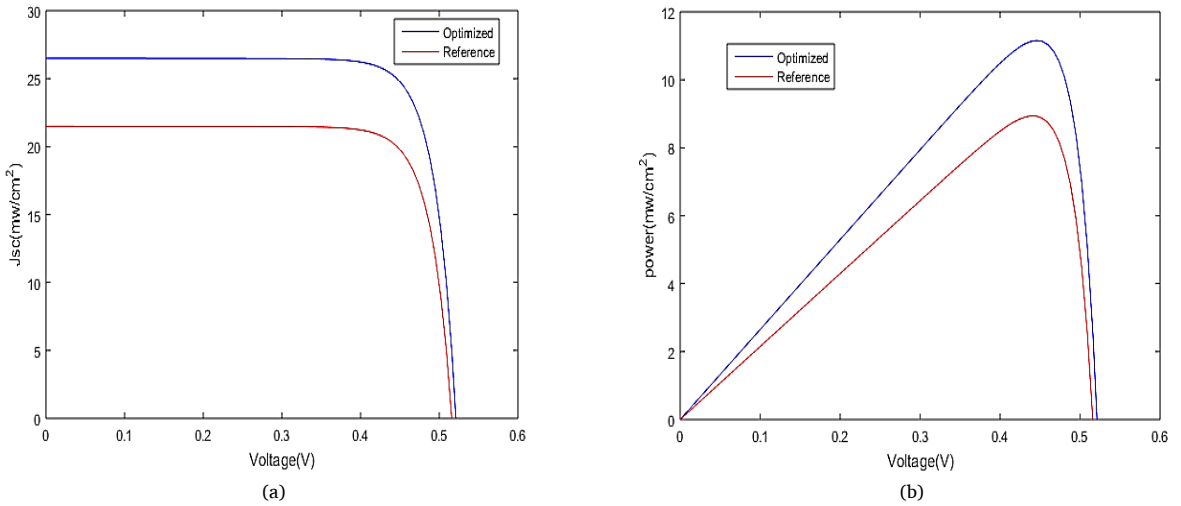

Figure 13. Comparison of the reference perovskite cell and the optimized perovskite cell, a) current-voltage characteristic, b) power-voltage characteristic.

4. Conclusion

This study emphasizes the importance of solar energy and presents various types of solar cells, particularly PSCs. It proposes a hybrid light trapping structure comprising silver core nanoparticles with a silica shell positioned beneath the active perovskite layer, along with a PMMA anti-reflective coating on the front surface, aimed at enhancing the absorption bandwidth in CBPSCs. The enhancement of light absorption can be attained through the meticulous selection of structural parameters, including the radius and period of the silver-silica nanoparticles, along with the thickness of the silica shell and the anti-reflective coating. In comparison to the reference CBPSCs lacking light management, the short-circuit current values with light trapping can be enhanced by 17 to 27%. Additionally, a substantial short-circuit current of 25.264 mA/cm^2 was attained for a 600 nm thick perovskite layer utilizing silver-silica nanoparticles having a radius of 100 nm and a periodicity of 280 nm, along with a 60 nm thick PMMA anti-reflection coating. The efficiency and short-circuit current of the carbon-based perovskite cell with the light trapping structure were enhanced; however, no notable alteration was seen in the open-circuit voltage and fill factor. This technique can serve as a general framework to enhance absorption efficiency while decreasing lead content through the utilization of thinner perovskite in CBPSCs. While the simulation results are promising, practical implementation faces challenges: (1) Precise alignment of Ag/SiO_2 nanoparticles within the perovskite layer requires advanced nanofabrication techniques (e.g., electron-beam lithography), which may increase cost. (2) Long-term stability of PMMA under UV exposure needs experimental validation. (3) Variability in nanoparticle size and distribution could affect performance reproducibility. Future studies should focus on scalable deposition methods (e.g., spin-coating with self-assembled nanoparticles) and accelerated aging tests to evaluate durability.

References

[1] W. S. Yang, B. Park, et al., "Iodide Management in Formamidinium-Lead-Halide–Based Perovskite Layers for Efficient Solar Cells," *Science*, vol. 356, no. 6345, pp. 1376–1379, 2017.

[2] M. Saliba, T. Matsui, et al., "Incorporation of Rubidium Cations into Perovskite Solar Cells Improves Photovoltaic Performance," *Science*, vol. 354, no. 6309, pp. 206-209, 2016.

[3] B. Boroomandnasab, and M. H. Zolfaghari, "Optimization CIGS/CIGS Tandem Solar Cells by Adjusting Layer Thickness Using Silvaco-TCAD," *Journal of Green Energy Research and Innovation*, vol. 1, no. 1, pp. 48–54, 2024.

[4] S. K. Sahoo, B. Manoharan, and N. Sivakumar, "Introduction," *Perovskite Photovoltaics*, pp. 1–24, 2018.

[5] T. Dai, Q. Cao, et al., "Strategies for High-Performance Large-Area Perovskite Solar Cells Toward Commercialization," *Crystals*, vol. 11, no. 3, p. 295, 2021.

[6] F. Ambrosio, J. Wiktor, F. De Angelis, and A. Pasquarello, "Origin of Low Electron–Hole Recombination Rate in Metal Halide Perovskites," *Energy & Environmental Science*, vol. 11, no. 1, pp. 101–105, 2018.

[7] Q. Lin, A. Armin, R. C. R. Nagiri, P. L. Burn, and P. Meredith, "Electro-Optics of Perovskite Solar Cells," *Nature Photonics*, vol. 9, no. 2, pp. 106–112, 2014.

[8] H. Dong, T. Lei, et al., "Plasmonic Enhancement for High Efficient and Stable Perovskite Solar Cells by Employing "hot Spots" Au Nanobipyramids," *Organic Electronics*, vol. 60, pp. 1–8, 2018.

[9] Y. Li, Z. Kou, J. Feng, and H. Sun, "Plasmon-Enhanced Organic and Perovskite Solar Cells with Metal Nanoparticles," *Nanophotonics*, vol. 9, no. 10, pp. 3111–3133, 2020.

[10] W. A. Murray, and W. L. Barnes, "Plasmonic Materials," *Advanced Materials*, vol. 19, no. 22, pp. 3771–3782, 2007.

[11] A. Benayad, D. Diddens, et al., "High-throughput experimentation and computational freeway lanes for accelerated battery electrolyte and interface development research," Advanced Energy Materials, vol. 12, no. 17, p. 2102678, 2022.

[12] E. Raoult, R. Bodeux, et al., "Optical Characterizations and Modelling of Semi-Transparent Perovskite Solar Cells for Tandem Applications," *in 36th European Photovoltaic Solar Energy Conference and Exhibition*, 2019, pp. 757-763.

[13] A. A. Tabrizi, H. Saghaei, M. A. Mehranpour, and M. Jahangiri, "Enhancement of Absorption and Effectiveness of a Perovskite Thin-Film Solar Cell Embedded with Gold Nanospheres," *Plasmonics*, vol. 16, no. 3, pp. 747–760, 2021.

[14] S. Royanian, A. Abdolahzadeh Ziabari, and R. Yousefi, "Efficiency Enhancement of Ultra-Thin CIGS Solar Cells Using Bandgap Grading and Embedding Au Plasmonic Nanoparticles," *Plasmonics*, vol. 15, no. 4, pp. 1173–1182, 2020.

[15] P. R. Pudasaini, and A. A. Ayon, "Nanostructured Thin Film Silicon Solar Cells Efficiency Improvement Using Gold Nanoparticles," *physica status solidi (a)*, vol. 209, no. 8, pp. 1475–1480, 2012.

Declaration of competing interest

The authors declare that they have no known competing financial interests or personal relationships that could have appeared to influence the work reported in this paper. The ethical issues, including plagiarism, informed consent, misconduct, data fabrication and/or falsification, double publication and/or submission, redundancy, have been completely observed by the authors.

Bibliography

Bahareh boroomandnasab was born in 1988, in Dezful, Iran. She received her Bachelor's, Master's, and Ph.D. degrees in Electronics Systems Engineering from Shahid Chamran University of Ahvaz, Ahvaz, Iran in 2011, 2013, and 2019, respectively. She is currently an Assistant Professor in Institute for Higher Education, ACECR, Khuzestan, IRAN. Her research interests include semiconductor device design, simulation and fabrication.

Email: boroomand@acecr.ac.ir

ORCID: 0009-0009-6083-3796

Contribution Statement: Data curation, Formal analysis, Software, Validation, Visualization, Roles/Writing-original draft.

Salem Doreghi is an Electronics Engineer at Karun Oil and Gas Exploitation Company. At work, he repairs all types of power supply and UPS. He was born in 1988. He is from Iran and the city of Ahvaz. He believes that electronic science helps people in all aspects of daily life. He has a master's degree from Institute for Higher Education ACECR Khuzestan.

Email: doraghi.1367@gmail.com

ORCID: 0009-0005-5025-2745

Contribution Statement: Investigation, Software.

Journal of Green Energy Research and Innovation

Challenges Ahead in Transmission Network Expansion Planning in The Presence of Renewable Energy Sources; An Updated Review

Abdollah Rastgou

Highlights

- **Transmission network expansion planning (TNEP) is vital for reliability in restructured power systems.**
- **Effective TNEP integrates renewable energy sources, supporting sustainability and reducing emissions.**
- **Proper transmission planning minimizes congestion, optimizing infrastructure for future demand and generation.**
- **A robust transmission network fosters competition, resilience, and public trust in the energy sector's evolution.**

Graphical Abstract

Use your device to scan and read the article online

Citation

A. Rastgou, "Challenges Ahead in Transmission Network Expansion Planning in The Presence of Renewable Energy Sources; An Updated Review," *Journal of Green Energy Research and Innovation*, vol. 2, no. 2, pp. 48-67, 2025.

https://doi.org/10.61186/jgeri.2.2.48

Journal of Green Energy Research and Innovation 2.2 (2025) 48-67

Online ISSN: 3041-9018

Journal of Green Energy Research and Innovation

Journal Homepage: www.jgeri.araku.ac.ir

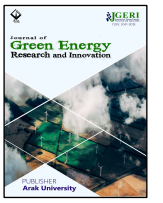

Challenges Ahead in Transmission Network Expansion Planning in The Presence of Renewable Energy Sources; An Updated Review

Abdollah Rastgou*

Department of Electrical Engineering, Kermanshah Branch, Islamic Azad University, Kermanshah, Iran.

ARTICLE INFO

Keywords:
Renewable energy sources,
Transmission network expansion planning,
Optimization,
Uncertainty.

Article History:
Received: 11 March 2025;
Revised: 21 March 2025;
Accepted: 26 March 2025.

Article type:
Review Article

* ***Corresponding author***
E-mail address
abdollah.rastgou@iau.ac.ir (A. Rastgou)

ABSTRACT

The significance of transmission network expansion planning (TNEP) in a restructured power system is underscored by the urgent need to integrate renewable energy sources. As the world shifts towards sustainability, effective transmission planning becomes critical for accommodating diverse energy sources, particularly wind and solar, which are frequently situated far from consumption centers. This integration is not only essential for achieving sustainability goals and reducing greenhouse gas emissions but also for ensuring a reliable and efficient power supply. Moreover, strategic transmission planning plays a vital role in minimizing congestion within the network, which can escalate costs and compromise reliability. By anticipating future demand and generation patterns especially the intermittent nature of renewables planners can optimize the placement of transmission lines and substations to mitigate potential bottlenecks. In a competitive market, a resilient transmission infrastructure is crucial for providing equitable access to all market participants, thereby fostering innovation and competition. Additionally, effective planning must address regulatory requirements and stakeholder interests, promoting transparency and collaboration among various entities in the power sector. This comprehensive approach not only ensures compliance but also builds public trust in the energy system. In summary, developing an efficient transmission network is imperative for supporting a reliable, competitive, and sustainable power system that prioritizes renewable energy sources. This paper aims to provide an overview of the challenges ahead in TNEP while proposing necessary solutions to effectively address these challenges.

1. Introduction

Energy planning refers to a set of activities that are carried out on a macro level to study the interrelationship between the energy sector and other economic sectors with an emphasis on environmental considerations to create coordination between supply and demand. In every country, one of the important issues in government policy is energy planning and management. Large-scale energy planning depends on many factors, including economic development prospects, political approaches, macro-management issues, economic situation, etc. According to Figure 1, one of the basic branches of energy planning is power system planning, which can be done even in a 50-year period. This planning includes generation expansion planning, transmission network expansion planning, and finally distribution network expansion planning (DNEP). After determining the share of electrical energy in meeting a country's energy needs, long-term production planning is conducted for a horizon of 30 to 40 years, during which the required capacities and types of power plants are specified. The TNEP is part of a broader process that begins with energy planning and concludes with operational planning. Once the expansion plan for generation is established, TNEP is carried out over a long-term horizon (up to 30 years), with updates occurring at shorter intervals. These updates and modifications to the expansion plans can even occur within horizons of 2 to 3 years depending on unforeseen events during the planning phase. After the TNEP is defined, reactive power planning is conducted in shorter intervals of 2 to 3 years. The goal here is to determine the type, capacity, and location of reactive power compensators needed to properly operate the network and to reduce losses. Finally, the operational planning process begins, covering a horizon from one year prior to one day before operation [1]. This phase addresses issues such as scheduling maintenance for power plants and lines, necessary switching operations in the transmission network, and establishing the production patterns for the units.

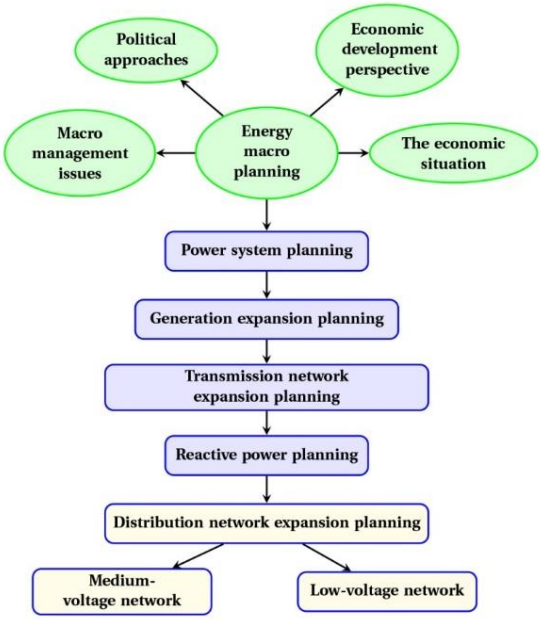

Figure 1. Energy planning procedure.

The significance of renewable energy sources (RESs) has become increasingly paramount in the face of climate change and the depletion of fossil fuels. As nations strive to reduce their carbon footprints and transition towards sustainable energy systems, harnessing the power of RESs such as solar, wind, hydro, and biomass is essential. These energy sources not only contribute to a cleaner environment but also enhance energy security by diversifying the energy mix. Furthermore, the adoption of renewables can stimulate economic growth by creating jobs in manufacturing, installation, and maintenance sectors, thus driving innovation and technological advancements. However, the effective integration of renewable energy into existing power grids necessitates comprehensive planning and expansion of transmission networks. As renewable energy generation is often decentralized and variable, a robust transmission infrastructure is crucial for transporting electricity from remote generation sites to urban centers where demand is highest. Strategic planning of these networks must consider factors such as geographical distribution, grid stability, and the incorporation of energy storage solutions. By investing in advanced transmission technologies and smart grid systems, countries can enhance their capacity to accommodate fluctuating renewable energy supplies, ultimately leading to a more resilient and sustainable energy future.

The TNEP is carried out in practice for four reasons, as illustrated in Figure 2, The primary goal of The TNEP is to develop a plan that ensures the economical supply of power while maintaining or improving the reliability of the network. Economical power supply means that, first, the investment costs for new lines and substations are minimized, and second, the transmission network does not impose any limitations on the economic operation of the power system. In the past, economic operation of the power system was synonymous with minimizing production costs; in restructured networks, it refers to the ability to create a competitive market for trading electrical energy. One of the reasons for expanding the transmission network is to connect newly constructed power plants to the grid. Naturally, the generated power must be transmitted to consumption points through the transmission system. Therefore, the expansion of the transmission network is inevitable, especially when considering the expansion and construction of new power plants.

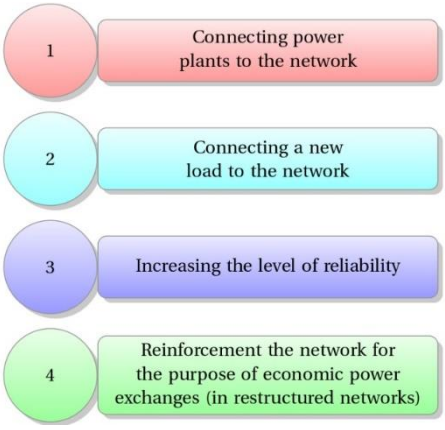

Figure 2. The main reasons for the TNEP.

Another reason for expanding the transmission system is to connect new load points to the grid. This connection primarily occurs at the sub-transmission level, and its impact is modeled as an increase in the load on transmission substations and a change in their loading patterns. In cases such as supplying large industries, their power needs can be met directly from the transmission network [2]. Maintaining and enhancing network reliability is also a key reason for network expansion. The most commonly used criterion for assessing the reliability of transmission networks is the *N-1* security criterion. According to this criterion, the power network must meet consumer needs without experiencing overload, unacceptable voltage drops, or load shedding, not only under normal conditions but also when one of its components is lost. Plans aimed at increasing reliability in power system planning can be categorized into two types:

• Expansion plans

• Reinforcement plans

In expansion plans, planners select new routes or locations for constructing new lines or substations while considering environmental constraints. This approach effectively adds new power transmission paths to the network [3]. In reinforcement plans, certain paths within the network are typically strengthened. Examples include converting an existing line into a double-circuit line, increasing the number of transformers at substations, or raising the transmission voltage level. Another reason for developing the transmission system is the economic exchanges of power, which becomes increasingly important in restructured power systems. In practice, since not all forecasts will be realized exactly, expansion plans are reviewed periodically (for example, every five years). Over time, some ambiguous information becomes clearer, allowing for more accurate predictions of the future. Additionally, the impacts of generation and the expansion of the distribution network must always be considered in the planning of the transmission network. This necessitates a feedback process between these optimization issues. The bar chart provided in Figure 3 illustrates the growth in transmission planning studies from 2016 to 2024.

Over this period, there has been a noticeable upward trend, with the number of studies increasing significantly, particularly in the last few years. This surge indicates a heightened focus on enhancing transmission infrastructure, likely driven by the growing demand for reliable energy supply and the integration of RESs into the grid. The substantial rise in studies during 2020 and beyond may reflect a response to emerging challenges in energy transition, regulatory changes, and technological advancements. Overall, this trend underscores the importance of strategic planning in ensuring that transmission networks can meet future energy needs efficiently and sustainably. Here's a more detailed breakdown of the trends and implications:

- Overall Trend: The data shows a consistent increase in the number of transmission planning studies each year. This upward trajectory indicates that there is an increasing recognition of the importance of thorough planning in transmission systems.
- Significant Growth Post-2020: Notably, there is a marked spike in the number of studies starting in 2020. This could be attributed to several factors:
    1. Energy Transition: As more countries and regions commit to transitioning to RESs, there is a greater need for comprehensive planning to ensure that the transmission infrastructure can accommodate these changes.
    2. Regulatory Changes: New policies and regulations may have been implemented that require more rigorous planning and analysis of transmission networks.
    3. Technological Advancements: Improvements in technology, such as smart grid solutions and advanced forecasting methods, may have made it easier and more effective to conduct these studies.
- Implications for Energy Supply: The increase in transmission studies suggests that utilities and energy planners are proactively addressing potential challenges in energy supply and reliability. This is crucial as electricity demand continues to rise, driven by factors such as population growth, increased electrification of transportation, and a shift towards electric heating.
- Integration of RESs: With the growing penetration of RESs like wind and solar, there is a need for enhanced transmission planning to ensure that these resources can be effectively integrated into the grid. This requires careful consideration of geographic locations, capacity needs, and potential bottlenecks in the existing infrastructure.
- Future Outlook: The trend indicated by the chart may continue as the energy landscape evolves. Ongoing studies will likely focus on resilience against climate change impacts, cybersecurity for grid operations, and optimizing existing infrastructure to meet future demands.

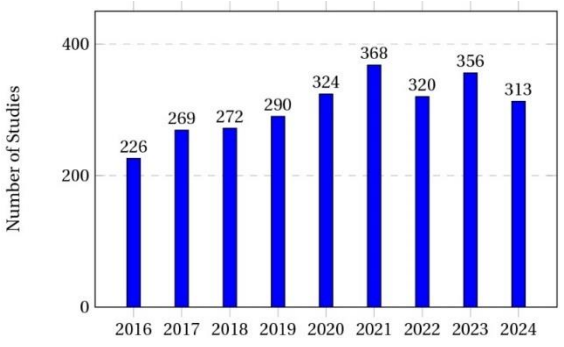

Figure 3. Number of studies on TNEP from 2016-2024 (adapted from Google Scholar).

Therefore, the bar chart reflects a vital aspect of energy management and planning, showcasing how stakeholders are increasingly prioritizing the expansion and enhancement of transmission networks to support a sustainable and reliable energy future. The following pie chart shown in Figure 4 represents the various components involved in the planning process, highlighting their relative contributions.

- Infrastructure Investment (40%): This segment represents the largest portion of the planning process, indicating that a significant amount of resources is allocated to upgrading and expanding physical infrastructure, such as substations and transmission lines.
- Regulatory Compliance (25%): A quarter of the planning effort goes into ensuring that all expansions comply with local, national, and international regulations. This includes environmental assessments and adherence to safety standards.
- Technological Innovation (15%): This portion signifies the investment in new technologies, such as smart grid solutions and renewable energy integration, which are essential for modernizing the network and improving efficiency.
- Stakeholder Engagement (10%): Engaging with stakeholders, including local communities, government bodies, and industry partners, is vital for gaining support and addressing concerns related to new projects.
- Risk Management (10%): This segment focuses on identifying and mitigating potential risks that could impact the transmission network's reliability and performance.

The Figure 4 clearly illustrates that infrastructure investment is the dominant factor in TNEP, reflecting the need for robust physical systems to support growing energy demands. Regulatory compliance is also a significant concern, emphasizing the importance of aligning projects with legal frameworks and environmental considerations. Technological innovation, while smaller in percentage, highlights a forward-looking approach to integrate advanced solutions that can enhance grid reliability and sustainability. Stakeholder engagement and risk management are equally important, ensuring that projects are socially acceptable and resilient against potential disruptions.

2. Problem formulation

The TNEP consists of two stages. In the first stage, various options for the expansion of the transmission network within the planning horizon are generated as a set of reinforcement and expansion plans using simplified models, such as the DC load flow model. In the second stage, the expansion options are evaluated through a more detailed analysis that includes maximum, average, and minimum load levels, short-circuit analysis, transient stability assessment, and reliability evaluation. In most studies, the TNEP primarily refers to the first stage mentioned above, although it can also incorporate more accurate load flow models and consider reliability in the planning process. The various methods used to generate transmission network expansion plans in the first planning stage typically focus solely on adequacy criteria in their models, while security aspects are deferred to the analyses conducted in the second planning stage.

3. TNEP challenges with RESs

The integration of RESs, such as solar and wind power, into the transmission network presents several challenges in the planning and expansion of electricity transmission systems. These challenges can significantly impact the reliability, efficiency, and overall effectiveness of the electrical grid [4-15]. Below are some of the key challenges associated with the installation of renewable energy plants in transmission network planning:

- Intermittency and Variability: RESs are inherently intermittent and variable, meaning their output can fluctuate based on weather conditions. This variability poses significant challenges for grid operators who must ensure a stable and reliable electricity supply. Planners need to develop strategies to accommodate these fluctuations, which may involve the integration of energy storage systems or demand response mechanisms.

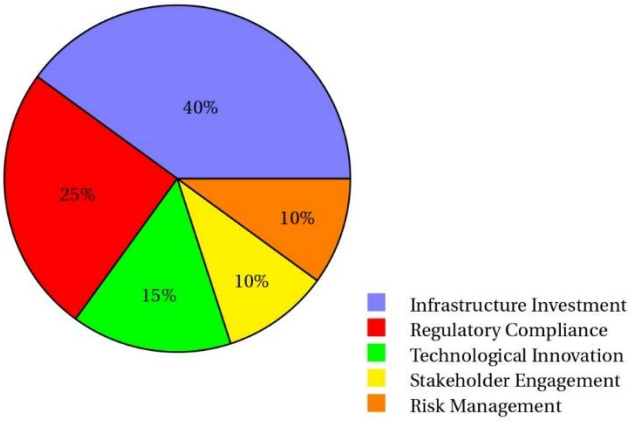

Figure 4. The various components involved in the planning process, highlighting their relative contributions.

- Grid Capacity and Infrastructure: The existing transmission infrastructure may not be adequately equipped to handle the additional load from renewable energy installations. Upgrading or expanding the grid may be necessary to accommodate new generation sources, which can be costly and time-consuming. Furthermore, planners must consider the location of renewable resources, as they are often situated far from existing transmission lines, necessitating new construction.
- Location and Resource Assessment: Identifying optimal locations for renewable energy plants is crucial for minimizing transmission losses and maximizing efficiency. However, suitable sites for wind and solar farms may not always align with existing transmission infrastructure. Comprehensive resource assessments and geographic analyses are required to determine the best locations while considering environmental impacts and land use.
- Regulatory and Policy Framework: The planning and installation of renewable energy projects are often subject to complex regulatory frameworks that can vary significantly by region. Navigating these regulations can be a challenge for developers and planners alike. Additionally, policies related to grid interconnection, permitting processes, and incentives for renewable energy can influence project timelines and feasibility.
- Technical Integration Challenges: Integrating renewable energy into the transmission network requires advanced technical solutions to manage issues such as voltage stability, frequency control, and power quality. Planners must consider the implementation of smart grid technologies, advanced forecasting tools, and real-time monitoring systems to effectively manage the integration of diverse energy sources.
- Economic Considerations: The economic viability of renewable energy projects is influenced by factors such as capital costs, operational expenses, and market prices for electricity. Planners must conduct thorough economic analyses to determine the cost-effectiveness of integrating renewables into the transmission network. This includes evaluating potential revenue streams from energy sales and considering the long-term impacts on electricity prices.
- Stakeholder Engagement: Successful planning for renewable energy integration requires collaboration among various stakeholders, including government agencies, utility companies, developers, and local communities. Engaging these stakeholders early in the planning process is essential to address concerns, gather input, and build support for renewable energy projects.
- Environmental Impact Assessments: The installation of renewable energy plants can have environmental implications that must be carefully evaluated. Conducting thorough environmental impact assessments is essential to understand potential effects on local ecosystems, wildlife habitats, and communities. Planners must balance the benefits of renewable energy with potential environmental trade-offs.

In summary, while the integration of RESs into the transmission network offers significant benefits in terms of sustainability and reducing greenhouse gas emissions, it also presents a range of challenges that must be addressed through careful planning and innovative solutions. By tackling these challenges head-on, planners can facilitate a smoother transition to a cleaner and more resilient energy future.

4. Restructuring power systems and its impact on TNEP

Restructuring power systems is a significant trend that has emerged in response to the challenges of traditional utility models. This transformation aims to enhance efficiency, promote competition, and improve service delivery in the electricity sector. One of the critical areas affected by this restructuring is the planning and expansion of transmission networks. The primary objective of restructuring is to separate generation, transmission, and distribution functions within the power sector. This unbundling allows for a more competitive market environment where multiple entities can participate in electricity generation. As a result, the transmission network must adapt to accommodate the new dynamics of competition among generators. In a restructured environment, independent system operators or regional transmission organizations often manage the transmission network. These organizations are responsible for ensuring reliable electricity delivery while facilitating market access for various generators. The planning process becomes more complex as it must consider not only technical constraints but also market signals and economic factors.

One significant impact of restructuring on transmission network expansion is the increased emphasis on interconnections. Enhanced interconnections between regions can facilitate electricity trading, improve reliability, and reduce costs. Planners must evaluate potential transmission upgrades or new lines that can connect regions with surplus generation to those with deficits. Moreover, the integration of RESs into the grid presents both challenges and opportunities for transmission planning. As more renewable generators enter the market, the need for flexible and robust transmission infrastructure becomes paramount. Planners must consider factors such as the geographical dispersion of renewable resources and their variability in generation. Another important aspect is the role of advanced technologies in transmission network expansion. Smart grid technologies enable better monitoring, control, and optimization of the transmission system. These innovations facilitate real-time data exchange and improve decision-making processes, which are crucial in a competitive market environment. Regulatory frameworks also play a vital role in shaping transmission expansion post-restructuring. Policies that promote investment in transmission infrastructure while ensuring fair access for all market participants are essential. Additionally, cost allocation methods must be transparent and equitable to encourage investment.

In summary, the restructuring of power systems significantly impacts transmission network expansion by introducing competition, enhancing interconnections, integrating RESs, and promoting technological advancements. Effective planning in this new paradigm requires a comprehensive understanding of market dynamics, regulatory frameworks, and technological innovations to ensure a reliable and efficient electricity supply for all consumers.

5. Congestion management and TNEP

Congestion management in the context of TNEP is a vital aspect of modern power system operations. As electricity demand grows and the integration of RESs accelerates, the need for effective congestion management strategies becomes increasingly important. Congestion refers to situations where the demand for electricity exceeds the available transmission capacity, leading to potential overloads, inefficiencies, and reliability issues within the power grid. As global electricity consumption continues to rise, driven by factors such as population growth, urbanization, and the proliferation of electric vehicles, the existing transmission infrastructure faces increasing pressure. This situation necessitates a proactive approach to managing congestion to prevent potential failures and maintain the stability of the power grid. Congestion occurs when the demand for electricity at certain points in the network exceeds the capacity of the transmission lines to deliver it. This imbalance can lead to several issues, including voltage fluctuations, thermal overloads, and, in extreme cases, blackouts. Such scenarios not only compromise the reliability of the power supply but also result in significant economic losses and risks to public safety. Therefore, effective congestion management is essential for safeguarding the integrity of the electrical system.

One of the primary challenges in congestion management is the integration of RESs, such as wind and solar power. While these sources are crucial for reducing greenhouse gas emissions and promoting sustainability, their intermittent nature can create additional complexities in power flow management. For instance, during periods of high generation from renewables and low demand, excess electricity may be produced, leading to potential congestion in certain areas of the grid. Conversely, during peak demand periods when renewable generation is low, traditional fossil-fuel-based plants may struggle to meet demand without causing congestion. To address these challenges, several strategies can be employed within TNEP. First, enhancing transmission infrastructure through the construction of new lines or upgrading existing ones can significantly alleviate congestion. This requires careful planning and investment to ensure that the network can accommodate future growth in electricity demand and renewable energy integration. Second, implementing advanced technologies such as Smart Grids and Flexible AC Transmission Systems (FACTS) can improve real-time monitoring and control of power flows. These technologies enable operators to respond dynamically to changing conditions on the grid, thereby optimizing the use of available capacity and reducing congestion risks. Demand response programs represent another effective strategy for managing congestion. By incentivizing consumers to adjust their energy usage during peak periods, utilities can flatten demand curves and reduce stress on the transmission system. This approach not only helps mitigate congestion but also promotes energy efficiency and cost savings for consumers.

Moreover, market-based mechanisms such as locational marginal pricing can provide economic signals that encourage efficient resource allocation across the grid. By reflecting the true cost of congestion in electricity prices, these mechanisms motivate generators and consumers to make decisions that align with system reliability and efficiency goals. Regulatory frameworks also play a crucial role in facilitating effective congestion management. Policymakers must create an environment that encourages investment in transmission infrastructure while ensuring equitable access for all market participants. This includes establishing clear guidelines for interconnection processes and addressing any barriers that may hinder new projects.

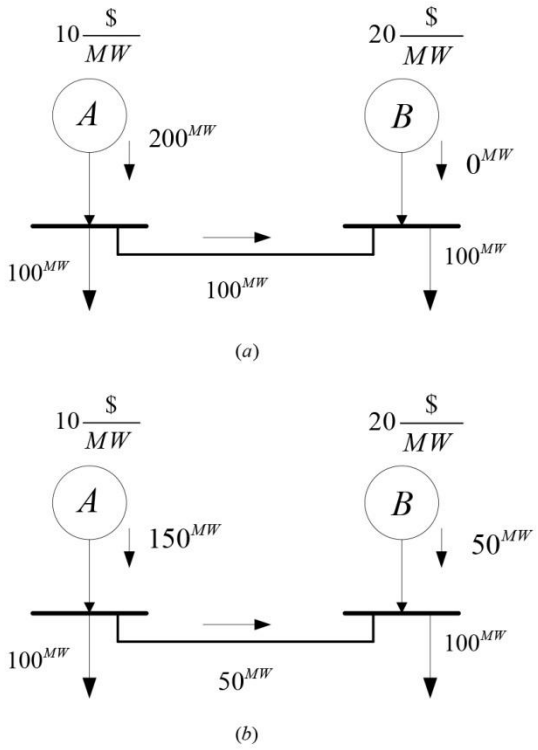

Figure 5. An example of the importance of congestion management in TNEP.

The occurrence of congestion in transmission lines is not a new issue and has also been present in traditional networks. However, in modern networks, this problem leads to complications, the most significant of which is a reduction in the competitiveness of the electricity market. Congestion in transmission lines causes the market to deviate from a perfectly competitive state, which in turn results in decreased social welfare and imposes additional costs on network users. To clarify this point, consider the following example. Figure 5 illustrates a two-area network connected by a transmission line. In scenario (*a*), the line between the two areas is considered to be without constraints. In this situation, based on the bids from the generating units, the loads in both areas prefer to purchase their required power from generator *A*, resulting in a flow of 100 megawatts across the line connecting the two areas. In this case, the total required power is purchased from the first generator at a price of 10 $ per megawatt, leading to a total supply cost of 2000 $ (calculated as 10 × 200).

In scenario (*b*), it is assumed that the transmission capacity of the line between the two areas is limited to 50 megawatts. In this case, the 100-megawatt load in area B must purchase at least 50 megawatts of its required power from the more expensive generator in its own area at a price of 20 $ per megawatt. Consequently, the total production cost for the loads in this network will be 2500 $, calculated as 20 × 50 + 10 × 150, which is 25% higher than the cost in the first scenario. It is assumed that both generators have submitted their bids based on their marginal costs, and generator *B* is unaware of the limitation on the interconnecting line and the behavior of generator *A*. It can be shown that in a perfect market, generators achieve maximum profit when they submit their bids based on their marginal costs. This example demonstrates that the increase in the cost of supplying electric energy is equal to the product of the flow through the congested line and the price differential of electric energy on either side of the line, which amounts to 500 $ (calculated as 50×(20 - 10)), representing the congestion cost. This can serve as a suitable metric for assessing the overall congestion level in the network. Given the network conditions, generator *B* can be confident that the 100 megawatt load in area *B* is compelled to obtain 50 megawatts of its required power from this generator; thus, generator *B* can propose any higher price to participate in the market. In this scenario, generator *B* can set prices in area *B* according to its preferences.

It should be noted that the network may not necessarily have zero congestion costs regarding line congestion levels. Therefore, it is essential to establish a compromise between investment costs in the network and congestion costs. For instance, consumers may prefer to pay higher energy prices due to line congestion; however, they may not want transmission usage tariffs to increase. This is because congestion and the resulting price increases typically occur only during peak load hours, and depending on their duration and extent of price increases, these additional costs during peak times may be negligible compared to a permanent increase in transmission tariffs. To keep transmission tariffs low, which can account for up to 11% of the total cost of delivered energy, operators are increasingly focused on maximizing the utilization of the existing transmission network. This is a key factor contributing to the increased density of transmission lines. High loading on existing lines, aside from issues related to line congestion (such as reduced competition in the market and higher energy prices for certain consumers), leads to a decrease in the reliability of the network and raises the risk of local or widespread blackouts.

6. New frameworks for the TNEP

TNEP often employs a two-level optimization framework, which consists of a main optimization problem and a sub-problem as shown in Figure 6. This dual-level approach allows for a systematic evaluation of both network development and generation patterns, ensuring that decisions made at one level are consistent with the operational realities at the other.

At the main level, the TNEP problem focuses on determining the optimal expansion plan for the transmission network. This involves identifying which new transmission lines should be built, where they should be located, and when they should be constructed.

The objective is typically to minimize the overall cost of the network while ensuring that it meets reliability standards and can accommodate future demand growth. Various constraints, such as budget limits, environmental regulations, and technical specifications of the network, must be considered in this optimization process. The sub-problem, on the other hand, deals with the generation patterns of power plants. It is essential to determine how much electricity each power plant should generate to meet the demand while minimizing operational costs. This is often formulated as an economic load dispatch problem, which seeks to allocate generation resources in a way that minimizes total generation costs while satisfying demand and operational constraints.

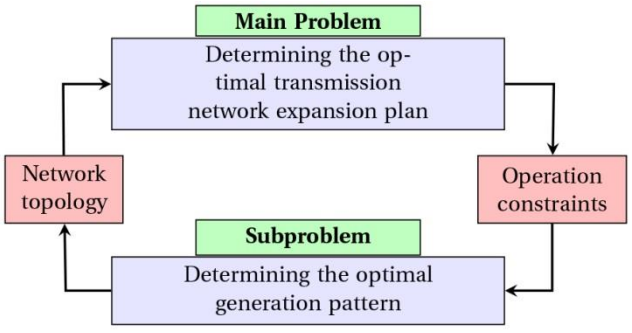

Figure 6. Model the TNEP problem as a main problem and a sub-problem.

The interaction between the two levels is critical. The main optimization problem relies on accurate generation patterns from the sub-problem to assess the flow capacities of existing and new transmission lines. Conversely, the results from the main problem can influence the operational decisions in the sub-problem by altering the available transmission capacity for power flows. This interdependence necessitates an iterative approach, where solutions from one level inform adjustments in the other until a satisfactory equilibrium is reached. Moreover, incorporating uncertainties such as fluctuations in demand or variations in renewable energy generation into this two-level optimization framework can enhance its robustness. Stochastic optimization techniques can be utilized to account for these uncertainties, allowing for more resilient planning outcomes that can adapt to changing conditions.

In summary, the two-level optimization framework in TNEP serves as a powerful tool for integrating network expansion decisions with generation dispatch strategies. By systematically addressing both aspects, engineers can develop comprehensive plans that not only enhance the transmission infrastructure but also ensure efficient and reliable electricity generation. This holistic approach is essential for meeting the evolving energy needs of society while maintaining economic and environmental considerations.

Considering generation costs in the objective function complicates the problem, and one of the common tools used in such cases is Benders Decomposition. Benders Decomposition is a powerful optimization technique that is particularly useful in TNEP due to its ability to manage complex problems [1-7]. One of the primary reasons for using this method is its capacity to reduce complexity by breaking down large-scale problems into smaller, more manageable sub-problems. This decomposition allows planners to focus on specific aspects of the network without being overwhelmed by the entire system's intricacies. Moreover, Benders Decomposition is highly scalable, making it suitable for large transmission networks that involve numerous decision variables and constraints. As a result, it enables the effective handling of extensive instances that would otherwise be computationally prohibitive with traditional optimization approaches. By solving these smaller sub-problems iteratively, the technique significantly improves solution times, which is essential for real-time decision-making in dynamic environments.

Another key advantage of benders decomposition is its flexibility in accommodating various types of constraints typical in transmission network planning, such as flow conservation and capacity limits. This flexibility allows for a more comprehensive optimization framework that can integrate multiple objectives, such as minimizing costs while enhancing reliability. Additionally, the method can be adapted to address uncertainty by incorporating stochastic elements, enabling planners to develop robust strategies that account for variations in demand and generation.

In summary, Benders Decomposition offers a structured and efficient approach to optimizing TNEP, effectively managing complexity, enhancing scalability, and facilitating robust decision-making under uncertainty.

6.1. Bi-level model

The increasing complexity of electricity markets and the growing demand for reliable and sustainable energy have necessitated advanced methodologies in the TNEP. Among these methodologies, bi-level programming has emerged as a particularly effective framework. A general structure of a bi-level problem in TNEP, represented in a textual format along with a description of the diagram the reader can visualize in Figure 7. The diagram illustrates a bi-level model used in TNEP. At the upper level, the "Upper-Level Problem" node represents strategic investment decisions that influence the overall network expansion. This level is connected to the "Investment Decisions" node, which highlights the decision-making process regarding investments in infrastructure. Below, the "Lower-Level Problem" node captures the operational aspects of the network, where the "Operational Decisions" node focuses on real-time operational strategies. The feedback loop between the lower and upper levels signifies the iterative nature of the planning process, where insights gained from operational decisions can inform and refine investment strategies, thereby creating a dynamic interplay between long-term planning and short-term operations. The rationale for employing bi-level models in TNEP can be understood through several key philosophical and practical considerations.

6.1.1. ierarchical Decision-Making

At the core of bi-level programming is the concept of hierarchical decision-making, where two distinct entities with different objectives interact. In TNEP, this typically involves a transmission planner (the upper level) and power generation companies (GENCOs) (the lower level). The upper-level planner aims to optimize the expansion of the transmission network, while the lower-level entities seek to minimize their operational costs in response to the network configuration. This dual perspective allows for a more realistic representation of the interactions between network infrastructure and generation strategies.

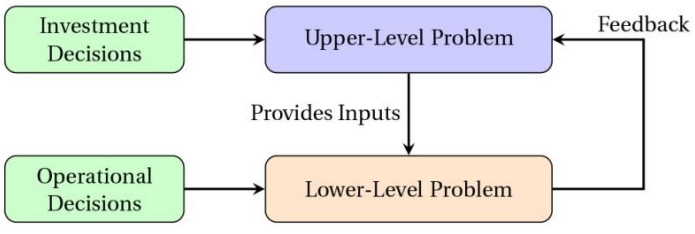

Figure 7. Bi-level model diagram in TNEP.

6.1.2. Capturing Strategic Interactions

Bi-level models effectively capture the strategic interactions between planners and generators. The decisions made by the transmission planner directly impact the operational landscape for GENCOs, influencing their generation dispatch and investment decisions. Conversely, the operational responses of GENCOs can affect the feasibility and cost-effectiveness of proposed expansions. By modeling these interactions, bi-level programming provides insights into how changes at one level affect outcomes at another, enabling better-informed decision-making.

6.1.3. Incorporating Uncertainty

Electricity markets are inherently uncertain due to fluctuations in demand, variable renewable generation, and regulatory changes. Bi-level models can incorporate stochastic elements, allowing planners to evaluate potential scenarios and their impacts on both network expansion and generation strategies. This capability is crucial for developing robust plans that can withstand unexpected changes in market conditions, enhancing the resilience of the power system.

6.1.4. Balancing Economic and Environmental Goals

Modern TNEP must balance economic efficiency with environmental sustainability. Bi-level programming allows planners to incorporate environmental objectives into their expansion decisions. For instance, planners can consider emissions reduction targets or renewable energy integration when determining network configurations. This holistic approach aligns with global efforts to transition to greener energy systems and ensures that expansion plans contribute positively to environmental goals.

6.1.5. Facilitating Regulatory Compliance

Regulatory frameworks often impose constraints on both transmission planning and generation operations. Bi-level models enable planners to account for these regulatory requirements systematically. By integrating compliance considerations into the optimization process, bi-level programming helps ensure that expansion plans meet legal standards while also being economically viable.

6.1.6. Enhancing Computational Efficiency

Bi-level programming can improve computational efficiency by decomposing complex problems into manageable sub-problems. The upper-level problem focuses on strategic planning, while the lower-level problem handles operational optimization. This separation allows for the application of specialized algorithms tailored to each level's unique characteristics, leading to faster convergence towards optimal solutions.

6.1.7. Supporting Multi-Objective Optimization

In practice, TNEP often involves multiple conflicting objectives, such as minimizing costs, maximizing reliability, and reducing environmental impact. Bi-level models can be extended to multi-objective frameworks, allowing planners to explore trade-offs between different goals. This flexibility is essential for stakeholders who must navigate competing priorities in a complex energy landscape.

6.1.8. Real-World Applicability

The real-world applicability of bi-level models is evident in their successful implementation in various case studies across different regions. These models have been used to analyze the impacts of new transmission lines, assess renewable energy integration, and evaluate the effects of policy changes on network expansion strategies. Their proven effectiveness enhances confidence in their use for future TNEP challenges.

In summary, the rationale for using bi-level programming in TNEP lies in its ability to model hierarchical decision-making processes, capture strategic interactions between planners and generators, and incorporate uncertainties and regulatory constraints. By balancing economic and environmental objectives while enhancing computational efficiency, bi-level models provide a robust framework for addressing the complexities of modern electricity markets. As the energy landscape continues to evolve, these models will play a crucial role in guiding sustainable and efficient transmission network development.

In [8], a bi-level TNEP model considering short-circuit current constraints is proposed. Refs. [9,10] present a new framework for addressing the expansion planning of distributed generation (DG) in sub-transmission substations, taking into account the capacity expansions of transmission substations and available incentives. The proposed model incorporates both firm contracts and capacity payments as incentive options and a bi-level model is developed for this problem, where the upper level focuses on the investor's optimal decision aimed at maximizing profit, while the lower-level addresses market clearing and substation expansion. Reference [11] presents a practical application of bi-level evolutionary optimization aimed at improving the electricity industry infrastructure. It provides a coordinated approach to generation and transmission expansion planning from the viewpoint of an independent system operator. The primary goal of this study is to demonstrate how optimizing generator capacity and location can reduce transmission investments while enhancing the reliability of the network. Reference [12] introduces a bi-level proactive transmission expansion framework where a centralized transmission system operator operates at the upper level, while decentralized generation companies

participating in the market function at the lower level. Reference [13] presents a novel dual-based bi-level approach for robust AC TNEP that accounts for uncertainties in RESs generation and load. The method employs convex relaxation and is solved using Benders Decomposition, with the master problem focused on determining the robust AC expansion plan. To effectively incorporate the impact of the electricity market, Reference [14] proposes a bi-level model for transmission expansion planning aimed at ensuring market fairness and investment efficiency. Reference [15] presents a bi-level model for TNEP that takes into account financial transmission right trading, along with a proposed comprehensive evaluation index for assessing TNEP schemes. Reference [16] proposes a bi-level optimization model for TNEP aimed at enhancing the network of an energy-exporting power grid with a hybrid AC/DC interface.

In [17], a bi-level transmission and generation expansion planning model that takes into account the correlation of wind power using mixed integer linear programming is proposed. Reference [18] introduces a bi-level proactive transmission expansion framework where a centralized Transmission System Operator operates at the upper level, while decentralized generation companies participating in the market represent the lower level. Reference [19] introduces a bi-level TNEP model that incorporates both prohibited operating zones and multi-fuel units.

6.2. *Multi-Stage Methods in TNEP*

Multi-stage methods provide valuable tools for optimizing TNEP in restructured power systems by enabling scenario analysis, investment timing, risk management, renewable integration, and comprehensive cost-benefit assessments. However, challenges such as model complexity, data availability, computational burdens, stakeholder coordination, dynamic market conditions, and regulatory hurdles must be addressed to fully leverage these methods. Overcoming these challenges is essential for ensuring that transmission networks are developed efficiently and effectively to meet future energy demands while supporting a sustainable energy transition [20-24].

6.2.1. *Key applications of multi-stage methods in TNEP*

- Scenario Analysis: Multi-stage methods enable the assessment of different future scenarios, such as varying demand levels, technological advancements, and regulatory changes. By evaluating multiple scenarios, planners can identify potential risks and opportunities in transmission network development.
- Investment Timing and Sequencing: These methods facilitate the strategic timing and sequencing of investments in transmission infrastructure. By analyzing costs and benefits over different stages, planners can determine the optimal schedule for upgrades and expansions, ensuring that investments align with market needs.
- Risk Management: Multi-stage approaches help in identifying and managing risks associated with uncertain factors, such as fluctuating energy prices or changes in policy. By incorporating risk assessments into the planning process, decision-makers can develop strategies to mitigate potential negative impacts on investments.
- Integration of Renewable Energy: As renewable energy sources become more prevalent, multi-stage methods can assist in planning for their integration into the transmission network. This includes evaluating the impact of variable generation on grid stability and determining the necessary infrastructure to accommodate future renewable projects.
- Cost-Benefit Analysis: Multi-stage methods allow for comprehensive cost-benefit analyses over time, considering both capital and operational expenditures. This helps stakeholders make informed decisions regarding the economic viability of transmission projects.

6.2.2. *Challenges arise in applying multi-stage methods for TNEP*

Despite their advantages, several challenges arise in applying multi-stage methods for TNEP:

- Complexity of Models: The complexity inherent in multi-stage models can make them difficult to develop and implement. Creating accurate models that capture all relevant variables and uncertainties requires significant expertise and resources.
- Data Availability and Quality: Reliable data is essential for effective multi-stage planning. However, obtaining high-quality data on demand forecasts, generation profiles, and regulatory environments can be challenging, leading to uncertainties in model outcomes.
- Computational Burden: Multi-stage optimization problems can be computationally intensive, especially when dealing with large networks and numerous scenarios. This can result in longer processing times and may require advanced computational tools.
- Stakeholder Coordination: In restructured power systems, multiple stakeholders (e.g., utilities, regulators, investors) are involved in transmission planning. Coordinating among these diverse entities can be challenging, particularly when interests and priorities differ.
- Dynamic Market Conditions: The rapidly changing nature of energy markets poses a challenge for multi-stage planning. Factors such as technological advancements, policy shifts, and economic fluctuations can render initial plans obsolete or less relevant over time.
- Regulatory Hurdles: Regulatory frameworks may not fully support or accommodate multi-stage planning approaches. Inflexible regulations can limit the ability of planners to adapt their strategies based on evolving circumstances.

6.3. Multi-criteria decision making

Multi-criteria decision making (MCDM) has become increasingly important in various fields, including the planning and development of electrical transmission networks. As the demand for electricity grows and the push for RESs intensifies, decision-makers must evaluate multiple conflicting criteria to ensure a sustainable and efficient energy transmission system. MCDM encompasses a range of methods designed to help decision-makers evaluate alternatives based on multiple criteria. Some popular MCDM techniques include:

- Analytic Hierarchy Process (AHP): This method decomposes a complex decision problem into a hierarchy of simpler sub-problems, allowing for pairwise comparisons among different criteria and alternatives. AHP is widely used in energy planning due to its structured approach [25-28].
- Technique for Order Preference by Similarity to Ideal Solution (TOPSIS): TOPSIS identifies solutions from a finite set of alternatives based on their geometric distance from an ideal solution. This method is particularly useful in energy transmission planning, where it helps prioritize projects that minimize costs while maximizing efficiency and sustainability.
- Weighted Sum Model (WSM): In this straightforward approach, each criterion is assigned a weight based on its importance, and alternatives are scored accordingly. WSM is easy to implement but may oversimplify complex decisions.
- Fuzzy MCDM: This approach incorporates fuzzy logic to handle uncertainty and imprecision in the decision-making process. Fuzzy MCDM is particularly beneficial in energy planning, where data may be uncertain or incomplete.

The TNEP involves numerous factors, including cost, reliability, environmental impact, and social acceptance. MCDM methods facilitate a comprehensive analysis of these factors:

- Cost-Benefit Analysis: MCDM allows for a detailed comparison of the economic viability of different transmission projects, helping stakeholders choose the most cost-effective solution.
- Environmental Considerations: As RESs gain prominence, MCDM can evaluate the environmental impacts of various transmission routes, ensuring that the least harmful options are selected.
- Social Impact Assessment: Public acceptance is crucial in energy projects. MCDM can incorporate social criteria, such as community impact and stakeholder preferences, into the decision-making process.
- Reliability and Resilience: MCDM methods can assess the reliability of different transmission configurations, ensuring that the chosen network can withstand disruptions and meet future demand.

Therefore, MCDM provides a robust framework for evaluating multiple criteria in the planning and TNEP. By employing various MCDM techniques, decision-makers can navigate the complexities of energy systems, balancing economic, environmental, and social considerations to achieve sustainable development goals. As the energy landscape continues to evolve, the integration of MCDM into transmission planning will be essential for optimizing resource allocation and ensuring reliable energy delivery.

7. Uncertainty

The restructuring of power systems and the integration of RESs have introduced significant uncertainties that pose challenges to the planning and development of electrical transmission networks. These uncertainties stem from various factors, including the variability of renewable energy generation, regulatory changes, technological advancements, and market dynamics.

7.1. Variability of renewable energy generation

One of the primary challenges in integrating RES, such as wind and solar power, is their inherent intermittency. Unlike conventional power plants that can provide a steady output, renewable sources are subject to fluctuations due to weather conditions and time of day. This variability complicates the planning of transmission networks, as operators must ensure that the infrastructure can accommodate sudden changes in generation levels. As a result, planners need to develop strategies that enhance grid flexibility and reliability, such as incorporating energy storage systems and demand response mechanisms.

7.2. Regulatory and policy uncertainties

The restructuring of power markets often involves changes in regulations and policies aimed at promoting renewable energy adoption. These changes can create uncertainties regarding financial incentives, grid access, and interconnection standards. For instance, shifts in government policies may affect the economic viability of certain renewable projects, leading to fluctuations in investment levels. Planners must stay abreast of regulatory developments and incorporate potential policy scenarios into their planning models to mitigate risks associated with these uncertainties.

7.3. Technological advancements

Rapid advancements in technology can also introduce uncertainty into transmission network planning. Innovations in energy storage, smart grid technologies, and demand-side management can significantly alter the landscape of energy generation and consumption. While these technologies offer opportunities for enhancing grid resilience and efficiency, they also require planners to adapt their strategies continuously. The challenge lies in accurately forecasting the impact of these technologies on future energy

demand and supply patterns.

7.4. Market dynamics

The restructuring of power systems has led to the emergence of competitive electricity markets, which can introduce additional uncertainties. Market prices for electricity can fluctuate based on supply-demand dynamics, leading to unpredictability in revenue streams for renewable energy projects. Planners must consider these market variations when designing transmission networks to ensure that they remain economically viable under different scenarios.

7.5. Strategies for addressing uncertainties

To effectively manage these uncertainties in TNEP, several strategies can be employed:

- Scenario Analysis: Planners can use scenario analysis to evaluate a range of possible futures, considering different levels of renewable energy penetration, regulatory changes, and technological advancements. This approach helps identify robust solutions that can withstand various uncertainties.
- Stochastic Modeling: Incorporating stochastic modeling techniques allows planners to account for the probabilistic nature of renewable generation and demand patterns. By simulating multiple scenarios, planners can develop more resilient transmission strategies.
- Flexible Infrastructure: Designing transmission networks with flexibility in mind is crucial. This includes investing in modular components that can be easily upgraded or expanded as new technologies emerge or demand patterns change
- Stakeholder Engagement: Collaborating with stakeholders, including regulators, utility companies, and community representatives, is essential for understanding diverse perspectives and addressing concerns related to uncertainty in transmission planning.

In summary, the challenges posed by uncertainties in restructured power systems and RESs significantly impact the planning and development of electrical transmission networks. By employing strategic approaches such as scenario analysis, stochastic modeling, and stakeholder engagement, planners can better navigate these complexities and create resilient transmission systems that support a sustainable energy future. As the energy landscape continues to evolve, addressing these uncertainties will be critical for ensuring reliable and efficient electricity delivery.

7.6. Scenario analysis

Scenario analysis is a strategic planning method used to make flexible long-term plans. It is particularly useful for analyzing uncertainties and understanding the potential impacts of different future conditions on an organization or project. Here, I will provide a detailed explanation of scenario analysis, its benefits, and how it compares to other methods of uncertainty analysis. Scenario analysis involves developing a set of plausible future scenarios based on varying assumptions about key drivers that affect outcomes. These scenarios are not predictions but rather narratives that help organizations visualize how different factors might interact and influence future events [21,29,30]. The process typically involves:

- Identifying Key Drivers: Recognizing the critical uncertainties that could impact the organization, such as economic trends, technological advancements, regulatory changes, and social dynamics.
- Developing Scenarios: Crafting distinct scenarios based on different combinations of these drivers. Each scenario represents a unique view of the future.
- Analyzing Impacts: Evaluating how each scenario would affect the organization's objectives, strategies, and operations.
- Strategic Planning: Using insights from the scenarios to inform decision-making, risk management, and strategic planning.

Advantages of scenario analysis are as follows:

- Comprehensive Understanding of Uncertainties: Unlike traditional forecasting methods that often rely on a single predicted outcome, scenario analysis embraces uncertainty by exploring multiple possible futures. This helps organizations prepare for various contingencies.
- Enhanced Strategic Flexibility: By considering a range of scenarios, organizations can develop more adaptable strategies that are resilient to changes in the external environment.
- Improved Risk Management: Scenario analysis allows organizations to identify potential risks associated with different futures and devise strategies to mitigate these risks effectively.
- Encourages Creative Thinking: The process of developing scenarios fosters creative thinking and innovation among team members, leading to more robust and diverse strategic options.
- Stakeholder Engagement: Scenario analysis can be a collaborative process that engages stakeholders across the organization, fostering a shared understanding of uncertainties and potential responses.

Scenario analysis is a powerful tool for navigating uncertainty, and it offers several advantages over other methods of uncertainty analysis. Below, I will explain these advantages in detail, comparing scenario analysis with other common techniques.

1. Holistic Perspective on Uncertainties

- Scenario Analysis: This method considers a wide range of uncertainties by developing multiple plausible scenarios based on various assumptions. Each scenario provides a narrative that captures different potential futures, allowing organizations to explore diverse outcomes and their implications.

- Other Methods (e.g., Sensitivity Analysis): Techniques like sensitivity analysis typically focus on how changes in individual variables affect outcomes, often in isolation. This can lead to an incomplete understanding of the complex interactions among multiple factors.
- Advantage: Scenario analysis provides a more comprehensive view of uncertainties by integrating multiple variables and their interdependencies.

2. Flexibility and Adaptability

- Scenario Analysis: By generating various scenarios, organizations can develop flexible strategies that can be adjusted as conditions change. This adaptability is crucial in dynamic environments where unexpected events can occur.
- Other Methods (e.g., Forecasting): Traditional forecasting methods often rely on historical data to predict future outcomes, assuming that past trends will continue. This can limit an organization's ability to respond effectively to sudden changes or disruptions.
- Advantage: Scenario analysis encourages strategic flexibility, allowing organizations to pivot their plans based on emerging trends or shifts in the environment.

3. Encouragement of Creative Thinking

- Scenario Analysis: The process of creating scenarios fosters creative thinking and innovation. It encourages teams to think outside the box and consider unconventional possibilities, which can lead to novel solutions and strategies.
- Other Methods (e.g., Quantitative Risk Analysis): Quantitative methods often focus on statistical models and data-driven predictions, which can stifle creativity and limit exploration of alternative futures.
- Advantage: Scenario analysis promotes a culture of innovation by challenging conventional thinking and encouraging diverse perspectives.

4. Enhanced Risk Management

- Scenario Analysis: By exploring different potential futures, organizations can identify risks associated with each scenario and develop targeted mitigation strategies. This proactive approach helps prepare for adverse events before they occur.
- Other Methods (e.g., Monte Carlo Simulation): While Monte Carlo simulations provide valuable insights into the probability of various outcomes, they may not capture qualitative risks or extreme events that are not easily quantifiable.
- Advantage: Scenario analysis allows for a more nuanced understanding of risks, including those that are difficult to quantify, thereby enhancing overall risk management efforts.

5. Stakeholder Engagement and Collaboration

- Scenario Analysis: The development of scenarios often involves collaboration across different teams and stakeholders, fostering a shared understanding of uncertainties and encouraging collective problem-solving.
- Other Methods (e.g., Traditional Forecasting): Many quantitative methods are conducted in isolation by analysts or modelers, which can lead to a disconnect between the analysis and the broader organizational context.
- Advantage: Scenario analysis promotes engagement and collaboration, ensuring that diverse viewpoints are considered in the decision-making process.

Therefore, scenario analysis offers significant advantages over other methods of uncertainty analysis by providing a holistic perspective, enhancing flexibility, encouraging creative thinking, improving risk management, and fostering stakeholder engagement. These strengths make scenario analysis an invaluable tool for organizations seeking to navigate complex and uncertain environments effectively. By incorporating scenario analysis into their strategic planning processes, organizations can better prepare for a range of potential futures and make more informed decisions.

8. Challenges of reliability assessment with TNEP

The restructuring of power systems, aimed at enhancing competition and integrating RESs, has introduced significant challenges in assessing the reliability of electricity supply. Reliability assessment is crucial for ensuring that the transmission network can meet demand consistently and effectively, especially as the energy landscape evolves. Below are some key challenges associated with this process:

- Increased Complexity of the Grid: The integration of diverse RESs, such as wind and solar, adds complexity to the power grid. These resources are inherently variable and uncertain, making it difficult to predict their output. This variability can lead to challenges in maintaining system reliability, particularly during peak demand periods or adverse weather conditions.
- Market-Driven Operations: In restructured power systems, market mechanisms dictate generation and transmission operations. This market-driven approach can lead to short-term decision-making that may not prioritize long-term reliability. The focus on cost minimization can result in underinvestment in critical infrastructure necessary for maintaining reliability.
- Regulatory Uncertainties: Frequent changes in regulatory frameworks can create uncertainties regarding reliability standards and requirements. This inconsistency can hinder effective planning and investment in transmission networks, as stakeholders may be unsure about future regulations impacting system reliability.

- Technological Integration: Emerging technologies, such as energy storage systems and demand response programs, can enhance reliability but also introduce new complexities. Understanding how these technologies interact with existing infrastructure is essential for accurate reliability assessments.
- Interconnectedness of Systems: As power systems become more interconnected, reliability assessments must account for the impacts of outages or failures in one region on neighboring areas. This interconnectedness complicates the analysis, as it requires a comprehensive understanding of the entire grid's dynamics.

To effectively address the challenges of reliability assessment in restructured power systems, several strategies can be implemented:

- Enhanced Modeling Techniques: Utilizing advanced modeling techniques, such as probabilistic load flow analysis and Monte Carlo simulations, can help assess the impact of renewable energy variability on system reliability. These models can incorporate a range of scenarios, providing a more comprehensive view of potential reliability issues.
- Robust Planning Frameworks: Developing robust planning frameworks that prioritize long-term reliability over short-term cost savings is essential. This includes establishing clear guidelines for investment in transmission infrastructure that considers future demand growth and renewable energy integration.
- Stakeholder Collaboration: Engaging stakeholders including regulators, utilities, and consumers in the planning process can ensure that diverse perspectives are considered. Collaborative efforts can lead to more informed decision-making regarding reliability standards and investment priorities.
- Regular Reliability Assessments: Conducting regular reliability assessments using updated data and models is crucial for adapting to changing conditions in the power system. Continuous monitoring allows for timely identification of potential reliability issues and facilitates proactive measures.
- Incorporation of Technological Innovations: Leveraging technological innovations, such as smart grid technologies and advanced energy management systems, can enhance real-time monitoring and control of the grid. These tools can improve operational flexibility and help mitigate reliability risks associated with variable RESs.
- Policy Stability: Advocating for stable regulatory frameworks can help reduce uncertainty related to reliability standards. Clear policies that support investment in reliable infrastructure are essential for maintaining system integrity in a restructured environment.

The assessment of reliability in restructured power systems with integrated RESs presents significant challenges due to increased complexity, market dynamics, regulatory uncertainties, technological advancements, and interconnectedness. By employing enhanced modeling techniques, robust planning frameworks, stakeholder collaboration, regular assessments, technological innovations, and advocating for policy stability, stakeholders can effectively navigate these challenges and ensure a reliable electricity supply for the future. Addressing these issues is vital for creating resilient power systems capable of meeting the demands of a sustainable energy landscape.

9. Challenges of Private Investment in TNEP

The restructuring of power systems has led to the emergence of competitive markets aimed at improving efficiency and integrating RESs. However, private investment in transmission network development faces several challenges that can hinder the effective planning and expansion of these critical infrastructures. Below are some of the key challenges associated with attracting private investment, along with strategies to enhance investment opportunities.

The main Challenges in this regard are:

- Item Regulatory Uncertainty: The regulatory environment in restructured power systems can be volatile, with frequent changes in policies and standards. This uncertainty can deter private investors who seek stable and predictable returns on their investments. Inconsistent regulations may also lead to confusion regarding the rights and responsibilities of private entities in the transmission sector.
- Long-Term Investment Horizon: Transmission projects typically require significant capital investment and have long payback periods. Private investors may be hesitant to commit to long-term projects without assurances of stable revenues and guaranteed returns. The mismatch between the short-term focus of many private investors and the long-term nature of transmission investments can create barriers to entry.
- Market Competition and Pricing: In competitive markets, the pricing mechanisms for transmission services may not adequately reflect the costs of infrastructure development. If transmission prices are kept artificially low due to market competition, it may not provide sufficient incentives for private investors to fund new projects.
- Risk Allocation: Investors are often concerned about the allocation of risks associated with transmission projects, including construction risks, operational risks, and demand risks. If the regulatory framework does not clearly define how these risks are shared between public and private entities, it can deter investment.
- Integration of RESs: The integration of variable RESs into the transmission network adds complexity to planning and investment decisions. Investors may perceive the uncertainties associated with RES output as a risk factor that complicates their financial models.
- Public Opposition and Environmental Concerns: Transmission projects often face opposition from local communities due to concerns about environmental impact, land use, and aesthetic issues. This public opposition can delay projects and increase costs, making them less attractive to private investors.

To address these challenges and enhance private investment in transmission network development, several strategies can be implemented:

- Stable Regulatory Frameworks: Establishing clear and stable regulatory frameworks is crucial for attracting private investment. Governments should work towards creating consistent policies that provide long-term visibility for investors regarding tariffs, revenue models, and regulatory requirements.
- Incentive Structures: Implementing incentive structures, such as tax breaks or guaranteed returns on investment, can make transmission projects more appealing to private investors. These incentives can help mitigate perceived risks and improve the overall investment climate.
- Public-Private Partnerships (PPPs): Developing public-private partnerships can facilitate collaboration between government entities and private investors. By sharing risks and responsibilities, PPPs can create a more favorable environment for investment while ensuring that public interests are met.
- Transparent Planning Processes: Ensuring transparency in planning processes can build investor confidence. Engaging stakeholders early in the planning phase and providing clear information on project timelines, costs, and expected returns can help attract private capital.
- Risk Mitigation Mechanisms: Implementing risk mitigation mechanisms, such as insurance schemes or government guarantees, can help reduce the financial risks associated with transmission projects. By providing a safety net for investors, these mechanisms can encourage greater participation.
- Facilitating Community Engagement: Actively engaging with local communities and addressing their concerns can help mitigate opposition to transmission projects. By incorporating community feedback into project planning and demonstrating commitment to environmental stewardship, developers can build trust and support.
- Promoting Technological Innovation: Encouraging the adoption of innovative technologies in transmission infrastructure can enhance efficiency and reduce costs. Public funding for research and development in smart grid technologies, energy storage solutions, and demand response programs can create a more attractive investment landscape.

Attracting private investment in transmission network development within restructured power systems is fraught with challenges, including regulatory uncertainty, long-term investment horizons, market competition, risk allocation, integration of RESs, and public opposition. However, by implementing strategies such as establishing stable regulatory frameworks, creating incentive structures, fostering public-private partnerships, ensuring transparency, mitigating risks, engaging communities, and promoting technological innovation, stakeholders can enhance the attractiveness of transmission projects for private investors. A collaborative approach that balances public interests with private investment objectives is essential for developing a resilient and efficient transmission network capable of supporting a sustainable energy future.

10. The effect of electrical energy storage devices and electric vehicles on TNEP

The integration of energy storage systems and electric vehicles (EVs) into TNEP presents a transformative opportunity for enhancing grid reliability, efficiency, and sustainability. Energy storage systems, such as batteries, can effectively balance supply and demand by storing excess energy during periods of low demand and releasing it during peak times. This capability is particularly beneficial in accommodating the variable nature of RESs like solar and wind. Moreover, electric vehicles can act as mobile energy storage units, offering the potential for vehicle-to-grid (V2G) technology, where EVs discharge stored energy back into the grid during high-demand periods. Consequently, when developing transmission networks, planners must consider the dual role of EVs as both loads and potential sources of energy. By strategically incorporating these technologies into transmission planning, utilities can reduce the need for costly infrastructure upgrades, improve grid resilience against outages, and facilitate a smoother transition to a low-carbon energy future. The synergy between energy storage and electric vehicles not only optimizes resource utilization but also enhances the overall stability of the electrical grid, paving the way for a more integrated and sustainable energy ecosystem [4,7,18] and [42-81]

The integration of energy storage systems and EVs into TNEP presents several significant challenges that need to be addressed. Energy storage systems must be carefully sized and strategically located to effectively mitigate these fluctuations, requiring advanced forecasting and modeling techniques. Additionally, the increasing penetration of EVs introduces new load patterns that can strain existing infrastructure, particularly during peak charging times. This necessitates a reevaluation of grid capacity and the potential for congestion in certain areas, demanding enhanced demand response strategies and dynamic pricing models to manage load effectively. Moreover, the interoperability of different technologies poses another challenge, as various energy storage systems and EVs may not seamlessly integrate with existing grid infrastructure or communication protocols. Regulatory frameworks also need to evolve to accommodate these technologies, ensuring that market structures incentivize investment in energy storage and EV charging infrastructure. Finally, there are concerns related to the lifecycle impacts of battery production and disposal, which must be considered in the broader context of sustainability. Addressing these challenges requires a collaborative approach involving utilities, policymakers, technology developers, and consumers to create a resilient and efficient transmission network that can support the growing role of energy storage and electric vehicles in the energy landscape.

11. Discussion

The restructuring of power networks has led to significant changes in the concepts of operation and planning due to various reasons. The requirement for open access for producers and consumers to the transmission network, the involvement of private investors in the generation and transmission sectors, the separation of generation and transmission sectors, and consequently the potential for achieving full coordination in the planning of these two sectors, as well as the increasing emphasis on investment

profitability in network development due to the presence of private investors, have all contributed to the diminishing effectiveness of conventional network planning approaches.

Network planning algorithms in a restructured environment must possess the following characteristics:

- Consider the diverse and often conflicting objectives of market players and investors
- Since the transmission network serves as a platform for power exchange and a more competitive market benefits all participants (as societal welfare), aim to eliminate barriers to competition within the market
- Model reliability in such a way that economic analysis can be performed, allowing for the determination of an optimal technical-economic level of reliability
- Model input uncertainties, which are significantly greater and more impactful than in the past, and effectively interact with the planning of other sectors, especially the generation sector
- Utilize a cost-benefit analysis approach instead of a cost-minimization approach to enable a thorough technical-economic evaluation of investments
- Facilitate the presence of private capital by shifting away from a fully centralized traditional approach

Since the introduction of transmission network planning models based on optimization with a single objective function in the 1970s, nearly all research efforts have focused on developing this model. Over the past three decades, research studies have been based on two main approaches:

- The introduction of new and more efficient methods for solving problems, including mathematical, intelligent, or hybrid methods
- Modifying the objective function of the initial model by incorporating factors such as operational costs and network losses

These approaches have not changed even with the restructuring of the network, such that most new planning models continue to follow the original single-objective structure, considering objectives such as minimizing congestion costs or maximizing overall welfare as their primary objective function. A suitable algorithm for TNEP in the new structure should possess the following capabilities and features:

- Pursue facilitating competition in the market as a goal
- Consider the interests of various stakeholders, including investors
- Take uncertainties in different sectors into account during the planning process
- Enable cost-benefit analysis

Figure 8 shows a bar chart that illustrates the trends in research studies related to transmission network development from 2016 to 2024. The horizontal axis represents the years, while the vertical axis indicates the number of studies conducted. The chart categorizes studies into five distinct types, each represented by a different color in the legend: Bi-level, Benders decomposition, Wind effect, Energy storage, and Multi-stage.

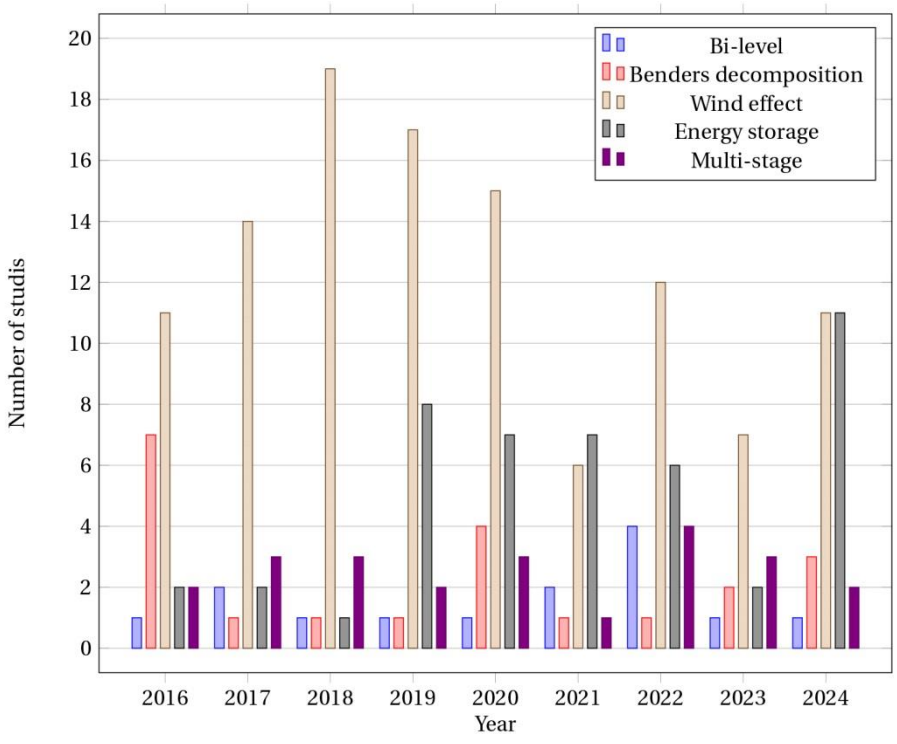

Figure 8. Trends in research studies related to transmission network development from 2016 to 2024.

The data shows that the Bi-level studies have shown significant variability, peaking in 2022 with four studies, indicating a growing interest in this approach for optimizing network planning. In contrast, Benders decomposition reached its highest point in 2018 with 19 studies but has since declined, suggesting a possible shift in focus towards other methodologies. The Wind effect category has gained traction, particularly in recent years, reflecting an increasing acknowledgment of renewable energy integration into transmission planning. Energy storage studies have fluctuated but saw a notable increase in 2024, highlighting the rising importance of energy storage solutions in managing grid stability and reliability. Lastly, multi-stage studies have remained relatively low but consistent, emphasizing their niche role in the broader context of transmission network research. Overall, this chart provides valuable insights into the evolving landscape of transmission network development research, showcasing how different topics have gained or lost relevance over time and guiding future research directions.

The optimization of TNEP faces several significant challenges that stem from the complexity of modern energy systems. As electricity demand continues to grow and the integration of RESs becomes more prevalent, traditional optimization methods may fall short in addressing the multifaceted nature of these challenges. One of the primary challenges is the inherent uncertainty associated with load forecasting and renewable generation. The variability of RESs, such as solar and wind, can lead to fluctuations in supply, making it difficult to ensure that the transmission network can reliably meet demand. This uncertainty necessitates the use of stochastic optimization techniques that can account for a range of possible scenarios, rather than relying solely on deterministic models.

Another challenge is the multi-objective nature of transmission planning. Planners must balance various competing objectives, including minimizing costs, maximizing reliability, and minimizing environmental impacts. Traditional optimization approaches often focus on a single objective, which may lead to suboptimal solutions when considering the broader implications of network development. Therefore, adopting multi-objective optimization frameworks is essential for finding solutions that satisfy diverse stakeholder interests. Additionally, regulatory and market uncertainties pose significant challenges to effective transmission planning. The evolving landscape of energy markets and regulations can affect investment decisions, making it crucial for planners to incorporate flexibility into their optimization models. This flexibility allows for adjustments in response to changing policies and market dynamics, ultimately leading to more resilient network designs.

In conclusion, addressing the challenges of optimization in transmission network development planning requires innovative approaches that incorporate uncertainty, multi-objectivity, and flexibility. By leveraging advanced optimization techniques and engaging with various stakeholders, planners can develop robust strategies that meet the demands of a rapidly changing energy landscape.

12. Conclusion

In conclusion, the importance of transmission network expansion planning (TNEP) in a restructured power system cannot be overstated. As we face the challenges of integrating diverse energy sources and meeting growing electricity demands, TNEP serves as a crucial framework for ensuring that the transmission infrastructure is capable of supporting a reliable and efficient energy supply. The transition to a more decentralized energy landscape, characterized by increased reliance on renewable resources, necessitates a forward-thinking approach to planning and investment in transmission networks. Effective TNEP not only facilitates the integration of renewable energy but also addresses issues related to network congestion and reliability. By strategically identifying areas where expansion or reinforcement is needed, TNEP helps to optimize the flow of electricity, reduce transmission losses, and enhance overall system performance. Furthermore, it plays a vital role in fostering competition among market participants by ensuring that all stakeholders have equitable access to the transmission network. Engaging with stakeholders including regulators, utility companies, and the public—is essential for successful TNEP implementation. Transparent communication and collaboration can help build trust and ensure that the planning process considers the diverse needs and concerns of all parties involved. Additionally, aligning TNEP with regulatory frameworks and policy objectives can facilitate smoother project approvals and encourage investment in necessary infrastructure. As we look to the future, it is clear that TNEP must adapt to evolving technologies and market dynamics. Innovations such as smart grid technologies, energy storage solutions, and demand response strategies offer new opportunities for enhancing transmission network efficiency and reliability. By embracing these advancements, we can create a more resilient power system capable of meeting the challenges of climate change and energy security. Ultimately, the successful implementation of TNEP will be instrumental in achieving not only economic growth but also environmental sustainability. A well-planned transmission network is essential for supporting clean energy transitions and ensuring that future generations have access to reliable and affordable electricity. As such, TNEP should be prioritized as a key component of energy policy and investment strategies moving forward.

References

[1] A. Rastgou, "Distribution Network Expansion Planning: An Updated Review of Current Methods and New Challenges," *Renewable and Sustainable Energy Reviews*, vol. 189, 114062, 2024.
[2] A. Rastgou, and J. Moshtagh, "Improved Harmony Search Algorithm for Transmission Expansion Planning with Adequacy–Security Considerations in the Deregulated Power System," *International Journal of Electrical Power & Energy Systems*, vol. 60, pp. 153–164, 2014.
[3] A. Rastgou, and J. Moshtagh, "Application of Firefly Algorithm for Multi-Stage Transmission Expansion Planning with Adequacy-Security Considerations in Deregulated Environments," *Applied Soft Computing*, vol. 41, pp. 373–389, 2016.
[4] E. Naderi, M. Pourakbari-Kasmaei, and M. Lehtonen, "Transmission Expansion Planning Integrated with Wind Farms: A Review, Comparative Study, and a Novel Profound Search Approach," *International Journal of Electrical Power & Energy Systems*, vol. 115, 105460, 2020.
[5] A. M. Alshamrani, M. A. El-Meligy, M. A. F. Sharaf, W. A. Mohammed Saif, and E. M. Awwad, "Transmission Expansion Planning Considering a High Share of Wind Power to Maximize Available Transfer Capability," *IEEE Access*, vol. 11, pp. 23136–23145, 2023.
[6] J. Hur, "Potential Capacity Factor Estimates of Wind Generating Resources for Transmission Planning," *Renewable Energy*, vol. 179, pp. 1742–1750, 2021.
[7] Y. Xie, and Y. Xu, "Transmission Expansion Planning Considering Wind Power and Load Uncertainties," *Energies*, vol. 15, no. 19, p. 7140, 2022.

[8] A. N. de Paula, E. J. de Oliveira, L. W. Oliveira, and C. A. Moraes, "Reliability-Constrained Dynamic Transmission Expansion Planning Considering Wind Power Generation," *Electrical Engineering*, vol. 102, no. 4, pp. 2583–2593, 2020.
[9] Z. Liang, H. Chen, et al., "Robust Transmission Expansion Planning Based on Adaptive Uncertainty Set Optimization Under High-Penetration Wind Power Generation," *IEEE Transactions on Power Systems*, vol. 36, no. 4, pp. 2798–2814, 2021.
[10] C. A. Moraes, L. W. de Oliveira, et al., "A Probabilistic Approach to Assess the Impact of Wind Power Generation in Transmission Network Expansion Planning," *Electrical Engineering*, vol. 104, no. 2, pp. 1029–1040, 2021.
[11] A. E. Ragab, and M. A. El-Meligy, "Transmission Expansion Planning in a Wind-Dominated Power System: A Closed-Loop Approach," *Sustainable Energy, Grids and Networks*, vol. 38, 101315, 2024.
[12] Y. Shi, R. Guo, Y. Tang, Y. Lin, and Z. Yang, "Integrated Transmission Network Planning by Considering Wind Power's Uncertainty and Disasters," *Energies*, vol. 16, no. 14, p. 5336, 2023.
[13] J. P. Pfeifenberger, A. Orths, W. Wang, and J. DeLosa III, "Planning for the Winds of Change: Coordinated and Proactive Offshore Wind Transmission Planning in Europe, China, and the United States," *IEEE Power and Energy Magazine*, vol. 22, no. 5, pp. 20–30, 2024.
[14] D. Liu, S. Zhang, et al., "Reducing Wind Power Curtailment by Risk-Based Transmission Expansion Planning," *International Journal of Electrical Power & Energy Systems*, vol. 124, 106349, 2021.
[15] M. Nazeri, M. Najafi, M. Hosseinpour, and M. Simab, "Simultaneously Planning of Transmission Line Expansion and Energy Storage in Order to Maximize the Capacity of Wind Farms," *Energy Science & Engineering*, vol. 12, no. 10, pp. 4308–4322, 2024.
[16] S. Borozan, S. Giannelos, P. Falugi, A. Moreira, and G. Strbac, "Machine Learning-Enhanced Benders Decomposition Approach for The Multi-Stage Stochastic Transmission Expansion Planning Problem," *Electric Power Systems Research*, vol. 237, 110985, 2024.
[17] S. Borozan, S. Giannelos, P. Falugi, A. Moreira, and G. Strbac, "Machine Learning-Enhanced Benders Decomposition Approach for the Multi-Stage Stochastic Transmission Expansion Planning Problem," *Electric Power Systems Research*, vol. 237, 110985, 2024.
[18] E. F. Alvarez, M. Paredes, and M. J. Rider, "Semidefinite Relaxation and Generalised Benders Decomposition to Solve the Transmission Expansion Network and Reactive Power Planning," *IET Generation, Transmission & Distribution*, vol. 14, no. 11, pp. 2160–2168, 2020.
[19] C. MacRae, A. Ernst, and M. Ozlen, "A Benders Decomposition Approach to Transmission Expansion Planning Considering Energy Storage," *Energy*, vol. 112, pp. 795–803, 2016.
[20] Y. Li, J. Wang, and T. Ding, "Clustering-based Chance-constrained Transmission Expansion Planning Using an Improved Benders Decomposition Algorithm," *IET Generation, Transmission & Distribution*, vol. 12, no. 4, pp. 935–946, 2018.
[21] S. Huang, and V. Dinavahi, "A Branch-And-Cut Benders Decomposition Algorithm for Transmission Expansion Planning," *IEEE Systems Journal*, vol. 13, no. 1, pp. 659–669, 2019.
[22] C. MacRae, A. Ernst, and M. Ozlen, "A Benders Decomposition Approach to Transmission Expansion Planning Considering Energy Storage," *Energy*, vol. 112, pp. 795–803, 2016.
[23] A. Rastgou, and S. Hosseini-Hemati, "Simultaneous Planning of the Medium and Low Voltage Distribution Networks Under Uncertainty: A Bi-Level Optimization Approach," *International Transactions on Electrical Energy Systems*, vol. 2022, pp. 1–19, 2022.
[24] H. Haghighat, and B. Zeng, "Bilevel Conic Transmission Expansion Planning," *IEEE Transactions on Power Systems*, vol. 33, no. 4, pp. 4640–4642, 2018.
[25] F. Misaghi, T. Barforoshi, and M. Jafari, "Distributed Generation Expansion Planning in Sub-Transmission Substations Considering Transmission Substations Expansions Using a Novel Bi-Level Model," Tabriz Journal of Electrical Engineering, vol. 47, no. 1, pp. 275–286, 2017.
[26] F. Misaghi, T. Barforoushi, and M. Jafari-Nokandi, "Regulatory Impacts on Distributed Generation and Upstream Transmission Substation Expansion Planning: A Novel Stochastic Bi-Level Model," *Iranian Journal of Electrical and Electronic Engineering*, vol. 13, no. 2, pp. 123–134, 2017.
[27] N. Gupta, M. Khosravy, N. Patel, and T. Senjyu, "A Bi-Level Evolutionary Optimization for Coordinated Transmission Expansion Planning," *IEEE Access*, vol. 6, pp. 48455–48477, 2018.
[28] I. C. González-Romero, S. Wogrin, and T. Gomez, "Considering Strategic Market Feedback in Transmission Expansion Planning: A Bi-Level Approach," in *2019 International Conference on Smart Energy Systems and Technologies (SEST)*, Porto, Portugal, pp. 1–6, 2019.
[29] N. Y. Puvvada, A. Mohapatra, and S. C. Srivastava, "Robust AC Transmission Expansion Planning Using a Novel Dual-Based Bi-Level Approach," *IEEE Transactions on Power Systems*, vol. 37, no. 4, pp. 2881–2893, 2022.
[30] F. Liu, Y. Su, et al., "A Bi-Level Transmission Expansion Planning Model Considering the Electricity Market," *2021 3rd International Conference on Electrical Engineering and Control Technologies (CEECT)*, pp. 126–130, 2021.
[31] J. Liu, Y. Liu, et al., "A Bi-Level Transmission Expansion Planning Method Considering Financial Transmission Rights," *2022 IEEE/IAS Industrial and Commercial Power System Asia (I&CPS Asia)*, pp. 1615–1619, 2022.
[32] L. Shen, L. Jiang, et al., "Bi-Level Transmission Expansion Planning Considering the Transfer Capacity of Hybrid AC/DC Interface," *2022 4th International Conference on Electrical Engineering and Control Technologies (CEECT)*, pp. 396–400, 2022.
[33] Y. Wang, R. Yang, F. Li, Y. Tang, and X. Zhao, "Variable-structure Copula Model for Multi-scenario Bi-level Transmission and Generation Expansion Planning," *IET Generation, Transmission & Distribution*, vol. 16, no. 21, pp. 4386–4399, 2022.
[34] I. C. González Romero, S. Wogrin, and T. Gómez San Román, "Considering Decentralized Storage and Renewable Investments in Transmission Expansion Planning: A Bi-Level Approach," *Universidad Pontificia Comillas*, Madrid, Spain, 2022.
[35] A. M. Alshamrani, K. A. Alnowibet, and A. F. Alrasheedi, "Bi-Level Transmission Expansion Planning Considering Prohibited Operating Zones and Multi-Fuel Units," *Sustainable Energy, Grids and Networks*, vol. 34, 101045, 2023.
[36] Y. Huang, X. Liu, et al., "Multi-Stage Transmission Network Planning Considering Transmission Congestion in the Power Market," *Energies*, vol. 13, no. 18, p. 4910, 2020.
[37] M. Taherkhani, S. H. Hosseini, M. S. Javadi, and J. P. Catalão, "Scenario-Based Probabilistic Multi-Stage Optimization for Transmission Expansion Planning Incorporating Wind Generation Integration," *Electric Power Systems Research*, vol. 189, 106601, 2020.
[38] S. Armaghani, A. Hesami Naghshbandy, and S. M. Shahrtash, "A Novel Multi-Stage Adaptive Transmission Network Expansion Planning to Countermeasure Cascading Failure Occurrence," *International Journal of Electrical Power & Energy Systems*, vol. 115, 105415, 2020.
[39] M. Franken, A. B. Schrief, H. Barrios, R. Puffer, and A. Moser, "Co-Optimization of Multi-Stage Transmission Expansion Planning and Grid Operation," *Electric Power Systems Research*, vol. 189, 106686, 2020.
[40] D. Sun, Y. Ma, et al., "Integrated Multi-Stage Coordination Planning of Transmission Network and Thermal Generation Units' Flexibility Reformation," *2020 IEEE 4th Conference on Energy Internet and Energy System Integration (EI2)*, pp. 1620–1625, 2020.
[41] S. Z. Moghaddam, H. Monsef, and M. Jafari, "A New Heuristic Method for Transmission Expansion Planning Using AHP," *2011 10th International Conference on Environment and Electrical Engineering*, pp. 1–4, 2011.
[42] S. Mou, N. Yang, H. Chen, Z. Liu, and S. Yang, "Integrating AHP and Entropy for Power Transmission Network Planning Evaluation," *2024 3rd International Conference on Energy and Electrical Power Systems (ICEEPS)*, pp. 621–624, 2024.
[43] Y. Hu, "Study on Comprehensive Evaluation of Transmission Grid Planning Based on Improved Fuzzy-AHP," M.S. thesis, *North China Electric Power University*, Beijing, China, 2016.
[44] Z. Yu, Q. Li, and Z. Lu, "Research on Gradual Planning Scheme of Power Grid Based on AHP and Entropy Weight Method," *Electronics Letters*, vol. 60, no. 14, p. e13280, 2024.
[45] K. Gholami, A. Azizivahed, et al., "Hybrid Uncertainty Approach for Management of Energy Storage-Embedded Soft Open Points in Distribution Grids," *Journal of Energy Storage*, vol. 87, 111394, 2024.
[46] P. Maghouli, S. H. Hosseini, M. Oloomi Buygi, and M. Shahidehpour, "A Scenario-Based Multi-Objective Model for Multi-Stage Transmission Expansion Planning," *IEEE Transactions on Power Systems*, vol. 26, no. 1, pp. 470–478, 2011.
[47] M. Majidi-Qadikolai and R. Baldick, "Stochastic Transmission Capacity Expansion Planning with Special Scenario Selection for Integrating *N-1* Contingency Analysis," *IEEE Transactions on Power Systems*, vol. 31, no. 6, pp. 4901–4912, 2016.
[48] A. Rastgou, J. Moshtagh, and S. Bahramara, "Probabilistic Power Distribution Planning Using Multi-Objective Harmony Search Algorithm," *Journal of Operation and Automation in Power Engineering*, vol. 6, no. 1, pp. 111–125, 2018.
[49] C. Rathore, "Static-Transmission Network Expansion Planning Considering Energy Storage Systems," International Journal of Innovations in Engineering, vol. 9, no. 7, pp. 1–7, 2022.

[50] J. Aguado, S. de la Torre, and A. Triviño, "Battery Energy Storage Systems in Transmission Network Expansion Planning," *Electric Power Systems Research*, vol. 145, pp. 63–72, 2017.
[51] H. Mazaheri, A. Abbaspour, M. Fotuhi-Firuzabad, H. Farzin, and M. Moeini-Aghtaie, "Investigating the Impacts of Energy Storage Systems on Transmission Expansion Planning," *2017 Iranian Conference on Electrical Engineering (ICEE)*, 2017.
[52] C. Bustos, E. Sauma, et al., "Energy Storage and Transmission Expansion Planning: Substitutes or Complements?," *IET Generation, Transmission & Distribution*, vol. 12, no. 8, pp. 1738–1746, 2018.
[53] I. Gonzalez-Romero, S. Wogrin, and T. Gomez, "Proactive Transmission Expansion Planning with Storage Considerations," *Energy Strategy Reviews*, vol. 24, pp. 154–165, 2019.
[54] S. Mahmoudi, M. Mirhosseini Moghaddam, and B. Alizadeh, "Transmission and Energy Storage–Expansion Planning in the Presence of Correlated Wind Farms," *International Transactions on Electrical Energy Systems*, vol. 29, no. 5, e2840, 2019.
[55] W. Gan, X. Ai, et al., "Security Constrained Co-Planning of Transmission Expansion and Energy Storage," *Applied Energy*, vol. 239, pp. 383–394, 2019.
[56] H. Nemati, M. A. Latify, and G. R. Yousefi, "Optimal Coordinated Expansion Planning of Transmission and Electrical Energy Storage Systems Under Physical Intentional Attacks," *IEEE Systems Journal*, vol. 14, no. 1, pp. 793–802, 2020.
[57] Z. Luburic, H. Pandzic, and M. Carrion, "Transmission Expansion Planning Model Considering Battery Energy Storage, TCSC and Lines Using AC OPF," *IEEE Access*, vol. 8, pp. 203429–203439, 2020.
[58] C. A. Mora, O. D. Montoya, and E. R. Trujillo, "Mixed-Integer Programming Model for Transmission Network Expansion Planning with Battery Energy Storage Systems (BESS)," *Energies*, vol. 13, no. 17, 4386, 2020.
[59] A. Amini, H. Falaghi, and M. Oloomi Buygi, "Energy Storage Systems Integrated Transmission Expansion Planning," *Journal of Energy Management and Technology*, vol. 4, no. 1, pp. 34–45, 2020.
[60] G. Pulazza, N. Zhang, C. Kang, and C. A. Nucci, "Expansion Planning Model Coordinated with Both Stationary and Transportable Storage Systems for Transmission Networks with High RES Penetration," *2020 IEEE International Conference on Environment and Electrical Engineering and 2020 IEEE Industrial and Commercial Power Systems Europe (EEEIC / I&CPS Europe)*, pp. 1–6, 2020.
[61] M. R. Ansari, S. Pirouzi, M. Kazemi, A. Naderipour, and M. Benbouzid, "Renewable Generation and Transmission Expansion Planning Coordination with Energy Storage System: A Flexibility Point of View," *Applied Sciences*, vol. 11, no. 8, p. 3303, 2021.
[62] M. Moradi-Sepahvand, and T. Amraee, "Integrated Expansion Planning of Electric Energy Generation, Transmission, and Storage for Handling High Shares of Wind and Solar Power Generation," *Applied Energy*, vol. 298, 117137, 2021.
[63] R. Hemmati, "Energy Storage Systems in Transmission Expansion Planning," *Transmission Expansion Planning: The Network Challenges of the Energy Transition*, pp. 249–268, 2020.
[64] H. Mazaheri, A. Abbaspour, et al., "An Online Method for MILP Co-planning Model of Large-scale Transmission Expansion Planning and Energy Storage Systems Considering N-1 Criterion," *IET Generation, Transmission & Distribution*, vol. 15, no. 4, pp. 664–677, 2020.
[65] I. Gonzalez-Romero, S. Wogrin, and T. Gomez, "Transmission and Storage Expansion Planning Under Imperfect Market Competition: Social Planner Versus Merchant Investor," *Energy Economics*, vol. 103, 105591, 2021.
[66] H. Nemati, M. A. Latify, and G. R. Yousefi, "Tri-Level Coordinated Transmission and Electrical Energy Storage Systems Expansion Planning Under Physical Intentional Attacks," *Journal of Energy Storage*, vol. 42, 103095, 2021.
[67] S. Liu, Y. Bai, et al., "Co-Planning of Transmission Expansion and Energy Storage in Electricity Spot Market," *2021 IEEE Sustainable Power and Energy Conference (iSPEC)*, pp. 1884–1890, 2021.
[68] M. Kazemi, and M. R. Ansari, "An Integrated Transmission Expansion Planning and Battery Storage Systems Placement - A Security and Reliability Perspective," *International Journal of Electrical Power & Energy Systems*, vol. 134, 107329, 2022.
[69] H. Mazaheri, M. Moeini-Aghtaie, M. Fotuhi-Firuzabad, P. Dehghanian, and M. Khoshjahan, "A Linearized Transmission Expansion Planning Model Under $N - 1$ *Criterion for Enhancing Grid-scale System Flexibility Via Compressed Air Energy Storage Integration," IET Generation, Transmission & Distribution*, vol. 16, no. 2, pp. 208–218, 2021.
[70] M. Moradi-Sepahvand, and T. Amraee, "Transmission and Energy Storage Co-Planning Expansion Considering Short-Term Uncertainties Under Renewable Penetration," *2022 30th International Conference on Electrical Engineering (ICEE)*, pp. 609–613, 2022.
[71] M. Rawa, Z. M. AlKubaisy, et al., "A Techno-Economic Planning Model for Integrated Generation and Transmission Expansion in Modern Power Systems with Renewables and Energy Storage Using Hybrid Runge Kutta-Gradient-Based Optimization Algorithm," *Energy Reports*, vol. 8, pp. 6457–6479, 2022.
[72] Y. Yuan, H. Zhang, H. Cheng, J. Zhang, and Z. Wang, "Transmission and Energy Storage Expansion Planning Against Extreme Event," *2022 IEEE 5th International Electrical and Energy Conference (CIEEC)*, pp. 4347–4352, 2022.
[73] Q. Yang, J. Wang, et al., "Tri-Level Expansion Planning for Transmission, Energy Storage, and Renewable Energy Considering Carbon Emission Limitation," *Energy Reports*, vol. 9, pp. 1169–1180, 2023.
[74] L. Qiu, Y. Dan, X. Li, and Y. Cao, "Decision-dependent Distributionally Robust Integrated Generation, Transmission, and Storage Expansion Planning: An Enhanced Benders Decomposition Approach," *IET Renewable Power Generation*, vol. 17, no. 14, pp. 3442–3456, 2023.
[75] M. Al-Dhaifallah, M. M. Refaat, et al., "Multi-Objectives Transmission Expansion Planning Considering Energy Storage Systems and High Penetration of Renewables and Electric Vehicles Under Uncertain Conditions," *Energy Reports*, vol. 11, pp. 4143–4164, 2024.
[76] D. H. Huanca, D. M. Falcão, and M. E. C. Bento, "Transmission Expansion Planning Considering Storage, Flexible AC Transmission System, Losses, and Contingencies to Integrate Wind Power," *Energies*, vol. 17, no. 7, p. 1777, 2024.
[77] H. Farokhzad Rostami, M. Samiei Moghaddam, M. Radmehr, and R. Ebrahimi, "Stochastic Security-constrained Transmission and Energy Storage Expansion Planning Considering High Penetration of Renewable Energy in Integrated Gas-electricity Networks," *Energy Storage*, vol. 6, no. 1, 2023.
[78] Q. Yang, J. Wang, Y. Zhang, and Q. Li, "A Network Search Space Reduction Method for Robust Coordinated Energy Storage and Transmission Expansion Planning," *IET Generation, Transmission & Distribution*, vol. 18, no. 7, pp. 1449–1465, 2024.
[79] K. Wu, R. Haider, and P. Van Hentenryck, "High-Spatial Resolution Transmission and Storage Expansion Planning for High Renewable Grids: A Case Study," arXiv preprint arXiv:2412.03799, 2024.
[80] L. Lu, M. Wei, et al., "Stochastic Programming Based Coordinated Expansion Planning of Generation, Transmission, Demand Side Resources, and Energy Storage Considering the DC Transmission System," *Global Energy Interconnection*, vol. 7, no. 1, pp. 25–37, 2024.
[81] N. Segura, A. Villarnarín-Jácome, D. Espín-Sarzosa, and F. Muñoz, "Assessing the Impacts of Electric Vehicle Demand Management on Transmission Expansion Planning," *2023 IEEE CHILEAN Conference on Electrical, Electronics Engineering, Information and Communication Technologies (CHILECON)*, pp. 1–6, 2023.

Declaration of competing interest

The author declare that he has no known competing financial interests or personal relationships that could have appeared to influence the work reported in this paper. The ethical issues, including plagiarism, informed consent, misconduct, data fabrication and/or falsification, double publication and/or submission, redundancy, have been completely observed by the author.

Bibliography

Abdollah Rastgou holds a Bachelor's, Master's, and Ph.D. degree in Power Electrical Engineering. He completed his Bachelor's degree at Tabriz University and went on to earn both his Master's and Ph.D. degrees with honors from Kurdistan University in Sanandaj. Dr. Rastgou has a keen interest in power system planning, bi-level planning, and renewable resource planning. His academic journey reflects a strong commitment to advancing the field of electrical engineering, particularly in optimizing power systems for sustainability and efficiency.

Email: abdollah.rastgou@iau.ac.ir

ORCID: 0000-0002-8620-2185

Contribution Statement: Conceptualization, Data curation, Formal analysis, Funding acquisition, Investigation, Methodology, Project administration, Resources, Software, Supervision, Validation, Visualization.

Journal of Green Energy Research and Innovation

Performance Analysis of a Three-Level Z-Source Inverter for Grid-Connected Photovoltaic Systems Using Model Predictive Control

Ali Nahavandi, Mohammad Reza Azizi

Highlights

- **Presentation of a single-stage boost z-source neutral point clamped (Z-NPC) Inverter.**
- **Use of model predictive control (MPC) to control the proposed three-level inverter.**
- **Tracking the maximum point of power for photovoltaic panel (PV) using model predictive control.**

Graphical Abstract

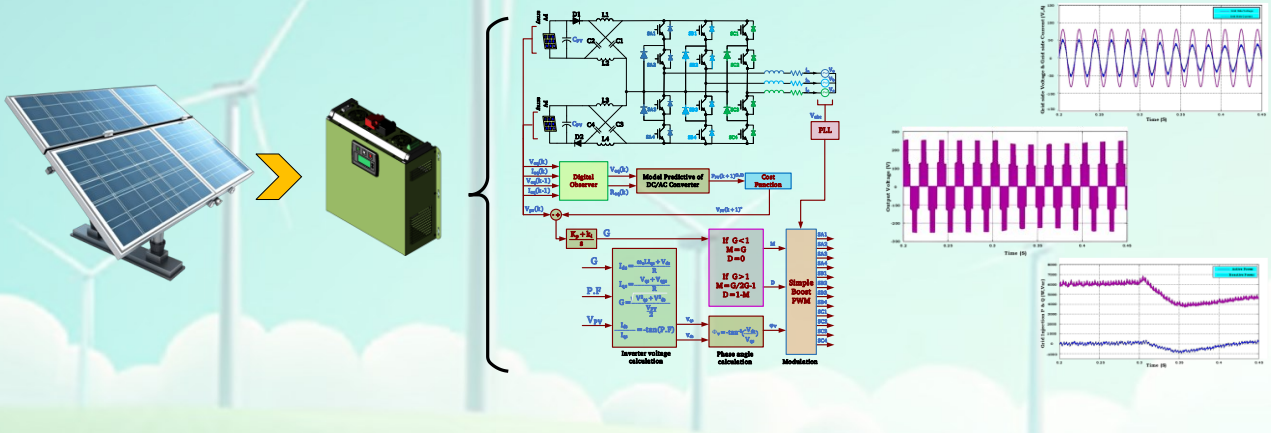

Use your device to scan and read the article online

Citation

A. Nahavandi, and M. Azizi," Performance Analysis of a Three-Level Z-Source Inverter for Grid-Connected Photovoltaic Systems Using Model Predictive Control," *Journal of Green Energy Research and Innovation*, vol. 2, no. 5, pp. 68-78, 2025.

https://doi.org/10.61186/jgeri.2.2.68

JGERI Journal of Green Energy Research and Innovation

Journal of Green Energy Research and Innovation 2.2 (2025) 68-78

Online ISSN: 3041-9018

Journal of Green Energy Research and Innovation

Journal Homepage: www.jgeri.araku.ac.ir

Performance Analysis of a Three-Level Z-Source Inverter for Grid-Connected Photovoltaic Systems Using Model Predictive Control

Ali Nahavandi *, Mohammad Reza Azizi

Department of Electrical Engineering, Faculty of Engineering, Malayer University, Malayer, Iran.

A R T I C L E I N F O

Keywords:
Photovoltaic System,
Three Level Z-Source Inverter,
Model Predictive Control,
Maximum Power Point Tracking
(MPPT).

Article History:
Received: 03 March 2025;
Revised: 07 April 2025;
Accepted: 09 April 2025.

Article type:
Research Article

* ***Corresponding author***
E-mail address
ali.nahavandi@malayeru.ac.ir (A. Nahavndi)

A B S T R A C T

In this paper, a single-stage three-level z-source inverter is utilized for connecting PV panels to the grid. The use of a three-level z-source inverter not only allows adjustment of output voltage but also facilitates the elimination of harmonic components. To extract maximum power from the PV panels, a model predictive control (MPC) strategy based on maximum power point tracking (MPPT) is employed. This method allows the MPC to predict the optimal operating point one step ahead, resulting in a faster response compared to conventional perturb and observe (P&O) method under rapid changes. Finally, the three-level z-source inverter is simulated using MATLAB/Simulink software, and its performance using the MPC method is analyzed. The simulation results have verified that the converter operates effectively.

1. Introduction

The increasing focus on renewable energy sources, driven by environmental concerns, decreasing prices of solar cells, and reductions in the costs of power electronic converters, has led to a significant rise in the use of solar panels for power supply and grid connectivity over the past decade [1]. The grid connection of solar panels is typically categorized into two forms: isolated and non-isolated. The non-isolated configuration is generally employed for low voltage applications, whereas the isolated configuration, which includes an iron core transformer, is used for high voltage applications. Although this transformer provides galvanic isolation between the power grid and photovoltaic systems, it is often bulky, heavy, and expensive due to its low operating frequency (50-60 Hz), leading to losses that diminish overall system efficiency. To eliminate the transformer, reduce costs, decrease weight, and enhance efficiency, there is a growing interest in transformerless systems [2,3].

Transformerless systems can be divided into single-stage and two-stage configurations. Grid-connected Photovoltaic (PV) systems typically employ two-stage architectures [4]. The first stage serves to boost the PV voltage and track the maximum power point using a DC-DC boost converter, while the second stage facilitates DC-AC power conversion. Although this two-stage structure has been tested successfully in recent years, it presents several disadvantages, including a high component count, lower efficiency, reduced functionality, increased costs, and bulkiness. To address these issues, there is growing interest in single-stage systems that can meet all requirements within a single power conversion stage. Several single-stage DC-AC inverters have been discussed in [5-7]. Among these single-stage systems, the impedance source inverter (ZSI) presents a particularly promising option for investigation. The ZSI possesses unique features that enable it to both increase and decrease the output voltage, capabilities that are not typically found in other types of inverters [8,9]. Generally, voltage source inverters (VSIs) can only decrease the output voltage, while current source inverters (CSIs) can only increase the output voltage. In [10] model predictive control was employed with a CSI to extract maximum power even when the PV voltage is less than its nominal value. One of the advantages of CSIs is their ability to deliver high-quality and robust current output.

However, a significant drawback of CSIs is the large DC link inductor, which can lead to high power losses. A ZSI with MPPT-based MPC was used in [11] to extract maximum power in a single stage, with satisfactory results.

PV arrays are inherently nonlinear, and they have a single operating point at which they generate maximum power. To maximize the efficiency of PV arrays, the implementation of Maximum Power Point Tracking control techniques is essential for extracting the maximum possible power [12]. Numerous MPPT techniques have been explored over the last couple of decades, with their respective advantages discussed in detail in [13]. Among these methods, the Perturb and Observe (P&O) technique is well-established and demonstrates satisfactory performance. However, its relatively slow response time can hinder its effectiveness in tracking rapid changes in solar irradiance [14,15]. A key contribution of this paper is the enhancement of the P&O method through the application of Model Predictive Control. By utilizing MPC, the P&O technique can predict the optimal operating point one step ahead compared to conventional P&O, allowing for a quick response to sudden changes in irradiance levels and temperature [16]. In [17], it was demonstrated that MPC can effectively improve the P&O method for MPPT, showing a strong response to rapid fluctuations in irradiance. Especially, this system is configured for grid connection using a two-stage approach, with each stage featuring independent control.

This paper focuses on a three-level impedance source inverter that employs MPPT-based MPC. This configuration not only facilitates the ability to increase or decrease output voltage and effectively implement MPPT but also reduces harmonic components in both the voltage and the current injected into the grid. Additionally, the inverter input is designed to incorporate two panels. Each panel is connected to its own impedance network, which enhances overall system performance. It is important to note that solar panels are typically constructed using low-voltage cells that are connected in series to achieve a reasonable output voltage. However, connecting a large number of cells in series can complicate the system and may negatively impact performance due to variations among cells and differing operating conditions. The subsequent sections of this paper are organized as follows: Section 2 describes the general components of the system. Section 3 presents the proposed MPPT-based MPC for z-source inverter. Section 4 provides simulation results that validate the effectiveness of the aforementioned control technique. Finally, Section 5 concludes the paper.

2. General Component of System

2.1. Three Level Z-Source Inverter

Three-level Neutral Point Clamped (NPC) inverters, known for their intrinsic advantages, are commonly employed as an effective architecture for medium voltage AC drives and, more recently, for grid-connected renewable energy applications at low voltage levels [18,19]. Despite their desirable output performance, these inverters have a limitation: they lack a DC-DC boost stage at the input, which restricts their functionality to only reducing the output voltage. To address this limitation, the NPC buck-boost impedance source inverter has been introduced [20,21]. This configuration incorporates two X-shaped impedance networks connected to two independent DC sources. The term "three-level Z-NPC" refers to this type of inverter. In a three-level Z-NPC inverter, instead of using two voltage sources or two capacitors with a common connection point, two Z-source inverters are employed without a common point. As a result, z-source inverters can operate within the structure of multilevel inverters. The added impedance networks are responsible for balancing and boosting the voltage by allowing short circuits at any inverter phase (known as the shoot-through state) without causing damage to the semiconductor switches. This is achieved through the inductances of the z-source, which help prevent sudden increases in current. As shown in Figure 1, the three-level Z-NPC inverter consists of two impedance networks, each connected to its own independent DC source. These impedance networks have the capability to enhance the input DC voltage.

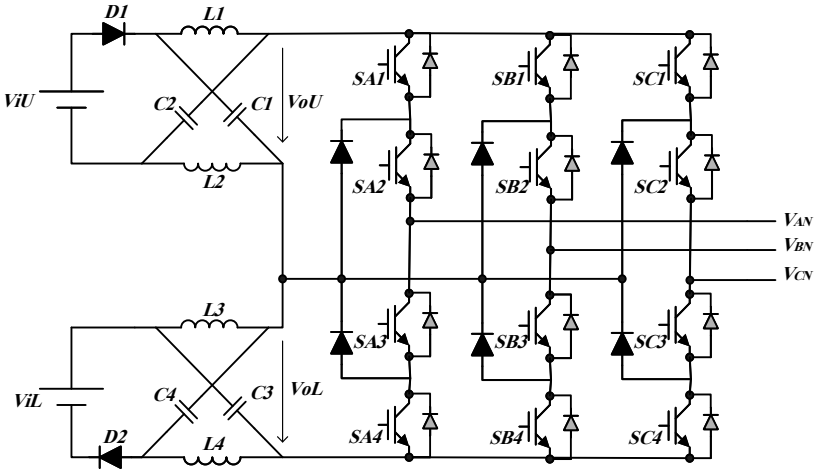

Figure 1. Three-level Z-source inverter with two impedance network.

Various modulation methods for z-source inverters have been proposed. Among these, in [22] the simple boost modulation strategy introduced which operates similarly to traditional carrier-based PWM, with its voltage gain defined by Equation (1):

$$G = M.B = \frac{V_{ac}}{V_o / 2} = \frac{M}{2M - 1} \tag{1}$$

Where M is the modulation index, B is the boosting factor of the impedance-network, V_{ac} is the amplitude of the output voltage of the inverter (equivalent to grid peak phase voltage when grid-tied), and V_o is the dc-link voltage. The boosting factor B is given by Equation (2):

$$B = \frac{1}{1 - 2D} \tag{2}$$

Where D is shoot-through duty cycle. Referring to the above equations, the boost factor of three level Z-NPC inverter for each impedance network can be derived as Equation (3):

$$\begin{cases} V_{oU} = B_U V_{iU} = \dfrac{V_{iU}}{1 - 2D_U} \\ V_{oL} = B_L V_{iL} = \dfrac{V_{iL}}{1 - 2D_L} \end{cases} \tag{3}$$

In which V_{iU} and V_{iL} are the DC input voltages and V_{oU} and V_{oL} are DC links output voltages and B_U and B_L for each impedance network are described as Equation (4):

$$\begin{cases} B_U = \dfrac{1}{1 - 2D_U} \\ B_L = \dfrac{1}{1 - 2D_L} \end{cases} \tag{4}$$

Where D_U is the shoot-through duty ratio for upper impedance network and for lower one is D_L as described in Equation (5):

$$\begin{cases} D_U = \dfrac{(T_{ShU} + T_{ShB})}{T} \\ D_L = \dfrac{(T_{ShL} + T_{ShB})}{T} \end{cases} \tag{5}$$

In these equations T_{ShU}, T_{ShL} and T_{ShB} represent the time durations of the short-circuit condition for the upper impedance network, the lower impedance network, and for both networks operating simultaneously, respectively. To minimize the output total harmonic distortion (THD), the boost factor must be determined such that the output voltages of both DC links in the networks are equal. When the DC link voltages of the NPC inverter are balanced, the same output power can be extracted from both DC links.

2.2. MPPT Techniques

Solar power generation systems utilize photovoltaic panels to convert sunlight directly into electricity. Under specific environmental conditions, there exists only one maximum power point (MPP) due to the nonlinear relationship between current and voltage (I-V). This peak power point fluctuates with changes in solar irradiance and operating temperature. The primary objective of implementing MPPT system is to ensure that the array of photovoltaic panels operates at the MPP, regardless of variations in irradiance, partial shading, or temperature. These factors can significantly impact the system's ability to achieve optimal performance. In recent years, many techniques have been proposed for MPPT, including the incremental conductance (INC) method, the P&O method, and the hill climbing method [13,15,23,24].

2.3. Model Predictive Control (MPC)

Model Predictive Control is a relatively new control technique applied for the control of power electronic converters [25]. Model predictive control has been used in low-switching-frequency power electronics for high-power applications since the 1980s [26]. Since high switching frequencies for the MPC algorithm required long calculation time, widespread adoption was not feasible at that time. In the past decade, with the improvement of high-speed microprocessors, interest in the application of MPC in power electronics with high switching frequency has increased considerably [27].

This method utilizes a mathematical model of the controlled system to predict its behaviour at each sampling instant k for the subsequent instant (k + 1). To determine the optimal state of the power converter, a cost function is defined. This function typically includes several constraints and control conditions. It generally encompasses the differences between reference values and predicted values of the controlled variables. Additionally, various components of this function represent specific constraints, such as limitations on switching frequency and other nonlinearities.

3. Proposed MPPT-Based Model Predictive Control Method

Figure 2 illustrates a grid-connected three-level Z-NPC inverter that utilizes two photovoltaic arrays in its DC links. Additionally, the control block diagrams for the proposed Maximum Power Point Tracking based model predictive control and other considerations are presented in this figure. The following sections will describe these blocks in detail, step by step.

3.1. Maximum Power Point Tracking- Based Model Predictive Control

The maximum power point tracking based on model predictive control is accomplished in two stages. In the first stage, the predictive model of the system is developed, and by applying the discrete-time model of the control variables used for predictions in the state-space model, two adaptive voltage values for the photovoltaic panels are predicted for the next sampling time. In the second stage, the cost function of the MPPT-based model predictive control tracks the voltage that maximizes the power drawn from the PV cells.

In this paper, due to the utilization of two panels, several approaches are suggested for implementing control methods:

1. Predictive equations can be extracted for each panel and its associated network, with the average modulation index considered. In this case, each network's impedance can be tailored to its specific conditions, allowing for different shoot-through duty cycles.

2. Regard to same conditions, predictive equations for one panel and its network be extracted, and other parameters appropriately be considered.

3. Both panels, be considered as a single panel and then predictive equations be extracted.

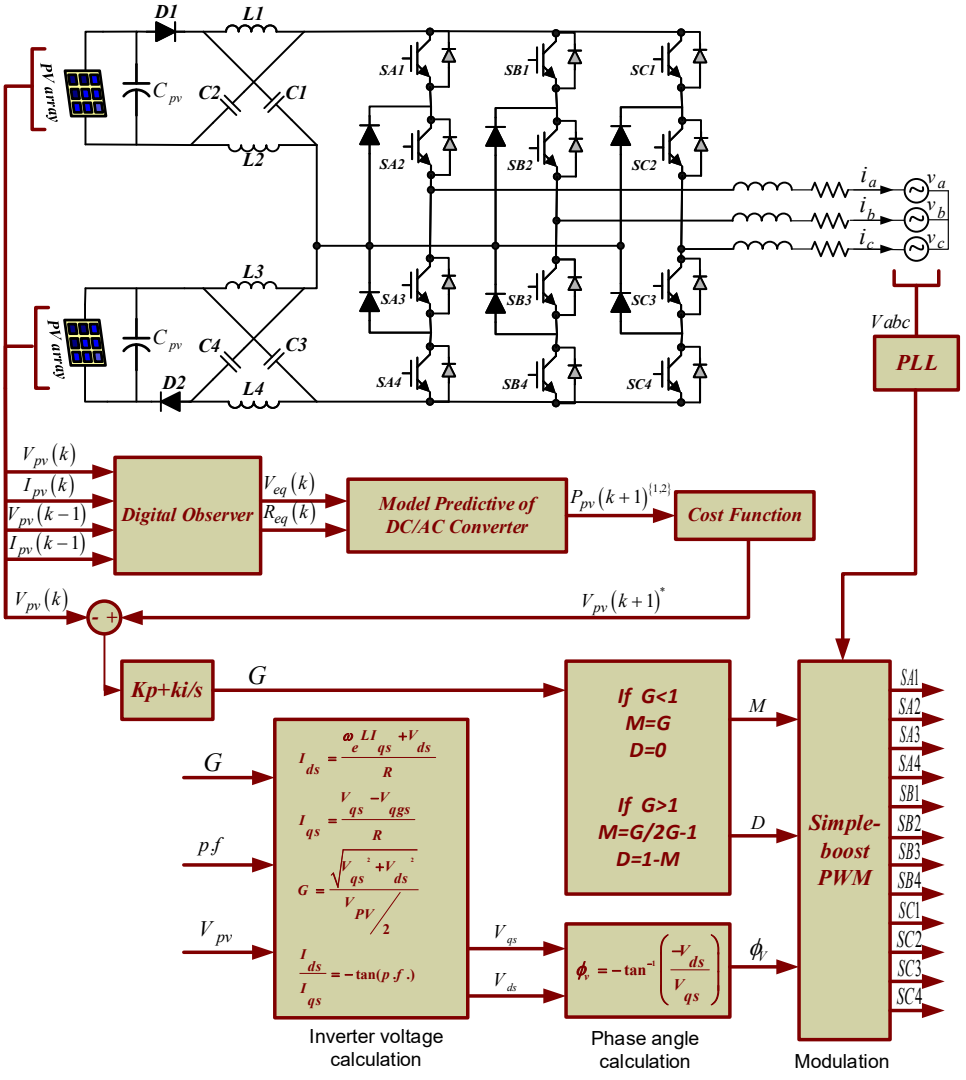

Figure 2. Three-level Z-source inverter with two impedance networks.

3.1.1. Stage1 Model Predictive Equation

By using KVL and KCL for non-shoot through state, Equation (6) is achieved.

$$\begin{cases} V_{PV} = R_{L_1} I_{L_1} + V_{L_1} + V_{C_1} \\ i_{L_1} = i_{C_1} + i_{inv} \end{cases} \tag{6}$$

Where R_{L1}, I_{L1} and V_{L1} are the inductor resistance, current and voltage respectively. Also, $V_{C1}$and i_{c1} are capacitor C_1 voltage and current respectively, and i_{inv} is inverter input current. By applying discrete time model with sample time T_s and replacing inductor voltage and capacitor current, this equation will be as Equation (7):

$$\begin{cases} I_{L_1}(k+1) = I_{L_1}(k) + \dfrac{T_s}{L_1}\left[(V_{PV} - V_{C_1}(k) - R_{L1} I_{L1}(K))\right] \\ V_{C_1}(k+1) = V_{C_1}(k) + \dfrac{T_s}{C_1}(I_{L_1}(k+1) - I_{inv}(k+1)) \end{cases} \tag{7}$$

Where I_{inv} is defined as Equation (8),

$$I_{inv}(k+1) = (S_{A1}.S_{A2}) \times I_a(k) + (S_{B1}.S_{B2}) \times I_b(k) + (S_{C1}.S_{C2}) \times I_c(k) \tag{8}$$

This equations for shoot through state are as Equation (9):

$$\begin{cases} V_{C2} = R_{L1} L_{L1} + V_{L1} \\ i_{L1} = -i_{C1} \end{cases} \tag{9}$$

As this topology is symmetrical and the values of inductance and capacitance is the same, $V_{L1} = V_{L2}$, $V_{C1} = V_{C2}$.

The discrete time model of above equation with sample time is as Equation (10):

$$\begin{cases} I_{L_1}(k+1) = I_{L_1}(k) + \dfrac{T_s}{L_1}(V_{C_1}(k) - R_{L_1} I_{L_1}(k)) \\ V_{C_1}(k+1) = V_{C_1}(k) - \dfrac{T_s}{C_1} I_{L_1}(k+1) \end{cases} \tag{10}$$

for sufficiently small sampling time (T_s), the change is negligible. Therefore, $V_{C_1}(k+1)$ is assumed to be approximately equal to $V_{C_1}(k)$. The average current flowing through C_{pv} and C_1 should be zero; thus, it can be concluded that I_{PV} is the same as Z-source inverter (ZSI) inductor current I_{L1}. Consequently, the predicted average PV current can be formulated using Equations (11) and (13) as follows:

$$I_{pv}^{ave}(k+1) = \left[I_{L_1}(k) + \frac{T_s}{L_1}(V_{PV} - V_{C_1}(k) - R_{L_1} I_{L_1}(k)) \right]\left[1 - D(k)\right] + \left[I_{L_1}(k) + \frac{T_s}{L_1}(V_{C_1}(k) - R_{L_1} I_{L_1}(k)) \right]\left[D(k)\right] \tag{11}$$

Considering the relationship between the PV voltage and V_{C_1} as follow in Equation (12):

$$V_{pv} = \frac{2}{B+1} V_{C_1} \tag{12}$$

The average PV voltage can be predicted using Equation (7), (10) and (12) as follows:

$$V_{pv}^{ave}(k+1) = \frac{2}{B+1} \times \left\{ \left[V_{C1}(k) + \frac{T_s}{C1}(I_{L1}(k+1) - I_{inv}(k+1)) \right]\left[1 - D(k)\right] + \left[V_{C1}(k) - \frac{T_S}{C1} I_{L1}(k+1) \right]\left[D(k)\right] \right\} \tag{13}$$

In following two possible values for PV voltage at sample time *(k+1)* will be predicted as follow in Equation (14):

$$\begin{cases} V_{pv}(k+1)^1 = V_{pv}(k) + \Delta V \\ V_{pv}(k+1)^2 = V_{pv}(k) - \Delta V \end{cases} \tag{14}$$

where ΔV is a voltage step that is adaptively predicted and can change based on its proximity to the Maximum Power Point (MPP). Equation (15) for ΔV is proposed:

$$\Delta V = \left| \tilde{V}_{pv}^{ave}(k+1) - V_{pv}(k) \right| \tag{15}$$

Where $V_{PV}^{ave}(k+1)$ is the predicted average voltage for PV at time n+1.

3.1.2. Stage2 MPPT Section & Cost Function

In this section, the MPPT technique tracks one of the two possible values of PV voltage that maximizes power extraction from the PV module. This MPPT algorithm requires understanding of the local P-V characteristics of the module around its operating point $V_{pv}(k)$. For this purpose, a digital observer (sensor) has been designed to generate the necessary information. The observer models the PV module with a Thevenin equivalent circuit. Since the characteristics of panel, at the time K and before it is available, Thevenin equivalent circuit of model can be achieved as shown in Figure 3. The elements of this circuit are equivalent voltage (V_{eq}) and equivalent resistance (R_{eq}) of the module and are calculated by Equation (16).

$$\begin{cases} R_{eq}(k) = -\dfrac{V_{pv}(k) - V_{pv}(k-1)}{I_{pv}(k) - I_{pv}(k-1)} \\ V_{eq}(k) = V_{pv}(k) + R_{eq}(k) \times I_{pv}(k) \end{cases} \tag{16}$$

Where $V_{pv}(k-1)$ and $I_{pv}(k-1)$ are the values of the PV module voltage and current from the previous sampling time. By calculating the panel voltage at the moment $k+1$ and having panel equivalent circuit, corresponding $I_{pv}(k+1)$ for each predicted value of voltage can be calculated in Equation (17):

$$\begin{cases} I_{pv}(k+1)^1 = \dfrac{V_{eq}(k) - V_{pv}(k+1)^1}{R_{eq}(k)} \\ I_{pv}(k+1)^2 = \dfrac{V_{eq}(k) - V_{pv}(k+1)^2}{R_{eq}(k)} \end{cases} \tag{17}$$

By estimating the equivalent resistance and voltage of the PV module and computing $I_{pv}(k+1)$ for each case, the two possible values for the generated power in the next sampling time can be easily predicted from Equation (18) and (19):

$$P_{pv}(k+1)^1 = V_{pv}(k+1)^1 \times I_{pv}(k+1)^1 \tag{18}$$

$$P_{pv}(k+1)^2 = V_{pv}(k+1)^2 \times I_{pv}(k+1)^2 \tag{19}$$

In next step, the predicted power value of the two cases will be used to evaluate the following cost function in Equation (20):

$$J^{\{1,2\}} = P_{pv}(k+1)^{\{1,2\}} - P_{pv}(k) \tag{20}$$

In order to track the MPP, the algorithm will choose the path that will result in the larger value of J from Equation (20). For instance, if $J_1 > J_2$, then the algorithm chooses to generate $P_{pv}(k+1)^1$ in the next sampling time, which correspondingly means the PV voltage will need to be shifted to $V_{pv}(k+1)^1$ by proper adjustment of controller. The desirable value of the PV voltage for the next step is denoted as $P_{pv}(k+1)^*$. Then $V_{pv}(k+1)^*$ will be compared with $V_{pv}(k)$ to generate the inverter gain.

3.2. Power Angle Control

The purpose of this section, is to control active and reactive power injected to the grid. To achieve such goal, inverter output voltages must be determined. The equivalent circuit of grid connected inverter in d-q rotating reference frame is shown in the Figure 4. Using the d axis and q-axis equivalent circuit, the relationship of d-q currents injected into the grid in terms of inverter output voltages is obtained as follow in Equations (21) and (22):

$$I_{ds} = \frac{\omega_e L I_{qs} + V_{ds}}{R} \tag{21}$$

$$I_{qs} = \frac{V_{qs} - V_{qgs}}{R} \tag{22}$$

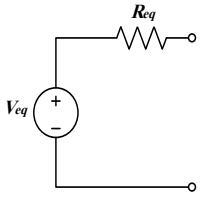

Figure 3. Equivalent circuit model of the PV module.

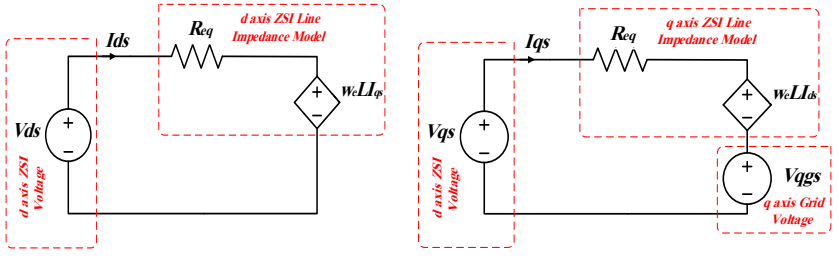

Figure 4. D-Q model of grid-connected Z-NPC system in rotating reference frame.

Where ω_e , L , R , V_{ds} , V_{qs} and V_{qgs} are grid angular frequency, line inductance, line resistance, inverter d-axis voltage, inverter *q*-axis voltage and the grid *q*-axis voltage, respectively.

According to Equation (1), the voltage gain of the inverter can be written as the follows in Equation (23):

$$G = \frac{V_{ac}}{V_{pv}/2} \tag{23}$$

In which we have V_{ac} as in Equation (24):

$$V_{ac} = \sqrt{V_{qs}^{\ 2} + V_{ds}^{\ 2}} \tag{24}$$

Also, there is Equation (25) for power factor:

$$\frac{I_{ds}}{I_{qs}} = -\tan(p.f) \tag{25}$$

Since unity power factor is concerned, by replacing 1 instead of $p.f$ in Equation (25), the *d*, *q* axis currents ratio will be obtained. By knowing inverter gain and solving these equations, the *d*, *q* axis voltages will be obtained. The power angle can be calculated using the following equation and be used in simple boost modulation as in Equation (26).

$$\phi_v = -\tan^{-1}\left(\frac{-V_{ds}}{V_{qs}}\right) \tag{26}$$

3.3. PI Controller & Calculation of M, D

In this section, the predicted voltage of the panel at a future time step is compared to the current panel voltage. The resulting error value is then fed into a PI controller to generate the inverter gain. This generated gain is subsequently utilized in the next block (Calculation of M and D) to determine the modulation index and duty cycle for the shoot-through state. The values of M, D determines how much the output voltage must be increased. In this block, the modulation index and duty ratio for the shoot-through state are defined according to the following equations:

For the case where the gain is less than or equal to unity we have Equation (27):

$$M = G,\ D = 0 \tag{27}$$

When the gain is greater than one we will have Equation (28):

$$M = G/2G - 1 \quad , \quad D = 1 - M \tag{28}$$

3.4. Switching of Three-Level Z-NPC Inverter

According to the three-level Neutral Point Clamped (NPC) inverter modulation based on the LS-PWM method, one of the three states presented in Table 1 is applied to the switches in the same leg at any given moment. A carrier wave with a frequency of 10 kHz and a range between (-1, 1) is compared with the values of positive and negative index modulation (-m, m), resulting in the generation of one pulse for each half-cycle. These pulses have been generated and added to conventional inverter pulses and create a shoot through state for Z-source inverter. If in mode 1 and 2 in the Table 1, the generated positive half-cycle pulses are applied to S_{A1} and S_{A3} at the same time, a shoot through state for upper impedance network will occur. Conversely, to achieve a shoot-through state in the lower impedance network, negative half-cycle pulses must be applied to the switches S_{A2} and S_{A4} , in the form of modes 2 and 3 in Table 1. It is important to note that in this method, there is no mode that allows both impedance networks to be in a shoot-through state simultaneously. In other words, there is no mode where all four switches in the same leg can be turned on at the same time.

Table 1. Switching table of three level NPC inverter.

Controller output	All switches in a leg			
	S_{A1}	S_{A2}	S_{A3}	S_{A4}
Mode 1	1	1	0	0
Mode 2	0	1	1	0
Mode 3	0	0	1	1

To achieve a shoot-through state in both impedance networks, the generated positive half-cycle pulses should be applied to S_{A1} and S_{A2} and the negative half-cycle pulses to S_{A3} add S_{A4}. According to the switching table, in modes 1 and 3, all four switches in a leg are turned on, resulting in both impedance networks being in a shoot-through state. It is important to note that this condition subjects the middle switches to increased voltage stress. Additionally, in mode 2 of the table, applying these pulses results in one of the two impedance networks entering a shoot-through state. Figure 5 illustrates the pulse generation for a leg of the inverter. In this figure, the black pulses correspond to the modulation of a three-level inverter, while the green pulses represent simple boost pulses. For clarity, the number of these pulses over a period (50 Hz) has been reduced.

As shown in Figure 5, in part A, it is indicated that simultaneously with the application of simple boost pulses to switches S_{A1} and S_{A2}, switch S_{A3} is also in inverter operation mode. The simultaneous turning on of these three switches causes the upper impedance network to be in shoot through state. In part B, with applying simple boost pulses to S_{A3} and S_{A4}, the switches S_{A1} and S_{A2} are switched in inverter operation mode. In this case, all four switches in a leg are turned on and both impedance network are in shoot through state. Similarly, in the specified part C, three lower switches are turned on. In this case, lower impedance network goes to shoot through state. Figure 6 illustrates the equivalent circuit for each of these states occurring in one leg of the inverter.

4. Simulation Results

In this section, the PV system is connected to the grid through a three-level Z-NPC converter. The effectiveness of the proposed MPC based MPPT strategy, along with other considerations discussed in the previous section, is evaluated using MATLAB/Simulink. The characteristics of SUNTECH270S-24-Vb module is used as an energy source of system. The P-V and I-V characteristic curves are illustrated in Figure 7, and the simulation parameters are summarized in Table 2. As mentioned in Section 3, a unity power factor is assumed for the system's operation. The performance of the MPC-based MPPT is assessed under three critical scenarios: response to a step change in solar irradiance, gradual changes in solar irradiance due to moving clouds, and steady-state performance around the maximum power point (MPP).

To begin evaluation, the operation of the system when the solar irradiance level decreases from 1000W/m^2 to 750W/m^2 at time t = 0.3 s is investigated. Figures 8 and 9 show the voltage and current of the upper PV panel connected to the three-level Z-NPC inverter, respectively. It is evident from these figures that the PV voltage and current at t = 0.3 s are affected by the change in irradiance level.

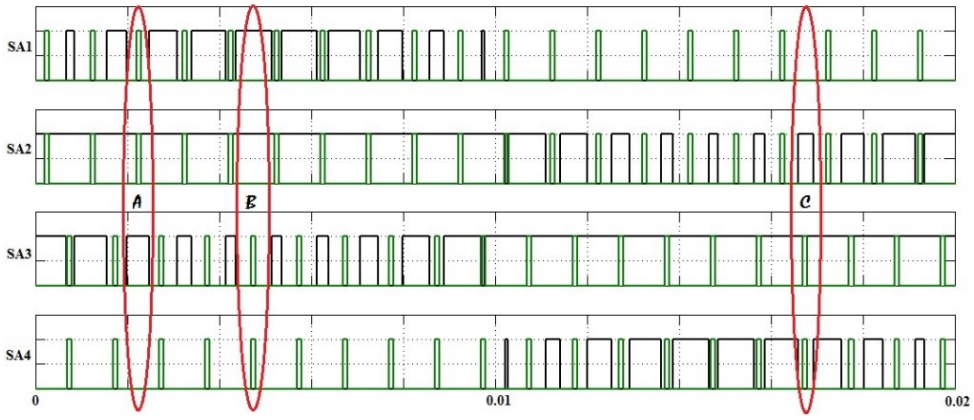

Figure 5. Modulation pulses for a leg of Z-NPC.

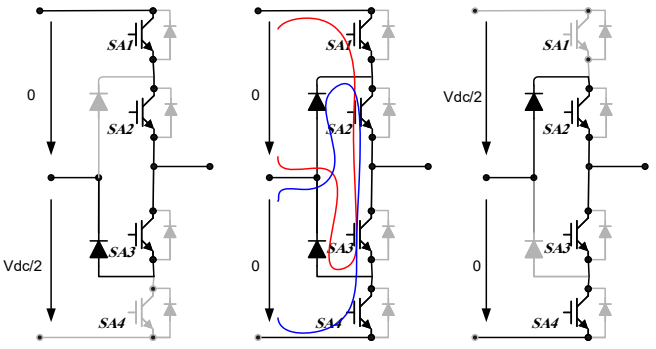

Figure 6. Shoot through states in a leg of Z-NPC.

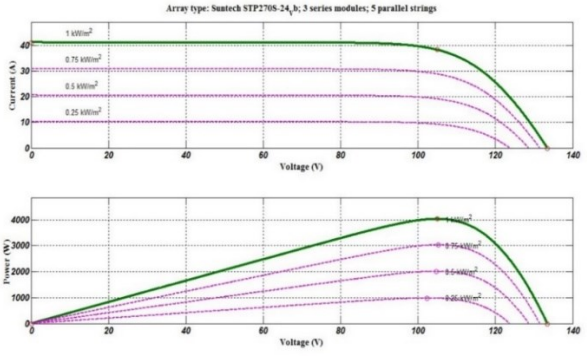

Figure 7. P–V and I–V characteristic curves of upper employed PV module.

Table 2. System parameters.

Parameters	Value
$L_1 = L_2 = L_3 = L_4 = L$	5 mH
$C_1 = C_2 = C_3 = C_4 = C$	1000 µF
C_{pv}	1000 µF
Sampling Time	5 µF
Switching frequency	10 kHz
L_{grid}	1 mH

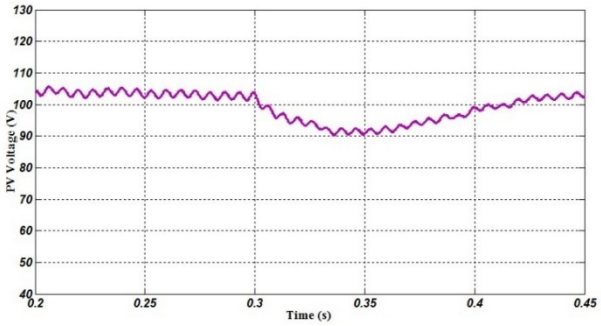

Figure 8. PV Panel Voltage for changing the irradiance level from 1000 W/m^2 to 750 W/m^2.

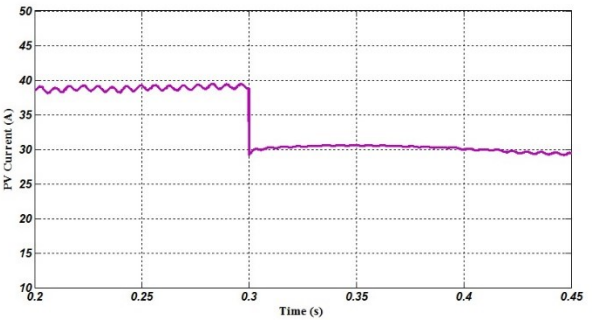

Figure 9. PV Panel current for changing the irradiance level from 1000 W/m^2 to 750 W/m^2.

The operating point of the PV system is optimized to extract maximum power. Figure 10 displays the output power of the upper panel, while the output power of the lower panel remains the same, as both impedance networks exhibit similar performance and operate at the same point. The overall power is obtained by sum of the power generated by each panel. As demonstrated, the proposed technique provides an acceptable response due to low convergence time and minimal oscillation around the maximum power point (MPP) in response to the applied step change in irradiance levels from 1000 to 750 W/m^2.

Figure 11 shows the unfiltered line output voltage of the inverter. The three-level waveform of the output voltage is clearly visible in this figure. At time t = 0.3 s, the output voltage is affected by a step change in irradiance. Subsequently, this voltage approaches the operating point value through the proposed control technique.

The generated power by the solar panels finally will be injected to grid through three-level Z-NPC inverter. It is important to note that during this transfer, some power is lost due to conduction and switching losses. Figure 12 shows the active and reactive power injected into the grid. As it's clear, the amount of power injected to grid, quickly decreases by applying step change in irradiance level. Also, with the aim of unity power factor that mentioned in previous part, it's visible that the reactive power is close to zero, means that the grid side voltage and current are in phase. Figure 13 shows the grid side voltage and current phase.

Figure 14 shows the harmonic components of the current injected into the grid using a three-level Z-NPC inverter. As can be seen from this figure, one of the advantages of the three-level Z-NPC inverter compared to the two-level Z-source inverter is its ability to reduce and eliminate high-order and even-order harmonics. Furthermore, the use of this inverter has led to decrease in the DC components of the grid-injected current. Table 3 compares the odd-order harmonic components of grid-injected current for both the two-level and three-level Z-source inverters. The table indicates that only the fifth and seventh harmonic components for the three-level inverter are greater than those for the two-level inverter, while all other odd harmonics in the two-level configuration have larger values.

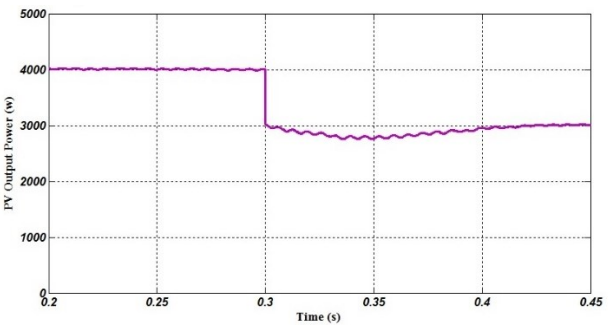

Figure 10. Extracted power from upper Solar Panel (extracted power from lower Panel is the same).

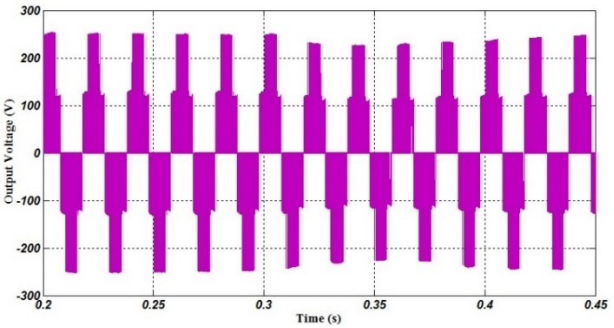

Figure 11. Line output voltage of three-level Z-NPC.

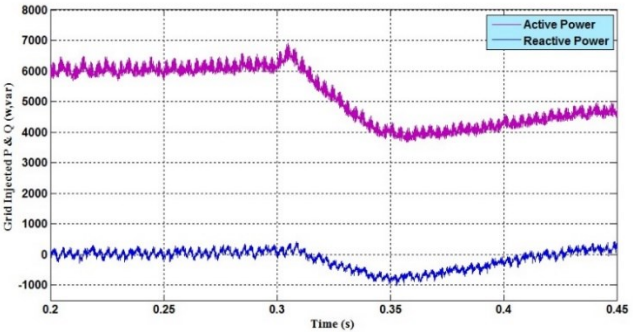

Figure 12. Injected Active and reactive power to grid.

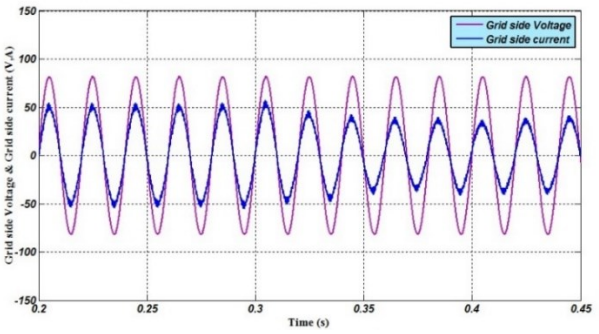

Figure 13. Grid side phase voltage and current.

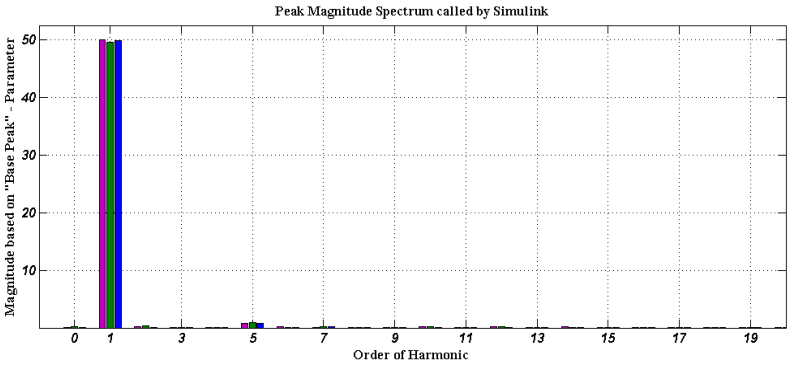

Figure 14. Spectrum of injected current to the grid.

Table 3. Comparison between the odd-order components of grid injected current for two-level and three-level Z-source inverter.

Harmonic order	Distortion in two-level inverter %	Distortion in three-level inverter %
Main component	48.91	49.95
3rd harmonic	0.7	0.1
5th harmonic	0.87	1.21
7th harmonic	0.67	0.24
9th harmonic	0.14	0.1
11th harmonic	0.51	0.02
13th harmonic	0.22	0.06
15th harmonic	0.06	0.08
17th harmonic	0.12	0.16
19th harmonic	0.12	0.04

5. Conclusion

In this paper, a model predictive control technique for maximum power point tracking in grid-connected PV panels was presented. The results showed that using the predictive control method, under step changes in solar irradiance, the maximum power point was tracked quickly with good convergence and minimal power ripple. Additionally, by incorporating both shoot-through and non-shoot-through states in the impedance source inverter, the PV panel was successfully connected to the grid while implementing MPPT. Using three-level Z-NPC inverter compared to the two-level Z-source inverter showed that the injected current in three-level mode, has fewer harmonic components. Furthermore, two panels were utilized, each with half the number of cells connected in series, which enhanced the performance capabilities of the PV system.

References

[1] P. Zhang, Y. Wang, W. Xiao, and W. Li, "Reliability Evaluation of Grid-Connected Photovoltaic Power Systems," *IEEE Transactions on Sustainable Energy*, vol. 3, no. 3, pp. 379–389, 2012.

[2] M. Shiravand, and A. Nahavandi, "Control and Improvement of Power Quality in Hybrid Three-Terminal AC/DC Microgrids," *Journal of Green Energy Research and Innovation*, vol. 1, no. 2, pp. 31–45, 2024.

[3] J. Ebrahimi, and M. Abasi, "Design of a Power Management Strategy in Smart Distribution Networks with Wind Turbines and EV Charging Stations to Reduce Loss, Improve Voltage Profile, and Increase Hosting Capacity of the Network," *Journal of Green Energy Research and Innovation*, vol. 1, no. 1, pp. 1–15, 2024.

[4] J. M. Kwon, B. H. Kwon, and K. H. Nam, "Three-Phase Photovoltaic System with Three-Level Boosting MPPT Control," *IEEE Transactions on Power Electronics*, vol. 23, no. 5, pp. 2319–2327, 2008.

[5] A. Nahavandi, M. Roostaee, and M. R. Azizi, "Single Stage DC-AC Boost Converter," *2016 7th Power Electronics and Drive Systems Technologies Conference (PEDSTC)*, pp. 362–366, 2016.

[6] S. Jain, and V. Agarwal, "A Single-Stage Grid Connected Inverter Topology for Solar PV Systems with Maximum Power Point Tracking," *IEEE Transactions on Power Electronics*, vol. 22, no. 5, pp. 1928–1940, 2007.

[7] E. Babaei, and A. Nahavandi, "Flexible Multilevel Boost DC-AC Converter," *2012 3rd Power Electronics and Drive Systems Technology (PEDSTC)*, pp. 506–511, 2012.

[8] F. Z. Peng, "Z-Source Inverter," *IEEE Transactions on Industry Applications*, vol. 39, no. 2, pp. 504–510, 2003.

[9] S. Patil, and P. Parikh, "Comparative Analysis of Simple Boost and Double Carrier PWM Control on PV Powered Z-Source Inverter," *2014 6th IEEE Power India International Conference (PIICON)*, pp. 1–6, 2014.

[10] B. Exposto, R. Rodrigues, et al., "Predictive Control of a Current-Source Inverter for Solar Photovoltaic Grid Interface," *2015 9th International Conference on Compatibility and Power Electronics (CPE)*, pp. 113–118, 2015.

[11] S. Sajadian, and R. Ahmadi, "Model Predictive-Based Maximum Power Point Tracking for Grid-Tied Photovoltaic Applications Using a Z-Source Inverter," *IEEE Transactions on Power Electronics*, vol. 31, no. 11, pp. 7611–7620, 2016.

[12] A. Bidram, A. Davoudi, and R. S. Balog, "Control and Circuit Techniques to Mitigate Partial Shading Effects in Photovoltaic Arrays," *IEEE Journal of Photovoltaics*, vol. 2, no. 4, pp. 532–546, 2012.

[13] T. Esram, and P. L. Chapman, "Comparison of Photovoltaic Array Maximum Power Point Tracking Techniques," *IEEE Transactions on Energy Conversion*, vol. 22, no. 2, pp. 439–449, 2007.

[14] H. Dong, H. Sugimoto, and N. Nishio, "A Maximum Power Tracking Control Method for Photovoltaic Power Generation System Based on Derivation of Output Power with Respect to Output Voltage," *IEEJ Transactions on Industry Applications*, vol. 118, no. 12, pp. 1435–1442, 1998.

[15] N. Femia, G. Petrone, G. Spagnuolo, and M. Vitelli, "Optimization of Perturb and Observe Maximum Power Point Tracking Method," *IEEE Transactions on Power Electronics*, vol. 20, no. 4, pp. 963–973, 2005.

[16] M. B. Shadmand, R. S. Balog, and H. Abu-Rub, "Model Predictive Control of PV Sources in a Smart DC Distribution System: Maximum Power Point Tracking and Droop Control," *IEEE Transactions on Energy Conversion*, vol. 29, no. 4, pp. 913–921, 2014.

[17] M. B. Shadmand, X. Li, R. S. Balog, and H. A. Rub, "Model Predictive Control of Grid-Tied Photovoltaic Systems: Maximum Power Point Tracking and Decoupled Power Control," *2015 First Workshop on Smart Grid and Renewable Energy (SGRE)*, pp. 1–6, 2015.

[18] Z. Tan, Y. Li, and M. Li, "A Direct Torque Control of Induction Motor Based on Three-Level NPC Inverter," *2001 IEEE 32nd Annual Power Electronics Specialists Conference (IEEE Cat. No.01CH37230)*, vol. 3, pp. 1435–1439, 2001.

[19] R. Strzelecki, "Three-Level Z-Source Neutral-Point-Clamped Inverter," *2006 8th International Conference on Actual Problems of Electronic Instrument Engineering*, pp. 172–179, 2006.

[20] P. D. Van den Heever, S. Oberholzer, and J. H. R. Enslin, "High-Efficient Solar Panel/Wind Turbine Converter with Maximal Power Control," in *Proceedings of the European Conference on Power Electronics and Applications*, pp. 663–668,1989.

[21] S. Alepuz, S. Busquets-Monge, et al., "Interfacing Renewable Energy Sources to the Utility Grid Using a Three-Level Inverter," *IEEE Transactions on Industrial Electronics*, vol. 53, no. 5, pp. 1504–1511, 2006.

[22] S. Dehghan, E. Seifi, M. Mohamadian, and R. Gharehkhani, "Grid Connected DG Systems Based on Z-Source NPC Inverters," *2011 2nd Power Electronics, Drive Systems and Technologies Conference*, pp. 104–110, 2011.

[23] P. C. Loh, D. Vilathgamuwa, Y. S. Lai, G. T. Chua, and Y. Li, "Pulse-Width Modulation of Z-Source Inverters," in *Conference Record of the 2004 IEEE Industry Applications Conference, 39th IAS Annual Meeting*, vol. 1, pp. 148–155, 2004.

[24] A. F. Boehringer, "Self-Adapting Dc Converter for Solar Spacecraft Power Supply Selbstanpassender Gleichstromwandler Für Die Energieversorgung Eines Sonnensatelliten," *IEEE Transactions on Aerospace and Electronic Systems*, vol. AES-4, no. 1, pp. 102–111, 1968.

[25] J. Rodriguez, and P. "Cortes, Predictive Control of Power Converters and Electrical Drives," *John Wiley & Sons*, 2012.

[26] J. Holtz, "A Predictive Controller for The Stator Current Vector of AC Machines Fed from A Switched Voltage Source," in *Proceedings of the International Power Electronics Conference (IPEC-Tokyo)*, pp. 1665–1675, 1983.

[27] J. Rodriguez, M. P. Kazmierkowski, et al., "State of the Art of Finite Control Set Model Predictive Control in Power Electronics," *IEEE Transactions on Industrial Informatics*, vol. 9, no. 2, pp. 1003–1016, 2013.

Declaration of competing interest

The authors declare that they have no known competing financial interests or personal relationships that could have appeared to influence the work reported in this paper. The ethical issues, including plagiarism, informed consent, misconduct, data fabrication and/or falsification, double publication and/or submission, redundancy, have been completely observed by the authors.

Bibliography

Ali Nahavandi was born in Malayer, Iran, in 1983. He received the B.Sc., M.Sc. and Ph.D. degrees in electrical power engineering from University of Tabriz, Tabriz, Iran, in 2006, 2008 and 2014 respectively. Since 2014 he is assistant professor in Faculty of Engineering, Malayer University, Malayer, Iran. His research interests include power electronic converters, renewable energy systems and power quality.

Email: ali.nahavandi@malayeru.ac.ir

ORCID: 0000-0002-8036-188X

Contribution Statement: Conceptualization, Project administration, Supervision, Validation, Roles/Writing - original draft, Writing-review & editing.

Mohammadreza Azizi received the B.Sc. degree in electrical engineering from the Shahid Madani University of Azerbaijan, Tabriz, Iran, and the M.Sc. degree in electrical engineering from Malayer University, Malayer, Iran. He acquired several years of experience as a Lecturer and a Research Assistant at Malayer University.

Email: Azizi.malayeru@gmail.com

ORCID: 0000-0002-5599-2276

Contribution Statement: Conceptualization, Data curation, Formal analysis, Investigation, Resources, Software.

Journal of Green Energy Research and Innovation

Illegal Miner Detection based on Dynamic Mode Decomposition and Unsupervised Machine Learning Algorithms

Alireza Simorgh, Khosro Khandani, Maryam Amiri

Highlights

- **Employing a real data set from Markazi Province Distribution Company to detect illegal miners.**
- **Dynamic Mode Decomposition (DMD) has been used to extract new features.**
- **Obtaining high accuracy of classification using unsupervised algorithms.**

Graphical Abstract

Use your device to scan and read the article online

Citation

A. Simorgh, K. Khandani, and M. Amiri," Illegal Miner Detection based on Dynamic Mode Decomposition and Unsupervised Machine Learning Algorithms," *Journal of Green Energy Research and Innovation*, vol. 2, no. 6, pp. 79-88, 2025.

https://doi.org/10.61186/jgeri.2.2.79

Journal of Green Energy Research and Innovation 2.2 (2025) 79-88

Online ISSN: 3041-9018

Journal of Green Energy Research and Innovation

Journal Homepage: www.jgeri.araku.ac.ir

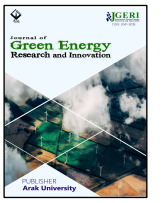

Illegal Miner Detection based on Dynamic Mode Decomposition and Unsupervised Machine Learning Algorithms

Alireza Simorgh [1], Khosro Khandani [1,*], Maryam Amiri [2]

[1] *Department of Electrical Engineering, Faculty of Engineering, Arak University, Arak, 38156-8-8349, Iran.*

[2] *Department of Computer Engineering, Faculty of Engineering, Arak University, Arak, 38156-8-8349, Iran.*

A R T I C L E I N F O

Keywords:
Miner detection,
Unsupervised algorithms,
Dynamic mode decomposition.

Article History:
Received: 19 February 2025;
Revised: 24 March 2025;
Accepted: 25 March 2025.

Article type:
Research Article

* ***Corresponding author***
E-mail address
k-khandani@araku.ac.ir (K. Khandani)

A B S T R A C T

Since the most important issue in the production of digital currencies is energy consumption, the use of illegal electricity in mining farms has become very popular. Illegal mining is particularly important in countries such as Iran where the price of electrical energy is extremely low. This issue has caused numerous problems such as frequent blackouts, large losses for industries and even daily power cuts in several large cities. Previous machine learning approaches for miner detection are mostly supervised methods which rely on labeled data. Due to the fact that the number of labeled data is very limited in reality, we propose unsupervised methods in this paper. A real data set from Markazi Province Distribution Company in Iran has been employed to produce the results. The classification process consists of two stages: in the first stage, Dynamic Mode Decomposition (DMD) has been used to extract new features which compose the set of features along with certain factors from the Advanced Metering Infrastructure (AMI). These features are selected for 58 subscribers with positive and negative labels. In the second stage, a number of unsupervised models are built from the results of the first stage. The highest accuracy of classification obtained is 74% from unsupervised algorithms and 85% for supervised algorithms, which is very significant considering the fact that unsupervised algorithms do not need labeled data.

1. Introduction

The energy needed to produce one bitcoin is almost equal to the energy needed by a house for a week. According to the Cambridge Centre for Alternative Finance (CCAF), bitcoin currently consumes about 110 terawatt hours per year – 0.55% of global electricity production, or roughly equivalent to the annual energy harvest of small countries like Malaysia or Sweden [1]. Around 4.5% of all bitcoin mining worldwide took place in Iran between January and April 2021. The price of electricity in Iran is much lower than the average price for households and businesses. Considering the prohibition of the production of digital currencies in some countries such as Iran, Algeria and Vietnam, or legal laws in other countries such as Denmark, the way to identify illegal miners is very important. Today, electricity distribution companies use different approaches to identify illegal miners. Some companies use algorithms based on comparing customers' current energy consumption with the past. Today, various methods are used to identify illegal digital currency mining facilities in electricity distribution companies. One of the most common methods is called AlgExp, which collects the characteristics of consumers' electricity consumption based on their activities, and the collected data are compared with past consumption data [1]. Identifying anomalies in electricity consumption is another approach which was proposed in [2] where an unsupervised method which combines clustering-based and prediction-based methods, has been employed for anomaly detection in power consumption. The authors hypothesized that the same daily consumption behavior appears repeatedly. Based on this assumption, the K-means algorithm has been applied to investigate behavioral scenarios in 24 different groups per day. In [3] Long Short-Term Memory (LSTM) neural network has been used to identify anomalies in electricity consumption data one hour ahead of time. Forecasting energy consumption was also addressed in [4] where LSTM networks have been used to predict future energy consumption. Li et al. in [5] proposed a framework for power consumption anomaly detection based on industrial wireless sensor networks. Their mechanism is based on machine learning and blockchain where the collected data are classified into three categories: outlier class, working day class, and holiday class. According to the types of power consumption anomalies, the extreme class is also divided into three subclasses. If the received data are beyond the normal range, abnormality will be detected.

In the last step, the K-nearest neighbor algorithm was used to detect anomalies that were not detectable in the previous step. Ouyang et al. in [6] have proposed a multidimensional cumulative ensemble model to detect abnormal energy consumption using various IoT sensors in an industrial environment. The authors considered the energy consumption data as a time series and used the hierarchical time series feature extraction method to extract different types of features, including decomposed features, transformed features, summarized features, and transformed features. Also, some machine learning models, such as the ensemble learning method, have been trained to discover classes. Nerurkar et al. proposed a graph-based deep learning model using spectral graphs and transactional features [7]. The proposed model is trained on complex features to classify illegal transactions on Bitcoin. This approach is also very complicated due to the need for a large number of labeled data and numerous features. In [8], a detection method called Bagging-GCN has been proposed based on the combination of the Bagging algorithm and the Graph Convolutional Neural Network (GCN) algorithm. The experiments conducted on the elliptic dataset showed that Bagging-GCN could superiorly identify legal and illegal transactions compared to the traditional learning methods such as logistic regression and support vector machine. In[9], the method of combining layers in Convolutional Neural Networks (CNN) has been used. The paper proposes a model of Bitcoin transaction analysis to identify anomalies related to money laundering. In [10], a machine learning method was introduced to analyze the complete Bitcoin user graph in order to identify suspicious actors potentially involved in illegal activities. Contrary to existing studies, the proposed method in [10] introduced a new set of features which were used to identify potential criminal activities more accurately. Regarding miner detection approaches, Amiri et al. [11] have used the INBORN model, which is one of the pattern-finding methods, to identify unauthorized miners. This research has considered the correlation between different characteristics and has clearly extracted customer behavior patterns.

In most of the previous works, only supervised methods have been used, which has its own difficulty due to the complexities of producing labeled data for this task. In addition, most of the previous papers have been conducted only on the basis of network factors and micro-consumption of subscribers, and no new innovations have been included in this field. For this reason, the lack of an explicit and efficient model without the need for labeled data and using advanced methods of feature creation motivates us to propose an efficient method to solve this problem in this paper. On the other hand, although the introduced methods can identify criminal activities such as illegal mining or electricity theft, they misclassify many subscribers, as well. If the number of false negative labels is large, the subscribers with illegal miners will be mistakenly assigned a negative label. Large number of false positive labels means that, the subscribers who do not possess illegal miners are mistakenly assigned a positive label. Although both of the numbers of false negative and false positive are preferred to be small, any algorithm which results in a fewer false negatives is considered to be more effective. The purpose of this paper is proposing an efficient method to identify unauthorized miners. For this purpose, 58 subscribers from Markazi province distribution company in Iran have been selected. This labeled data set includes 41 subscribers with positive labels and 17 subscribers with negative labels. Some features are extracted from this data set and then Dynamic Mode Decomposition (DMD) is applied to extract some other features. In the next step, various pre-processing methods are applied to the data, and then, different unsupervised models are applied to them. Eventually the models are evaluated based on the accuracy of the miner detection. Figure 1 shows the structure of the proposed method. The innovation of this paper is extracting novel features by employing DMD which helps obtain more effective and reliable unsupervised models. The set of features are composed of DMD features and other features obtained from AMI. This new feature selection approach paves the way for constructing more effective models in similar classification problems. The rest of the paper is organized as follows: Basic concepts and definitions are explained in Section 2. Section 3 introduces the proposed method in detail. Then we evaluate the results in Section 4. Finally, this paper concludes with our future works in Section 5.

2. Basic concepts and definitions

This section introduces the main concepts and definitions including k-means, mean shift, DBSCAN, Agglomerative Clustering and dynamic mode decomposition.

2.1. K-means

The K-means clustering algorithm calculates the center points and repeats this until it finds the optimal center point. This algorithm needs to determine the number of clusters. The number of specified clusters is represented by k. In this algorithm, the data are assigned to a cluster in such a way that the sum of the squares of the distance between the data points and the central point is minimal. It is understandable that the smaller the changes in the clusters, the more similar data we will have within the cluster [12].

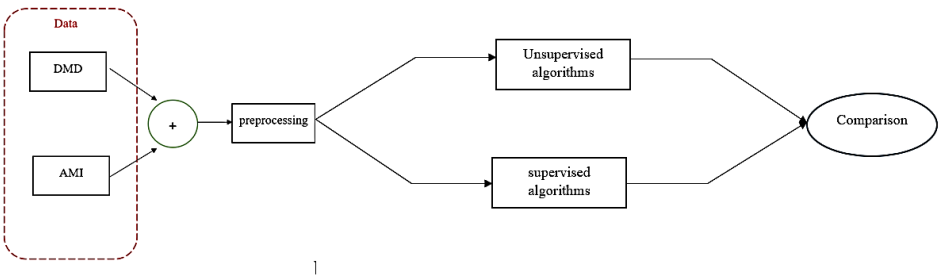

Figure 1. The procedure of the miner detection based on DMD and machine learning.

This algorithm continues to work so that the sum of squared differences from the mean is minimized for each cluster. The objective function of this algorithm is defined as follows. In this regard, μ_m is the center of cluster m, $c^{(1)}$ is the number of the cluster assigned to the data $x^{(i)}$ and $\mu_c(i)$ is the center of the cluster assigned to the data $x^{(i)}$.

$$J\left(c^{(1)}, c^{(2)}, \dots, c^{(k)}, \mu_1, \mu_2, \dots, \mu_m\right) = \frac{1}{2}\sum_{i=1}^{m}\left\|\mathrm{x}^{(i)} - \mu_c(i)\right\|^2 \tag{1}$$

As illustrated in the pseudo-code of Figure 2, first, the number of clusters is determined, then the initial centers of the clusters are determined, and finally, in each step, the distance between the calculated points and the centers of the clusters are updated until the objective function is minimized and there are no more data. In this research, since our goal is to identify miner subscribers from non-miners, the number of clusters is equal to 2. Also, the selection of the center of primary clusters is performed using K-means $++$ method.

2.2. DBSCAN

DBSCAN algorithm is the basis of density-based clustering methods, which has the ability to discover clusters of different sizes and shapes from a large volume of data and is also resistant to noise. Despite these advantages, this algorithm has problems such as the difficulty of determining the exact value of the input parameters, not recognizing clusters with different densities, and not correctly recognizing clusters when the clusters are close to each other [13]. In DBSCAN algorithm, the two main parameters are the minimum sample and the neighborhood radius, where the minimum sample is the minimum number of samples required to form a cluster, and the neighborhood radius is defined as the maximum distance between two points while they still belong to a cluster [12]. Any data point whose distance with an assumed data point is smaller than the radius is considered as a neighbor of that data point. The main idea of DBSCAN is that for each sample of a cluster, a neighborhood with a certain radius eps should contain a minimum number of objects. The neighborhood of a point like p is defined as in Equation (2):

$$N_{eps} = \left\{q \in \frac{D}{dist(p,q)} < eps\right\} \tag{2}$$

where D is the data set, dist(p,q) is the distance between points p and q, and eps is the neighborhood radius. If there is at least one predetermined number of points in the neighborhood radius of eps from a point like p, then this point is called the central point. The central point is defined as in Equation (3):

$$N_{eps}(p) > min\ sampels \tag{3}$$

The objective function in this algorithm is defined in Equation (4):

$$min\ W_1\left(\frac{1}{k}\sum_{i=1}^{k} s(i)\right) + W_2\left(\frac{k}{N_g}\right) \tag{4}$$

$$s.t: 0 < eps < D_{max}$$

$$2 < \min sampels < N_{max}\ ;\ \min sampels \in Z$$

where D_{Max} and N_{Max} are the Euclidean distance between the farthest point in the data set and the maximum number of data points respectively, k is the number of clusters and W_1 and W_2 are the weights to be determined.

2.3. Mean Shift

This method is a non-parametric approach with the aim of finding local maxima or clustering data. In using this method, the number of clusters is not necessary to be determined. It also has no restrictions on the shape of the data distribution or the shape of the generated clusters. This method finds local maxima with an iterative method, in such a way that for each data point in the feature space, the center of a search window is placed at that point, then it is checked whether that data point is located in a local maximum in terms of statistical distribution. If it is not located in a local maximum, the neighborhood center is moved and checked again.

input: K, number of clusters; D, a data set of N points
1. Initialization.
2. **Repeat**
3. **For** each point p in D **do**
4. Find the nearest center and assign p to the
5. Corresponding cluster.
6. **End for**
7. Update clusters by calculating new centers using Mean of the members.
8. **Until** stop- iteration criteria satisfied
9. **Return** clustering result

Figure 2. K-means algorithm [11].

The above comparison continues until reaching convergence and finding data on the local maximum. Data points that are associated with this local maximum are considered as cluster members [14]. The objective function of this algorithm is as follows in Equation (5):

$$f(x) = \frac{1}{nh^d}\sum_{i=1}^{R} K[\frac{x - x_i}{h}] \tag{5}$$

where x_i is a sample in the data set, h is the bandwidth, n is the number of samples, and d is the dimension of the examined space. Also, K is an optimal kernel that is usually considered in the following two ways [15] as in Equations (6) and (7):

$$K(x) = \begin{cases} 1, & -1 \le |x| \le 1 \\ 0, & else \end{cases} \tag{6}$$

$$\text{Gaussian } K(x) = \frac{1}{(2\pi)^{\frac{d}{2}}} e^{\frac{-1}{2}|x|^2} \tag{7}$$

First the appropriate bandwidth and the kernel function are determined. Then, this algorithm chooses the central points which are updated in each step based on the mean shift vector. In this research, the bandwidth is estimated based on the k-nearest neighbor method.

2.4. Agglomerative clustering

In data mining and statistics, hierarchical clustering is a clustering method whose purpose is to build a hierarchy of clusters. Hierarchical clustering methods are divided into two categories. Agglomerative approach: starting from the bottom, at each stage, two clusters are merged together and form a new cluster. Divisive approach: starting from the top, at each stage a cluster is decomposed into smaller clusters that are located at a lower level. New clusters are placed at higher levels and this process is repeated [16]. Each level of the hierarchy represents a category of data that can be viewed as a tree. Each leaf of the tree represents an initial observation, and the root of the tree is the collection of all observations. The results of a hierarchical clustering are generally displayed in the form of a dendrogram [17]. In order to understand which clusters should be grouped together or separated from each other, a measure of difference between clusters must be defined. In most methods, this criterion is achieved by defining a link criterion. The distance criterion determines the distance between two observations and the link criterion defines the distance between two sets of observations by a function of the distance between the observations of each set. Choosing an appropriate distance measure affects the shape of the clusters owing to the fact that for one distance measure, several observations can be close to each other. Some common distance measures for use in hierarchical clustering are given in Table 1 .

The link criterion defines the distance between two sets by a function of the pairwise distance between the observations of each set. Some common link criteria are listed in Table 2. In maximum distance, the distance between two observations a and b of two sets A and B is calculated based on the maximum, in minimum distance, this distance is calculated based on the minimum, and in average distance, it is calculated based on the average.

Table 1. Types of distance measure in hierarchical clustering [18].

Function	Formula
Euclidean	$\sum_{i=1}^{d}\sqrt{(x_i - y_i)^2}$
Manhattan	$\sum_{i=1}^{d}\lvert x_i - y_i\rvert$
Euclidean squared	$\sum_{i=1}^{d}(x_i - y_i)^2$
Maximum	$\sum_{i=1}^{d}\max_i\lvert x_i - y_i\rvert$

Table 2. Types of link criteria in hierarchical clustering [17].

Function	Formula
Maximum distance	$\max\{d(a,b): a \in A, b \in B\}$
Minimum distance	$\min\{d(a,b): a \in A, b \in B\}$
Average distance	$\frac{1}{\lvert A\rvert\lvert B\rvert}\sum_{a\in A}\sum_{b\in B} d(a,b)$

Agglomerative clustering starts with one cluster for each observation and at each step, two clusters that have the least difference from each other are aggregated using the criteria of Tables 1 and 2. This continues until the number of clusters reaches one. Agglomerative algorithm is shown in Figure 3. According to this figure, first each sample is considered as a cluster, then the distance between the clusters is calculated, and the clusters that have the smallest distance from each other are merged together. This process continues until only one cluster remains. In this research since our goal is to distinguish miners from non-miners, the number of clusters will be two in agglomerative algorithm. Also, the distance criterion is based on the Euclidean distance and the link criterion is chosen as the average distance.

2.5. Dynamic Mode Decomposition

Dynamic mode decomposition (DMD) is an equation-free data-driven matrix decomposition method developed in 2008. This method can provide an accurate reconstruction of coherent spatio-temporal structures resulting from nonlinear dynamical systems or an estimate of the short-term future of such systems. DMD approximates the modes of the Koopman operator, which is a linear operator and can represent nonlinear dynamics without linearization. This algorithm is also a dimensionality reduction algorithm which produces a set of modes based on a time series of data, each of which grows with a constant frequency. In particular, for linear systems, these modes and frequencies are similar to the normal modes of the system. The figure below shows the algorithm of this method based on singular value decomposition [19]. DMD algorithm is shown in Figure 4. According to this figure, the decomposition of singular values of the input matrix is first calculated. Then the first r singular values are selected and the $\Sigma_r$matrix is generated. Also $R^{r\times r}$ is a diagonal matrix comprising the first r singular values. Then the matrix $\tilde{A}$ is calculated. The eigenvectors of this matrix are the modes of the dynamic state decomposition, and its eigenvalues are the eigenvalues of the dynamic state decomposition.

3. Proposed Method

As stated earlier, the previous methods in the field of illegal miner detection have employed supervised learning methods. Since such algorithms need labeled data, and the generation of these labeled data is complicated, time consuming and expensive, It is preferable to choose unsupervised methods to detect miners. Additionally, supervised models are often trained based on grid factors obtained from AMI, and innovation in this field has been very limited. In this paper, our approach is to use unsupervised algorithms which do not require labeled data. In addition, the features created by DMD have been used in addition to the AMI features to build models. This has brought significant improvements. In this research, the features from AMI that are used are: power factor (phases 1, 2, 3), active power and reactive power. Furthermore, from the dynamic mode decomposition method, new features i.e. the modes and eigenvalues are produced. Then, various pre-processing methods including normalization, filling missing data, checking the correlation between features, summarizing data and removing outliers are applied to the data. Eventually, unsupervised algorithms are applied to the standardized data and the data are classified into two clusters. Then the best models were selected and the produced results were compared with supervised methods. The stages of this research are outlined as follows:

3.1. Data extraction

A real data set from Markazi Province Distribution Company including 58 labeled subscribers, of which 41 subscribers with positive labels and 17 subscribers with negative labels, has been used in this research. The sampling interval for all subscribers is 15 minutes.

3.2. Feature selection

In this research, the features are: power factor (phase 1, 2, 3), active power and reactive power. Additionally, DMD has been applied to produce new features. From DMD method, new features such as mode and eigenvalues are produced, which indicate the inherent behavior of the data, such as stability or instability .

3.3. Preprocessing

In this step, we prepare the extracted data for applying machine learning algorithms, which includes several parts:

3.3.1. Missing data

In the data set used for this research, there are missing data that are replaced by the two methods of feature average and previous moment sample, and the obtained results are checked.

Input: number of clusters, data
1. $C_{|X|} \coloneqq \{\{x\}|x \in X\}$
2. ***for*** i =|X|-1,….1 **do**
3. $find\ distinct\ clusters\ A, B \in C_{i+1} minimizing\ diam(A \cup B)$
4. $C_i \coloneqq (C_{i+1}\{A, B\}) \cup \{A \cup B\}$
5. **End for**
6. **Return** $C_1 \ldots \ldots C_{|X|}$

Figure 3. Agglomerative Algorithm [17].

input: $Matrices\ X, Y \in R^{m*n}, rank\ r(\leq \min(m,n))$
1. $Compute\ the\ truncated\ SVD\ of\ X(\approx U_r\Sigma_r V_r^T)$: $U_r \in R^{m\times r}$ $comprised\ the\ first\ r\ left\ singular\ vectors, \Sigma_r \in R^{r\times r}$ $is\ a\ diagonal\ matrix\ comprising\ the\ first\ r\ singular\ values,$ $V_r \in R^{n\times r}$ $comprices\ the\ first\ r\ right\ \ singular\ vectors$
2. $\tilde{A} = U_r^T Y V_r \Sigma_r^{-1}$
3. $compute\ the\ eigenpairs\ of \tilde{A}\ \tilde{w} = \lambda\tilde{w}\ , and\ let\ w = U_r\tilde{w}$

Figure 4. Dynamic mode decomposition Algorithm [20].

3.3.2. Outliers

To detect noisy or outlier data, two methods of box diagram and displaying the probability distribution of data are used, and finally, outlier data that reduce the quality of the algorithms are removed .

3.3.3. Data normalization

Data normalization is one of the most important pre-processing steps in data mining. Since the used features may have different intervals and lower the quality of clustering or supervised algorithms, in order to achieve more accurate results, it is necessary that the intervals of different features be somehow the same or close to each other. For this research, minmax and z-score methods are used and the results are compared with each other.

3.3.4. Data aggregation

Since the data used in this research are in the form of time series, in order to be able to use machine learning algorithms, summarization is obvious. For this reason, aggregation is done using two aggregation methods based on maximum and average, and the results are compared with each other.

3.3.5. Data Correlation

Correlation is a statistical term that examines whether two variables are related to each other or not. Features with high correlation are linearly related to each other and have approximately the same effect on the dependent variable; Therefore, when two features have a high correlation, one of these two features can be left out. In this research, the correlation between the characteristics is checked and the characteristics that have a high correlation are removed.

3.4. Model selection

At this stage, a model must be selected that can be used to separate and categorize the data. In this research, since the labeled data are available, however, the goal is to build an unsupervised method, various unsupervised algorithms are applied to the data and the results obtained are compared with the results of supervised algorithms. Different clustering algorithms are used for data classification, which can be based on distance (k-means), density (DBSCAN and mean shift) and rank order (agglomerative). In the supervised method, neural network, decision tree, support vector machine and ensemble learning algorithms are used and the obtained results are compared.

3.5. Selection of hyperparameters

In k-means and agglomerative algorithms, since our goal is to distinguish miners from non-miners, the number of clusters is equal to 2; But in other algorithms, other hyperparameters must be determined. For example, in the average transfer algorithm, the bandwidth is estimated based on the k-nearest neighbor method. To put it more clearly, the average distance between samples located in a cluster is calculated. In this paper the bandwidth in mean-shift algorithm is chosen as a value between 0 and 2 according to KNN. And in the DBSCAN algorithm, hyperparameter selection is done according to the accuracy of the silhouette index; The higher the index, the better hyperparameters are selected. In this paper the hyper-parameters of DBSCAN are set based on the grid search algorithm [21]. In fact, eps has been selected as a number between 0.1 and 2 and minimum samples are numbers between 1 and 10.

3.6. Prediction

In this step, the model built by clustering and supervised algorithms is applied to new data to predict their labels. In the following, the work done in this research will be examined in the form of several models.

In the next step, according to the mentioned points, unsupervised models NF, FNF, MNF, ZNF, CNF were built based only on the recorder features from the AMI. Then, the features created with the use of DMD method were used and unsupervised models MO, EV, MOEV were created which are based on mode features, eigenvalues and a combination of the two. Finally, the unsupervised models MONF, NFEV, MONFMEM, MONFME, which are based on a combination of recorded features and DMD ones were built. Mean shift, agglomerative k-means, and DBSCAN algorithms are used in all these models and their only difference was in the used features and pre-processing methods. Finally, in order to compare the results obtained with the supervised models, MONFMEM, MONF, NFEV, MNF, NF were built. In these models, neural network algorithms, ensemble learning, support vector machine, and decision tree are used. Figure 5 shows the structure of this research. According to this figure, first the appropriate features for the Distribution Company of Markazi Province data set are selected, then they are prepared using pre-processing methods such as data normalization, data aggregation, filling missing values and determining the correlation between features for applying unsupervised algorithms. Then, in order to evaluate the obtained results, supervised algorithms are also applied and the obtained results are compared.

4. Evaluation

In this section, the results obtained from the models built in the previous chapter are evaluated. The results obtained with the help of DMD features have the highest quality. Also, the agglomerative algorithm, which is a type of hierarchical algorithm, had the highest accuracy in data classification, and this accuracy was evaluated at 74%. By evaluating the results of supervised models, it was found that DMD features performed best and the highest accuracy achieved was 85%. By examining the two results obtained from the unsupervised and supervised models, it can be seen that there is almost a ten

percent difference between the two aproaches. Figures 6 and 7 show the comparison of the results of the supervised and unsupervised models. In the models built with the help of unsupervised methods, when only features recorded from the AMI were used, the highest accuracy of 62% was achieved. With the addition of built-in features using DMD, this value has increased to 74%. For monitoring models, when only AMI features were used, the highest accuracy achieved was 79%. With the addition of constructed features with the help of DMD, this value increased to 85%. Therefore, it can be concluded that the accuracy in both cases was higher when the DMD features were used. In Figures 8 and 9, a comparison between true positive and true negative labels is made. As it can be seen, when the features made from DMD were used along with the AMI features, there were more true positive labels, while when only AMI features were used, there were more true negative labels. In Figures 10 and 11, a comparison is made between false positive and false negative labels. As it can be seen, when the features made from DMD were used along with the AMI features, there were more false positive labels, while when only AMI features were used, there were more false negative labels .

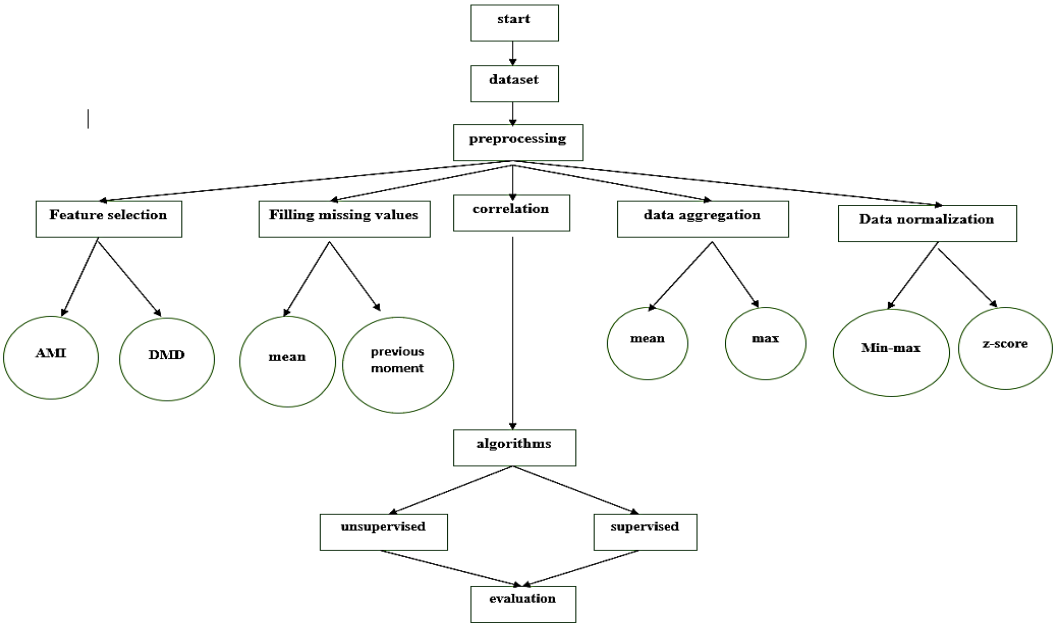

Figure 5. The procedure of the miner detection based on DMD and unsupervised learning.

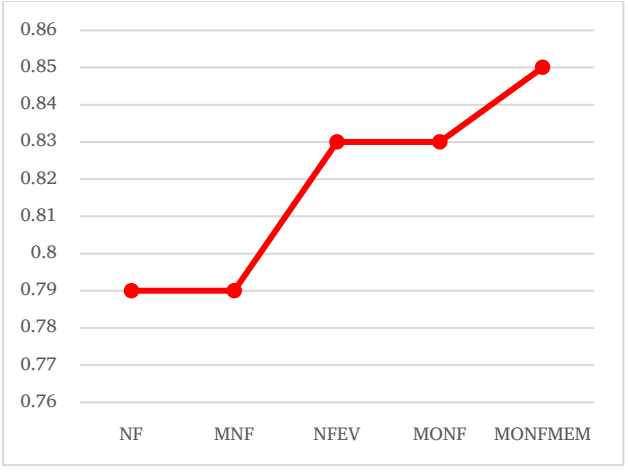

Figure 6. Accuracy of supervised models.

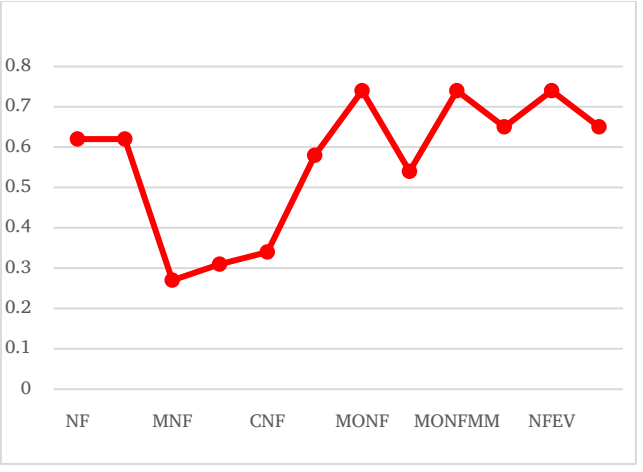

Figure 7. Accuracy of unsupervised models.

In Figures 12, 13 and 14, a comparison has been made between precision, recall and support of unsupervised models. In this research, precision measures how good the model is at assigning positive samples to the positive class. That is, how accurate the miner prediction is. Recall measures how good the model is in detecting positive samples. The measures provide valuable information, but the objective is to improve recall without affecting precision. Sensitivity measures how apt the model is to detect samples in the positive class. Therefore, given that miners are a positive class, sensitivity quantifies how many of the actual miners are correctly predicted as miners. As it is known, the values of sensitivity, recall and precision in the three models MONF, NFEV and MONFMEM had the highest value, which means that these models have performed well in detecting subscribers with miners.

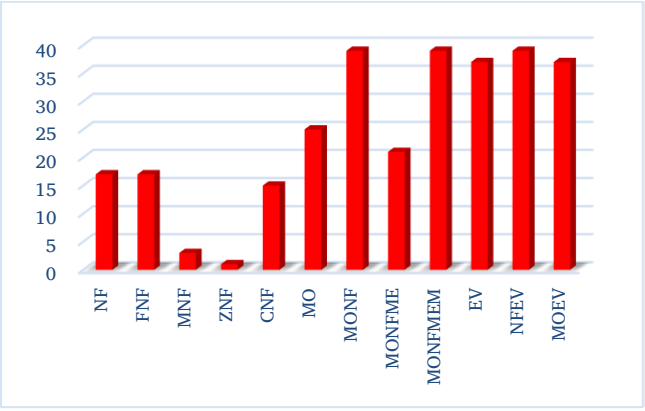

Figure 8. Number of true positive labels of unsupervised models.

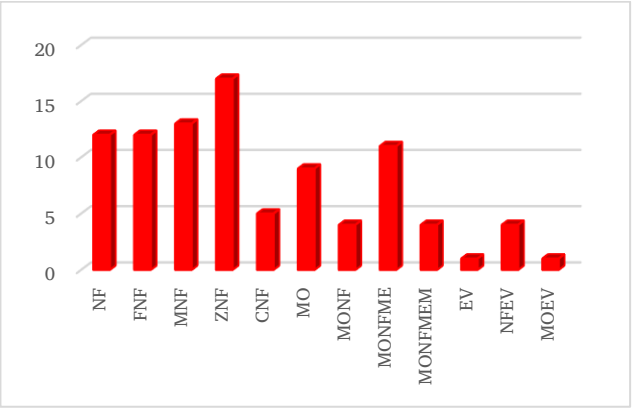

Figure 9. Number of true negative labels of unsupervised models.

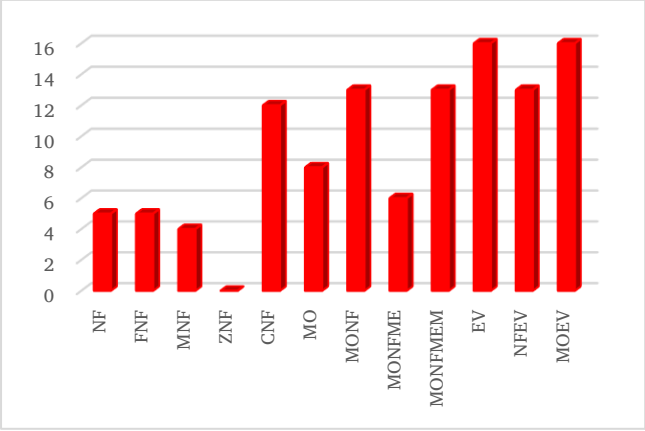

Figure 10. Number of false positive labels of unsupervised models.

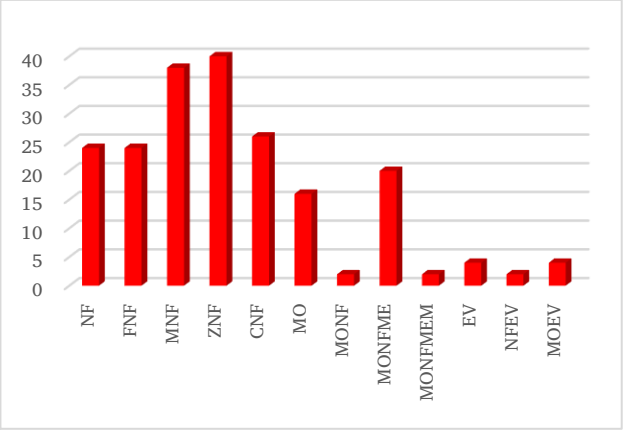

Figure 11. Number of false negative labels of unsupervised models.

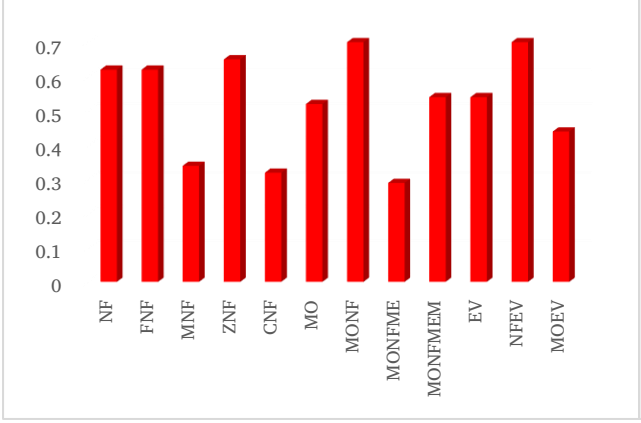

Figure 12. Precision for unsupervised models.

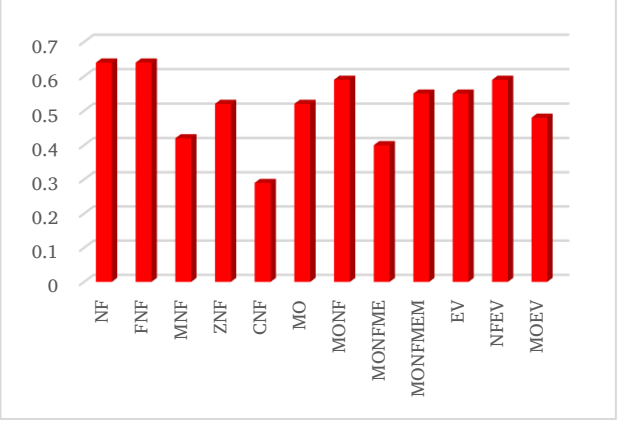

Figure 13. Recall for unsupervised models.

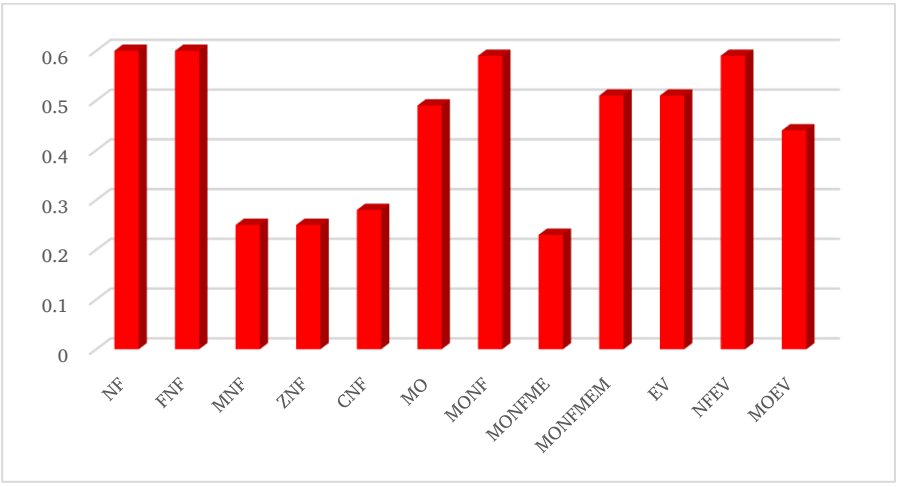

Figure 14. Sensitivity for unsupervised models.

5. Conclusion

This research seeks to provide a method to provide an efficient method to identify unauthorized miners. The proposed models which used AMI and DMD features together produced the most superior results in detecting miners by using unsupervised algorithms. Unsupervised algorithms MONF, NFEV and MONFMEM showed 74% accuracy which is significant compared to the supervised algorithms. The DMD method has produced useful features that have increased the accuracy of the algorithms. Since the data of the consumers collected at distribution companies are highly confidential and accessibility to these data is difficult, data augmentation for improving model generalizability and scalability is suggested as future work.

References

[1] B. Dindar, and Ö. Gül, "The Detection of Illicit Cryptocurrency Mining Farms with Innovative Approaches for the Prevention of Electricity Theft," *Energy & Environment*, vol. 33, no. 8, pp. 1663-1678, 2022.
[2] C. Chahla, H. Snoussi, L. Merghem, and M. Esseghir, "A Deep Learning Approach for Anomaly Detection and Prediction in Power Consumption Data," *Energy Efficiency*, vol. 13, no. 8, pp. 1633-1651, 2020.
[3] M. Kardi, T. AlSkaif, B. Tekinerdogan, and J. P. S. Catalao, "Anomaly Detection in Electricity Consumption Data using Deep Learning,"*2021 IEEE International Conference on Environment and Electrical Engineering and 2021 IEEE Industrial and Commercial Power Systems Europe,* pp. 1-6, 2021.
[4] C. Zhou, Z. Fang, et al., "Using Long Short-Term Memory Networks To Predict Energy Consumption Of Air-Conditioning Systems," *Sustainable Cities and Society*, vol. 55, 102000, 2020.
[5] M. Li, K. Zhang, J. Liu, H. Gong, and Z. Zhang, "Blockchain-Based Anomaly Detection of Electricity Consumption in Smart Grids," *Pattern Recognition Letters*, vol. 138, pp. 476-482, 2020.
[6] Z. Ouyang, X. Sun, J. Chen, D. Yue, and T. Zhang, "Multi-View Stacking Ensemble for Power Consumption Anomaly Detection in the Context of Industrial Internet of Things," *IEEE Access*, vol. 6, pp. 9623-9631, 2018.
[7] P. Nerurkar, "Illegal Activity Detection on Bitcoin Transaction using Deep Learning," *Soft Computing*, vol. 27, no. 9, pp. 5503-5520, 2023.
[8] S. Wu, Q. Liu, and J. Li, "Research on the Detection of Illegal Transactions in Currency Transactions Based on Blockchain Technology," *International Journal of Network Security*, vol. 26, no. 1, pp. 19-24, 2024.
[9] K. Kolesnikova, O. Mezentseva, and T. Mukatayev, "Analysis of Bitcoin Transactions to Detect Illegal Transactions using Convolutional Neural Networks," *IEEE International Conference on Smart Information Systems and Technologies,* pp. 1-6, 2021.
[10] A. Wahrstätter, J. Gomes, S. Khan, and D. Svetinovic, "Improving Cryptocurrency Crime Detection: Coinjoin Community Detection Approach," *IEEE Transactions on Dependable and Secure Computing*, vol. 20, no. 6, pp. 4946-4956, 2023.
[11] M. Amiri, and H. Askari, "Illegal Miner Detection Based on Pattern Mining: A Practical Approach," *Journal of Computing and Security*, vol. 9, no. 2, pp. 1-10, 2022.
[12] M. Ahmed, R. Seraj, and S. M. S. Islam, "The K-Means Algorithm: A Comprehensive Survey and Performance Evaluation," *Electronics*, vol. 9, no. 8, p. 1295, 2020.
[13] J. Qian, Y. Zhou, et al. "MDBSCAN: A Multi-Density DBSCAN Based on Relative Density," *Neurocomputing*, vol. 576, 127329, 2024.
[14] C. Cariou, S. Le Moan, and K. Chehdi, "A Novel Mean-Shift Algorithm for Data Clustering," *IEEE Access*, vol. 10, pp. 14575-14585, 2022.
[15] Y. A. Ghassabeh, and F. Rudzicz, "Modified Subspace Constrained Mean Shift Algorithm," *Journal of Classification*, vol. 38, pp. 27-43, 2021.
[16] X. Ran, Y. Xi, Y. Lu, X. Wang, and Z. Lu, "Comprehensive Survey on Hierarchical Clustering Algorithms and the Recent Developments," *Artificial Intelligence Review*, vol. 56, no. 8, pp. 8219-8264, 2023.
[17] G. J. Szekely, and M. L. Rizzo, "Hierarchical Clustering via Joint Between-Within Distances: Extending Ward's Minimum Variance Method," *Journal of classification*, vol. 22, no. 2, pp.151-184, 2005.
[18] M. R. Ackermann, J. Blömer, D. Kuntze, and C. Sohler, "Analysis of Agglomerative Clustering," *Algorithmica*, vol. 69, pp. 184-215, 2014.
[19] P. J. Schmid, "Dynamic Mode Decomposition and its Variants," *Annual Review of Fluid Mechanics*, vol. 54, pp. 225-254, 2022.
[20] J. A. Rosenfeld, R. Kamalapurkar, L. F. Gruss, T. T. ND Johnson, "Dynamic Mode Decomposition for Continuous Time Systems with the Liouville Operator," *Journal of Nonlinear Science*, vol. 32, pp. 1-30, 2022.
[21] K. Khan, S. U. Rehman, K. Aziz, S. Fong, and S. Sarasvady, "DBSCAN: Past, Present and Future," *The Fifth International Conference on the Applications of Digital Information and Web Technologies*, pp. 232-238, 2014.

Declaration of competing interest

The authors declare that they have no known competing financial interests or personal relationships that could have appeared to influence the work reported in this paper. The ethical issues, including plagiarism, informed consent, misconduct, data fabrication and/or falsification, double publication and/or submission, redundancy, have been completely observed by the authors.

Bibliography

Alireza Simorgh was born in 1997 in Boroujerd, Iran. He obtained his Bachelor's and Master's degrees in Electrical Engineering and Electrical Control Engineering, respectively, from Ayatollah Boroujerdi University in Boroujerd, Iran, and Arak University in Arak, Iran, in 2021 and 2024. Currently, he is working as an Industry Liaison Officer at Shoroue Innovation Center. His specialized interests include robotics, multi-agent systems, data science and machine learning, and fuzzy systems.
Email: alirezasimorgh76@gmail.com
ORCID: 0009-0000-8996-0355
Contribution Statement: Data curation, Formal analysis, Investigation, Methodology, Resources, Software, Validation, Visualization, Roles/Writing - original draft.

Khosro Khandani received his BS degree in electrical engineering from Sahand University of Technology, Tabriz, Iran, in 2007; MS degree in electrical engineering from Iran University of science and Technology, Tehran, Iran, in 2011; Ph.D. degree in electrical engineering from Tarbiat Modares University, Tehran, Iran, in 2016. He is currently an associate professor in electrical engineering department, faculty of engineering, Arak University, Arak, Iran. His research interests include cooperative control of multi-agent systems, fuzzy systems, fractional-order systems and machine learning.
Email: k-khandani@araku.ac.ir
ORCID: 0000-0002-1762-3541
Contribution Statement: Conceptualization, Investigation, Project administration, Supervision, Roles/Writing-original draft, Writing-review & editing.

Maryam Amiri received the BS degree in computer engineering from Arak University, Arak, Iran, in 2009; the MS degree in computer engineering from the Bu-Ali Sina University, Hamedan, Iran, in 2012; the Ph.D. degree in computer engineering from the University of Tabriz, Tabriz, Iran, in 2018. She is currently an assistant professor in the Department of Computer Engineering, the faculty of engineering, Arak University, Arak, Iran. Her research interests include cloud computing, machine learning, and data mining.
Email: m-amiri@araku.ac.ir
ORCID: 0000-0002-7411-9552
Contribution Statement: Conceptualization, Data curation, Project administration, Resources, Writing-review & editing.